A DIGITAL HUMAN PHANTOM FOR USE IN THE FDTD COMPUTATION OF BODY SURFACE POTENTIAL DURING CARDIAC ARRHYTHMIA

A thesis submitted to the University of Manchester
for the degree of Master of Science
in the Faculty of Engineering and Physical Sciences

2008

By
Michael Knight
School of Computer Science

Contents

Abstract **11**

Declaration **12**

Copyright **13**

Acknowledgements **14**

1 Introduction **15**

2 Cardiac Arrhythmia **18**

2.1 Electrocardiography 19

2.1.1 Body Surface Potential Mapping 22

2.2 Causes of Cardiac Arrhythmia 22

2.2.1 Ectopic Pacemakers 24

2.2.2 Irregular Pacemaker 24

2.2.3 Abnormal Conduction 25

2.3 Treating Cardiac Arrhythmia 25

2.3.1 Psychology and Lifestyle 25

2.3.2 Medication 27

2.3.3 Physical and Electrical Treatment 27

2.3.4 Ablation 28

3 Digital Human Phantoms **31**

3.1 Requirements for this Project 31

3.2 Types of Model 33

3.2.1 Mathematical Models 34

3.2.2 Tomographic Models 34

3.2.3 Hybrid Models 36

3.3 Selecting a Phantom Type 39

4 Available Data Sources and Phantoms 41
4.1 The Visible Human Project 41
4.1.1 Photographic Data 42
4.1.2 Radiological Data 45
4.1.3 Applications of the VHP 49
4.1.4 Problems with the VHP 50
4.1.5 Using the VHP 51
4.2 The Tomographic Models 51
4.3 The Basis for the Phantom 55

5 Increasing Resolution 56
5.1 Smoothing in Two Dimensions 60
5.1.1 Convolution Filter Based 60
5.1.2 Look-Up Table Based 65
5.2 Smoothing in 3 Dimensions 69

6 Implanting the Isolated Heart Model 72
6.1 The Heart Model 72
6.1.1 Reformatting and Viewing the Isolated Heart Model . . . 72
6.2 Insertion of the Isolated Heart 75
6.2.1 Orientation 75
6.2.2 Insertion 76
6.3 Preparing the phantom for use 78

7 Conclusions 79
7.1 Future Work 80

A Methods for the Visualisation of Data 82
A.1 Viewing VHP data 82
A.1.1 Photographic 82
A.1.2 Radiological 84

B Methods for Scaling and Smoothing 87
B.1 Modal Filter 87
B.2 Look-Up Table 90

B.2.1 The Main Program 90
B.2.2 The Look-Up Table 93
B.2.3 Pictoral Representation of the LUT Shape Choices 111
B.2.4 Recombining the Files 112

C Isolated Heart Codes **118**
C.1 Reformatting 118
C.2 Mirroring 119
C.3 Extracting a Phantom Section for Visualising 120
C.4 Insertion 122
C.5 Reducing the Range of Tissue Values 123

D Contents of the Final Phantom **127**

Bibliography **130**

List of Tables

4.1 Imaging specifications for the Male normalCT data 49
4.2 Imaging specifications for the Female CT data 49
4.3 Imaging specifications for the Male frozenCT data 50

List of Figures

2.1 A common placement of the ten electrodes used for taking 12-lead ECG measurements 20
2.2 An example ECG output waveform with the five primary components labelled 21
2.3 The Cardiac Conduction system, image taken from `http://www.nottingham.ac.uk/nursing/practice/resources/cardiology/function/conduction.php` 23
2.4 The formation of a cardiac re-entry circuit 26

3.1 A rendering of an example MIRD-type mathematical phantom . . 35
3.2 The female voxel phantom Naomi, produced by Peter Dimbylow[40] 37
3.3 A 3-D rendering of the 4-D NCAT Phantom developed by Paul Segars[44] 38

4.1 Image produced from a_vm1420.raw of the Visible Human Male, the image has been rotated 90° anti-clockwise. The body segment visible is arranged such that the rear of the torso is at the top and being viewed from the bottom, with the right arm on the right hand side of the image. 44
4.2 Axial and Coronal MRI scans from the VHP Female data set . . . 45
4.3 MRI scans of the same section of the VHM using a) T1, b) T2 and c) proton density imaging. 46
4.4 A CT scan from the VHM. 48
4.5 A Rendering of the TARO voxel phantom produced with the ParaView visualisation software 53
4.6 File 611.txt from the voxel phantom NORMAN converted to a .pgm image 54

4.7 Z-normal plane 220 from the voxel phantom TARO converted to a .pgm image 54

5.1 The results of increasing the resolution of a 3 pixel wide square image by 2×, 1.66× and 2.66× using a nearest neighbour algorithm 57
5.2 Nearest neighbour scaling to increase the resolution of a small section of a TARO z-plane from 2 mm to 0.33 mm. Pixel size has been kept constant. 58
5.3 The same section of a TARO z-plane enlarged from 2 mm to 0.33 mm resolution using the standard bilinear and bicubic smoothing filters included in the GNU Image Manipulation Program version 2.2.13[54] 59
5.4 The result of applying a 3×3 mean filter to the central portion of a 5×5 grid of values 61
5.5 The result of applying a 3×3 and 5×5 modal filters in an example situation 63
5.6 One quarter of TARO z-normal plane number 220, scaled by 6 times without smoothing (top) and with smoothing from a 5×5 modal filter(bottom) 64
5.7 One quarter of TARO z-normal plane number 220, scaled by 6 times and smoothed with a 9×9 modal filter 65
5.8 An example of the Look-Up Table process. The original data is used to select a output shape, and then this is used with the original data to apply values to the output pixels 67
5.9 The four pixel arrangement on the left could be interpreted to produce either of the two 144 pixel outputs on the right. As there is no reason to pick one over the other, the region will simply be scaled without smoothing. 68
5.10 One quarter of TARO z-normal plane 220 scaled by 6 times and smoothed with the LUT method. 69
5.11 A section of TARO z-normal plane 220 after nearest neighbour scaling, scaling and smoothing with a 5×5 mode filter, scaling and smoothing with a 9×9 mode filter and scaling and smoothing via the LUT method. 70

6.1 The position and large anatomy of the human heart, as shown in Gray's Anatomy[56] figure 490. 73
6.2 The isolated heart rendered in ParaView and viewed from the front. 74
6.3 The heart (blue) - and local blood (red) - of the TARO model, extracted and rendered in ParaView and viewed from the front. . 75
6.4 The TARO model heart (top) and the isolated heart (bottom) rendered in ParaView and viewed from below. 77

Glossary and Acronyms

Atria The upper chambers in the heart which receive blood from the veins and push it in to the ventricles.

AV(node) The Atrioventricular node. A region of myocardial tissue between the atria and the ventricles that (in a healthy heart) serves as the relay station and barrier for conduction between the two sets of chambers.

BSPM Body Surface Potential Mapping. Recordings taken across the whole torso of the electrical potential at the body surface caused by cardiac activity.

Cardiac Relating to the heart

Chordae Chordae Tendinae, tendons inside the heart that restrict the movement of the valves.

CT Computed Tomography. A method of constructing three-dimensional images from a series of two-dimensional x-rays taken around an axis of rotation.

ECG Electrocardiography. Recording the electrical activity of the heart at specific points on the body surface.

Endocardium The inner layer of the heart that lines the heart chambers. The Purkinje fibres are contained within the deepest layer of the endocardium.

FDTD Finite-Difference Time-Domain. A computational method of solving electrodynamic problems that operates in the time domain and so can cover a range of frequencies in a single simulation.

Infarction Death of tissue due to loss of blood supply.

Ischaemia An insufficient supply of blood reaching an organ.

MIRD Medical Internal Radiation Dose. Commonly refers to the MIRD Committee who develop standards and schema for the measuring of received internal radiation doses.

MRI Magnetic Resonance Imaging. An imaging technique that uses powerful magnetic fields to align atoms within the human body and then measure the response as they return to their original position.

Myocardium The muscular tissue of the heart. Unlike muscle throughout the rest of the body, the Myocardium is capable of transmitting an action potential.

NCAT NURBS-based Cardiac-Torso. A model of a male head and torso defined by NURBS surfaces.

NLM The US National Library of Medicine

NURBS Non-Uniform Rational B-Splines. A method for mathematically defining smooth curves and surfaces.

Pericardium A double-walled sack that surrounds the heart and its intersections with the vascular system. The outer layer is thick and fibrous, while the inner layer is thin and adheres to the outer surface of the heart. Between the two layers is a small amount of fluid to lubricate their motion over each other.

Pixel A picture element. The smallest piece of information in a digital image. Normally arranged as a regular two dimensional grid.

SA (node) The Sinoatrial node. The primary pacemaking region of the heart and the generator of sinus rhythm.

Sinus Rhythm The term used to describe a healthy heart rhythm.

Ventricles The lower and larger chambers of the heart that collect blood from the atria and pump it out into the rest of the body.

VHP The Visible Human Project.

Voxel A volume element. The three dimensional equivalent of a pixel.

Abstract

There is increasingly large amount of interest in biophysical simulation and the modelling of biological systems. Digital Human Phantoms are anthropomorphic models which originally developed in the field of radiation dosimetry but are now being applied to broader medical concerns.

Cardiac Arrhythmia is a reasonably common affliction which can vary in severity from an unnoticed condition of no consequence to a fatal condition that can kill in minutes. Many arrhythmias can be successfully controlled or cured if their source can be localised, but this localisation can involved extensive intrusive procedures. Body Surface Potential Mapping offers a non-intrusive localisation method, but there is a lack of available data to connect output readings with physical conditions.

This thesis addresses the reasons for, requirements of and construction of a Digital Human Phantom for the simulation of Cardiac Arrhythmia. The simulations will use the FDTD method of computational electrodynamics to simulate the body surface response produced by various arrhythmogenic sources and the final model is compatible with this technique.

Declaration

No portion of the work referred to in this thesis has been submitted in support of an application for another degree or qualification of this or any other university or other institute of learning.

Copyright

i. The author of this thesis (including any appendices and/or schedules to this thesis) owns any copyright in it (the "Copyright") and s/he has given The University of Manchester the right to use such Copyright for any administrative, promotional, educational and/or teaching purposes.

ii. Copies of this thesis, either in full or in extracts, may be made only in accordance with the regulations of the John Rylands University Library of Manchester. Details of these regulations may be obtained from the Librarian. This page must form part of any such copies made.

iii. The ownership of any patents, designs, trade marks and any and all other intellectual property rights except for the Copyright (the "Intellectual Property Rights") and any reproductions of copyright works, for example graphs and tables ("Reproductions"), which may be described in this thesis, may not be owned by the author and may be owned by third parties. Such Intellectual Property Rights and Reproductions cannot and must not be made available for use without the prior written permission of the owner(s) of the relevant Intellectual Property Rights and/or Reproductions.

iv. Further information on the conditions under which disclosure, publication and exploitation of this thesis, the Copyright and any Intellectual Property Rights and/or Reproductions described in it may take place is available from the Head of School of School of Computer Science (or the Vice-President).

Acknowledgements

Firstly, I would like to thank my supervisor Dr. Fumie Costen, who has provided continued guidance throughout the course of this project and never failed to provide support and encouragement when needed.

I would also like to thank the Biological Physics group here in Manchester for providing the isolated heart model that forms a key part of this work and their guidance in using the ParaView visualisation software.

I am grateful to Dr. Len Freeman and Dr. Tony Shardlow for their support throughout a difficult and complicated academic year. Without them, I may never have reached this stage.

Finally, I would like to thank my family, for their unwavering support, endless patience and continued encouragement over the years and through the most difficult of times.

Chapter 1

Introduction

Cardiovascular disease is currently the leading cause of death worldwide[1], estimated to be the primary cause in some 17 million cases every year, almost 30% of total global mortality. Of the various cardiovascular disorders, the primary lethal conditions are coronary heart disease, in which the hearts own blood supply is blocked leading to a myocardial infarction - commonly referred to as a heart attack - and stroke, in which the output of the heart is depleted leading to cerebral ischaemia, a lack of blood reaching the brain.

The developed world has an increasingly elderly society [2], and an increasingly high survival rate after a first heart condition arises. These statistics combined lead to an increasingly large population who are suffering from heart conditions, or have suffered a cardiac disorder at some point in their history that has damaged their cardiovascular system. An increasing need for medical care targeted at this population is therefore developing, and is reliant on the advancement of cardiac medicine, and a greater understanding of cardiac function in both the structurally normal heart, and those with previously damaged myocardial tissue.

Damaged myocardial tissue can be caused by a variety of illnesses, environmental effects and surgical complications. The damaged tissue alone may not be a serious problem, though sufficiently large quantities may reduce overall blood flow, but the way in which a small region of damaged tissue can affect the rest of the heart may produce serious problems. Cardiac arrhythmia is a common result, and the occurrence of an arrhythmia can greatly decrease survival prospects[3]. Arrhythmia can also occur in otherwise healthy people, with a variety of contributing factors. The treatment of arrhythmia is therefore a prominent frontier in modern medicine.

The contents of this work are intended to form a component part of a larger piece, one that intends to provide a realistic, numerical simulation of the electromagnetic effects produced by the heart during normal function and various types of cardiac arrhythmia. This simulation will operate at a very fine resolution for a body of such size, with key regions described at 0.33 mm intervals, and take into account the electromagnetic properties of the various tissues and organs that the waves will pass through to accurately describe the spatio-temporal behaviour that can be measured on the body surface. Currently, the connection between body-surface response and cardiac condition is known through empirical means; readings taken from a patient are matched with the previously diagnosed underlying condition.

The numerical simulator produced will solve the forward problem, correlating the inter-cardiac activity with the surface response. This information can then be integrated into an inverse problem solver, one intended to accurately predict the physical and electrical condition of the heart from a set of non-invasive readings. Inverse algorithms already exist, such as that of Armoundas et al.[4], which calculate the instantaneous electrical activity in the heart from a single time sample of a multiple-lead body surface electrocardiograph. The accuracy of systems of this type will be improved using the information that can be gathered from a successful detailed forward problem.

This long-term project is an exploration into the feasibility of the technique, as there is a lack of prior study incorporating models with such high spatial and temporal resolution. Previous works have not used a detailed model of the whole heart embedded in a realistic torso and so are unable to ascertain the precise relationships between arrhythmic tissue location and ECG response. This project combines the propagation of the action potential with the propagation of the electromagnetic waves through a far more detailed biophysical model than has previously been used. It is hoped that the results will provide a step towards computative cardiology, and verify the viability of a much larger study.

The contents of this report

This work is concerned with the development of the digital human body that will provide the simulation space. The model will be used in Finite-Difference Time-Domain codes, and so must be constructed in a manner than can be easily

incorporated into pre-existing codes and those currently under development. An externally developed heart model has been provided by the Biological Physics Research Group at Manchester that is rich in detail and already at the 0.33 mm resolution sought. Incorporation of this heart into the final body model provides reliability in this most important region.

The construction of a digital model for simulations requires an understanding of the problem under consideration. The specifics of cardiac arrhythmia are discussed in chapter 2, with attention paid to the identification, causes and treatment of the condition. The mechanisms of studying the hearts rhythmic function are described, as it these which the final simulation will hope to emulate.

The structure of the model desired, the features we require of it and the various types of model it could imitate or be based upon are discussed in chapter 3. Information upon which a model can be based and previously developed models which have been made available to us are discussed in chapter 4. From this information a model type and the specific model basis are chosen.

Chapter 5 concerns the adaptation of the chosen model base to better fit the requirements. This involves the rescaling and smoothing of a previous model. The chapter discusses some standard smoothing techniques and how they are largely incompatible with the properties of the data being used. The complexity of operating in three dimensions while still generating a surface of acceptable quality and methods that are used to overcome this are considered, and the final body model is produced.

The heart model, and its insertion into the completed body, is detailed in chapter 6. The Paraview[5] visualisation software is used to find an optimal position for the external heart model to be implanted into the main body. Implantation is then a matter of overwriting the original data with the contents of the heart model. The final model is produced, and its successes and limitations described.

Finally, conclusions are drawn over the project, and potential for improvements and future developments are discussed.

Chapter 2

Cardiac Arrhythmia

Cardiac arrhythmia is a condition in which normal heart function is impaired or otherwise affected, producing a beat rhythm that is of abnormal speed or structure. A minor arrhythmia may go completely unnoticed, and many more do little other than cause minor palpitations, causing the sufferer to be abnormally aware of their heart beat. Indeed, in many cases the arrhythmia itself is not dangerous or is not the underlying condition, but a symptom of a larger problem[6].

Arrhythmic action can produce a range of beat variations. The most common variations are simply of tempo. The heart may beat too quickly (tachycardia) or too slowly (brachycardia), both resulting in a lack of blood flow throughout the body. The heart rhythm is expected to change with regard to a variety of external factors, but unexplained variation too far in either direction can be a sign of a potentially serious problem. As well as these, there may be problems with anomalous beats inserted into the normal rhythm, the atria and ventricles may become desynchronised, or the heart chambers may not contract properly resulting in a loss of blood flow and the potential formation of blood clots in the heart, leading to a greatly increased risk of stroke.

Common complaints from people suffering arrhythmic disorders include shortness of breath, dizziness, pain and fainting. In many cases these occur for a few short periods over an extended interval and can be easily treated or even just accepted as a minor inconvenience that will occur a few times a month. However in some cases the attacks will be more frequent or more severe, leading to a significant decrease in the quality of life or possible damage to the cardiac tissues. In people who have suffered from previous cardiac disorders or have any of a range of cardiovascular problems, an arrhythmia that could be ignored in an otherwise

healthy patient can become a serious concern.

Cardiac arrhythmias are often categorised as being disorders of rate, rhythm or conduction, or a combination thereof. Commonly the only way to determine the existence, and type, of arrhythmia is through the use of electrocardiogram (ECG) supported with ultrasound-based echo-cardiography. For successful treatment it is important that the specific details of the arrhythmia are known in order to provide maximum benefit with minimal risk. Once an arrhythmia has been identified non-invasively, treatment may require invasive methods than can further localise the source.

2.1 Electrocardiography

The basic concept of the ECG has existed for over a century. Electrodes are attached to a patients skin at various points around the torso and extremities, and the electric potential between combinations of these creates a 'lead', the output of which is recorded over a period of time. Interpretation of the readings can provide a large amount of detail into the hearts functioning, along with the general electrical rhythm pattern, different leads provide information from a different 'perspective'. The most common form of ECG in use is 12 lead electrocardiography. This system involves 10 electrodes, which produce 12 leads of information. The mismatch in number is due to the specific way in which the electrodes are used.

One electrode is placed at a specific position on each arm and the left leg. These are used in pairs, with positive or negative defined by the potential between the two, to form three 'bipolar leads' named as I,II and III and called the 'limb leads'. These three electrodes are also used to form the three 'augmented limb leads' - aV_R, aV_L and aV_F (augmented vector Right/Left/Foot) - where the electrode at each point is defined as positive and compared with the average of the two others set as negative.

Six more electrodes are positioned on the torso around the heart, these form six 'Unipolar leads', known as V_1-V_6, where the electrical potential at a each electrode is positive and compared with a reference point that averages the output of the three limb leads. The final electrode is a ground that contributes nothing to the waveforms. It can be put anywhere on the body, but is usually positioned on the right leg to complement that on the left.

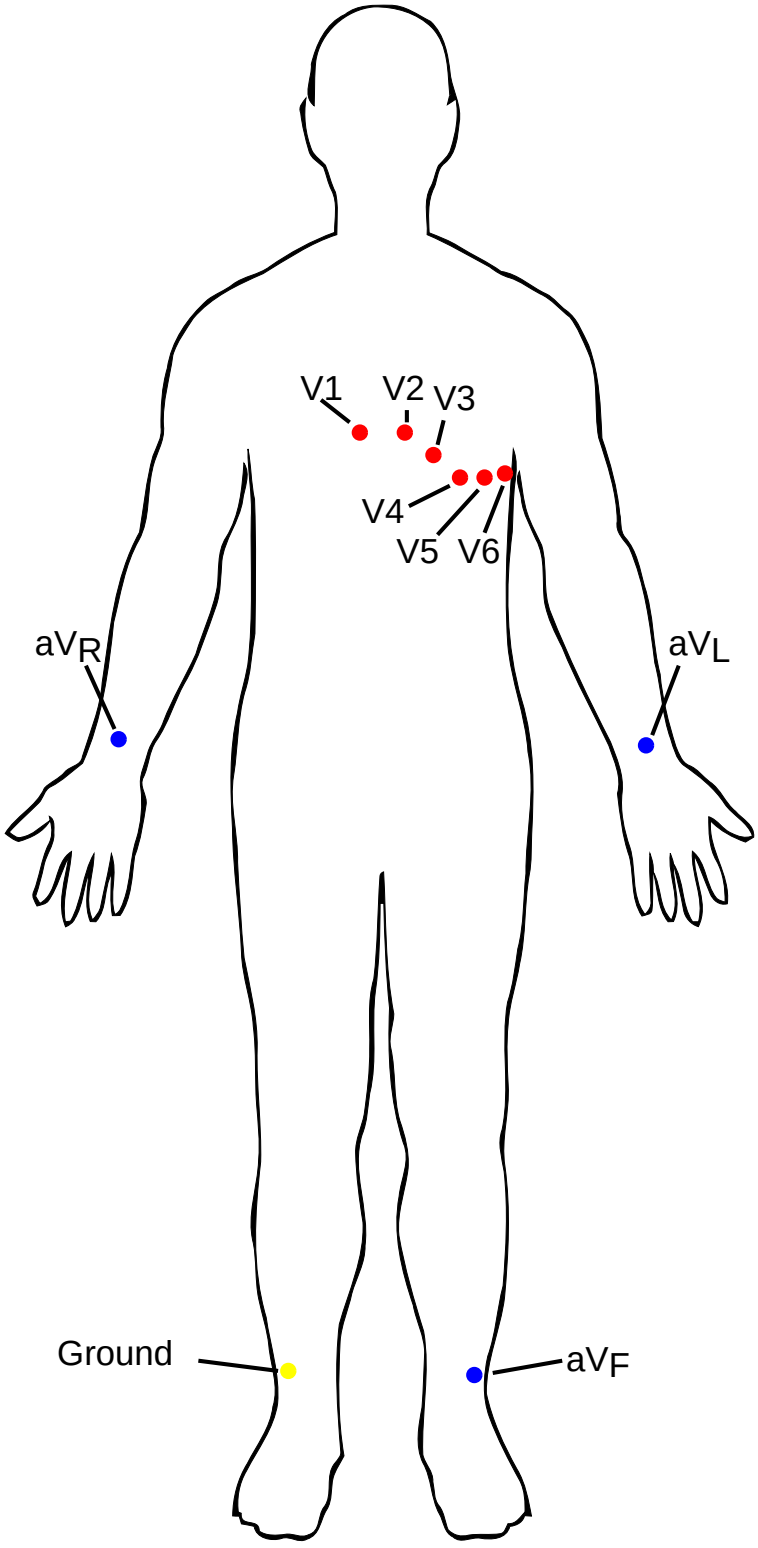

Figure 2.1: A common placement of the ten electrodes used for taking 12-lead ECG measurements

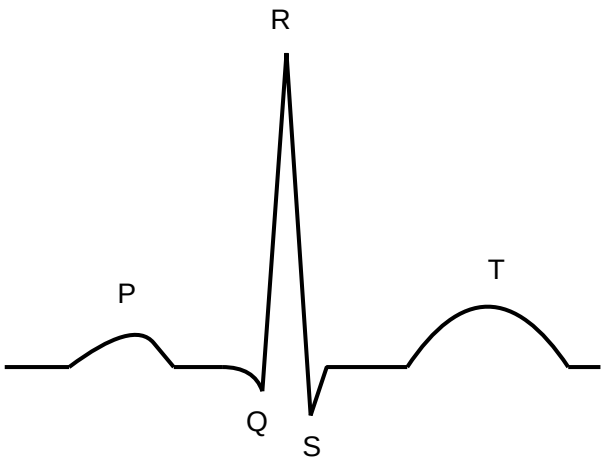

Figure 2.2: An example ECG output waveform with the five primary components labelled

An ECG output shows a waveform with 5 primary components. Each of these is known by a letter, one of P, Q, R, S or T, and in a normal rhythm should occur in alphabetical order with regularity in tempo and amplitude. Inspection of individual lead outputs, and direct comparison between two or more, with attention paid to the spacing between these events, their relative amplitudes and regularity of their occurrence can provide a significant amount of insight into the type of aberration and its general location within the heart structure.

A 12 lead ECG will output either all leads concurrently, or switch between groups of leads at regular intervals. Identification of a problem may require only a short period of recording, with the anomaly showing up in every beat, or may require long term observation to catch an irregular occurrence that may last for only a few seconds in 24 hours. Some modern machines will provide automatic interpretation of the readings to allow operation by non-specialist staff[7].

While widely utilised, the 12-lead ECG is inherently limited by the small number of locations at which data is collected [8]. This provides a clear and definitive constraint on the maximum amount of information extractable, and exists largely because of convention to traditional practice rather than technological limitation. More sources of data would allow for more precise diagnosis of arrhythmic conditions and more precise localisation of defects.

2.1.1 Body Surface Potential Mapping

Body surface potential mapping works in a manner similar to that of the 12 lead ECG, but rather than using 10 electrodes, it incorporates anywhere between 32 and 219 electrodes arranged around the whole torso[9]. This produces considerably more data, and so is considerably more complicated to interpret, but recognition of the presence of complex arrhythmia and correlation of BSPM features during arrhythmia with the location of structural and conductive defects can lead to huge advances over 12 lead ECG in the accuracy and reliability of diagnoses[10].

Despite the benefits, the relationships between BSPM output and cardiac function are not completely understood, and so only limited utilisation of the technique is possible. The large amounts of output information can make human interpretation of the readings extremely time consuming, while the lack of knowledge makes automated interpretation an inexact process.

Commonly, BSPMs are used as a means of supporting a previous diagnosis, with specifically chosen lead locations designed to pick up optimal information about a specific defect[8]. 32 electrodes is considered a practical diagnostic amount, but the specific locations of these electrodes is likely to have been chosen by taking measurements of patients with well documented conditions. Measurements will be taken from this patient using over a hundred electrodes, and from these, a subset can be taken that produce an output that is similar within an acceptable level of error.

2.2 Causes of Cardiac Arrhythmia

The myocardial tissue that makes up the majority of the heart is muscle unlike that found in the rest of the body[11]. As well as the standard muscle properties, the myocardium has the ability to conduct electrical signals in a manner similar to that of neurons. Moreover, not only can the tissue conduct electricity, it is also capable of generating an action potential, providing a signal that is transmitted to the rest of the heart. Regions that act in such a way are described as possessing automacity, and they form the pacemaking regions that generate and regulate the heart beat pattern.

The primary pacemaking region in a healthy heart is the Sino-Atrial (SA)

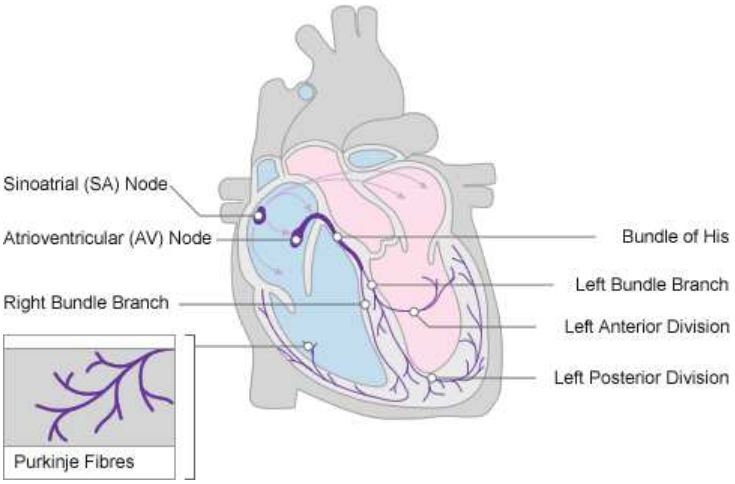

Figure 2.3: The Cardiac Conduction system, image taken from `http://www.nottingham.ac.uk/nursing/practice/resources/cardiology/function/conduction.php`

node, however it is not the only region. Automacity is also found in the Atrio-Ventricular (AV) node and the bundle of His, both located at the junction between the atria and ventricles; the right and left bundle branches, conductive fibres that extend from the bundle of His out to the ventricles; and the Purkinje fibres, which spread from the bundle branches to reach all over the ventricle walls. While all of these tissues are capable of generating their own electrical signals, a healthy SA node will dominate by having the shortest time period, overriding the activity in the other regions. The SA node is therefore the source of what we consider a normal heartbeat, the Sinus Rhythm[6].

Myocardial calls at rest are in a polarised state, with a negative potential difference compared to the extracellular space[12]. When excited, the cell depolarises, resulting in either a less negative or slightly positive potential difference. The magnitudes of the resting potentials differ among the cells, but are generally between -50 and -95 mV, with the SA node having the smallest PD and the Purkinje fibres the largest. When excitation occurs, the depolarisation can produce a change of 60-120 mV at a rate of up to 800 Volts per second. As each cell is excited it becomes unexcitable and causes the excitation of all available cells surrounding it. The cells remain unexcitable for a period, and so the signal sweeps across the heart chamber in a single wave.

Cardiac arrhythmia is thus the result of something disrupting an element within this system.

2.2.1 Ectopic Pacemakers

Ectopic pacemakers are regions other than the primary regions of automacity that have become excited and begun acting as pacemakers. The additional stimulation produced by an ectopic focus can cause additional beats in the regular rhythm, or cause beats to happen early or late. If there is only ectopic focus and it produces signals irregularly, it may be best left untreated. However, if the focus is consistent in its activity, or more than one such region is present, it can lead to tachycardia or fibrillation.

In the atria, ectopic foci are most commonly found in the region of the Pulmonary veins in the left atrium[13]. These ectopic foci frequently occur in multiple sites in the same patient, and left untreated can heavily increase the risk of stroke. Ectopic foci in the junctional regions surrounding the AV node and bundle of His are rare, but difficult to treat [14].

Ventricular ectopic beats are relatively common in patients with otherwise normal hearts. These can be of little clinical significance but sometimes lead to an enlarged ventricle, which is frequently a precursor to cardiac dysfunction[15]. Ventricular tachycardia and fibrillation are more serious conditions than their atrial and supra-ventricular counterparts, especially following recent surgery or infarction, and so even foci with no symptoms presenting will receive treatment.

2.2.2 Irregular Pacemaker

If the SA pacemaker fails due to cardiac disease, or the automacity otherwise falls below that of the AV node, the AV junction will take over as the primary pacemaker in the heart. This is not usually a problem, though it may lead the the discovery of a previously unknown condition that is retarding the output of the SA node. The role of primary pacemaker may switch between the two nodes, but this is a symptom of the underlying problem rather than a direct concern[6].

If the SA node fails and the AV junction does not take over the pacemaking role, or if the AV junction fails to transmit signals from the atria to the ventricles, an ectopic area of automacity in the ventricles can instead perform the duty. This 'complete heart block' is a serious problem, with the pulse being as low as 20-40 beats per minute and producing a low cardiac output. It is also possible for the atria and ventricles to become driven by separate pacemakers without there being conduction problems in the AV node. This problem is rare as it requires

synchronicity between the pacemakers and the situation will collapse if one gains dominance.

2.2.3 Abnormal Conduction

While the conductive cells in the heart normally transmit only one way, they are theoretically capable of transmitting in any direction. Normally the conduction system transmits the signal from the SA node through the whole of the heart in one movement before it ceases. Cells in the myocardium are depolarised sequentially and then spend a short period repolarising and in a refractory phase, during which time they cannot be stimulated. The signal is passed on to any myocardial cell that is not in this state and therefore excitable. Problems occur when a conductive fibre either conducts slowly, or ceases to allow transmissions in one direction.

Slow conduction results in the signal that would ordinarily be travelling as a smooth front through the tissue becoming discontinuous. Cells that have been stimulated from one direction have time to depolarise before the signal arrives from the slow region. This allows a secondary rhythm to form resulting in tachycardia. If the situation is correct, the cells may "trap" a signal in a re-entry circuit as shown in figure 2.4.

2.3 Treating Cardiac Arrhythmia

Once an arrhythmia has been diagnosed, and it is decided that direct treatment of the arrhythmia rather than an underlying condition is necessary, the response can take one of many forms[6].

2.3.1 Psychology and Lifestyle

Some disorders can be treated through psychological therapy or alteration of lifestyle. The heart is highly susceptible to influence from the mental state of the patient, and simply being aware of a problem can lead to it worsening as the patient's anxiety and focus on every minor event compliment each other to produce a significant decrease in their quality of life. Patients who smoke, consume too much alcohol or caffeine, or use other narcotics may be providing

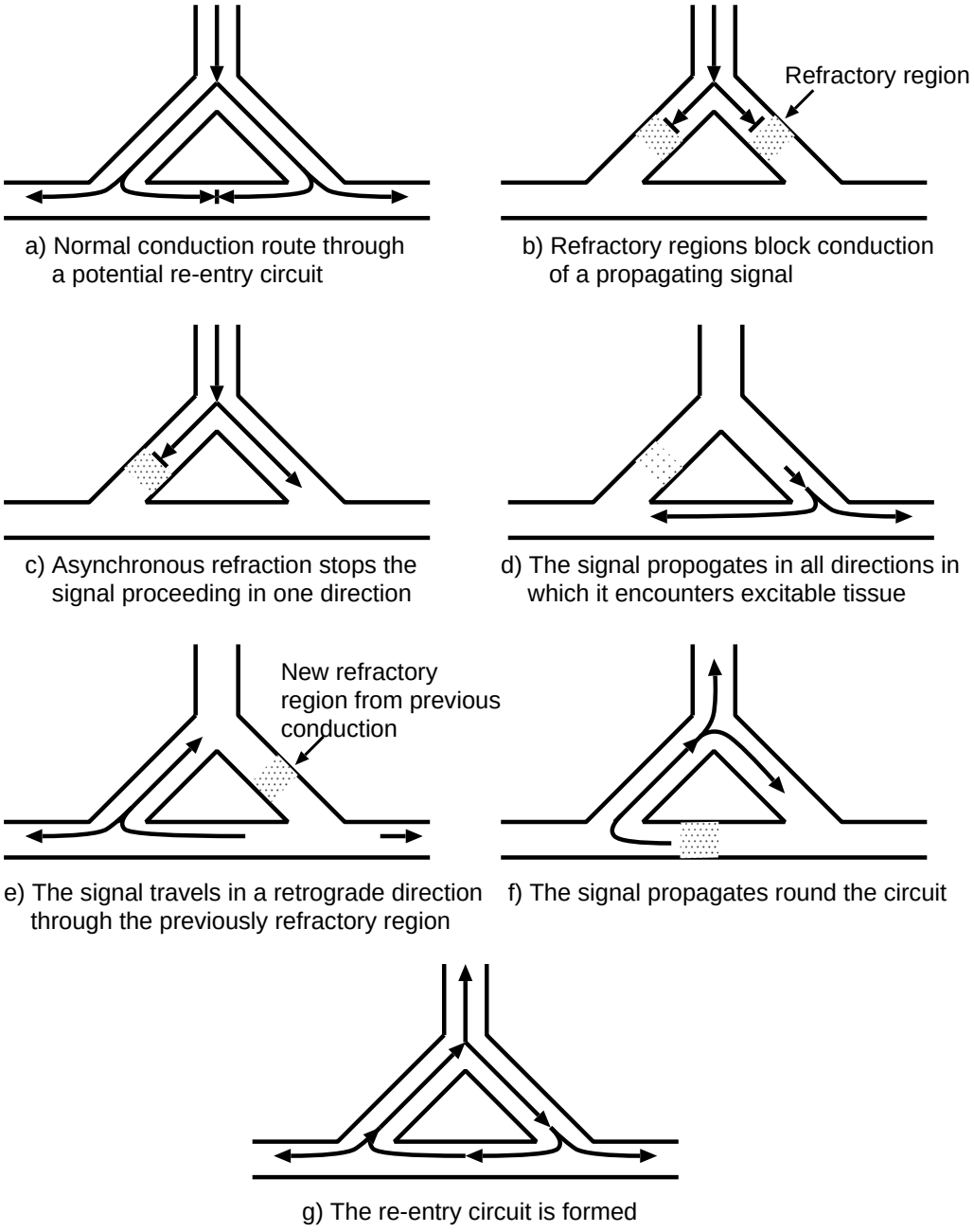

Figure 2.4: The formation of a cardiac re-entry circuit

a chemical augmentation that turns an insignificant problem into a more serious one, and cessation of these substances may be sufficient to provide relief.

2.3.2 Medication

Many disorders can be treated pharmacologically, with a variety of medications available that act on specific elements of the heart function. These medications may alter: the action potential in the whole heart, or just certain areas; the speed of conduction through certain junctions; ectopic activity; the automacity of the myocardium; and a variety of other attributes. These medications can require careful and regular monitoring as their primary action may be beneficial, but cause impairment of general cardiac function.

Side effects with these medications can range from the unpleasant to the fatal. Inappropriate prescription can cause a pre-existing, or even new, condition to develop, or could lead to cardiac arrest. The effects mean that dosage and sensitivity are extremely important to minimise the risk of toxicity, and some are prescribed only for short periods while under ECG monitoring. Frequently, medications will only suppress the symptoms of arrhythmia, rather than having a curative effect[16]. .

2.3.3 Physical and Electrical Treatment

Direct stimulation of the heart rhythm is another option available. The least aggressive of these is Vagal stimulation, in which the vagal nerve that connects to the SA and AV nodes is stimulated by physical means, a manoeuvre that would normally reduce the heart rate. This is rarely curative as it frequently only works while the stimulation is being applied, but can be used in the control of transient atrial and supra-ventricular tachycardia and also as a diagnostic tool when determining the type of tachycardia occurring.

Serious disorders of rhythm can be terminated by electrical Cardioversion or Defibrillation, application of electric current to the heart either directly or through the chest wall. The severity of the action and distress it causes a patient generally limits use of this procedure to life-threatening situations such as ventricular fibrillation, tachycardia that is leading to circulatory failure or heart rhythm failing to return during cardiac surgery.

Defibrillation is designed to depolarise a critical mass of the myocardium,

allowing the SA node to reassert authority over the pacemaking and returning the patient to sinus rhythm. Cardioversion can be thought of as a more refined version, with an ECG equipped machine delivering the charge just after the peak of the R-wave. This specific time is chosen to minimise risk of the shock inducing Ventricular fibrillation.

Implantable Cardioverter-Defibrillators (ICD) are an option for patients with recurring fibrillation or tachycardia or the potential for sudden onset of either arrhythmia[17]. The ICD is implanted in the chest with leads inserted into the heart where it monitors the heart rhythm. If tachycardia or fibrillation occur the device interprets the readings as such and delivers a shock appropriate to halt the arrhythmia and reinstate sinus rhythm.

When the heart becomes incapable of maintaining a sinus rhythm under its own automacity, possibly due to disorders such as the SA node failing, conduction problems or asynchronicity between the ventricles, an implanted artificial pacemaker can be installed to take over the pacing. This battery powered device may have one, two or three leads that enter the heart to provide stimulation at certain points. It can pace constantly, or provide signals only when a normally regular heart misses beats or falls below a certain rate. Modern pacemakers will adapt to the users need, increasing the heart rate in response to the bodies metabolic requirements[18].

Some implants serve the role of both ICD and artificial pacemaker, providing capabilities that can keep a diseased heart functioning for long periods. These devices are more complicated than their single purpose counterparts, being required to both distribute low energy signals for pacing and high voltage shocks for defibrillation.[18]

2.3.4 Ablation

In situations with arrhythmia being caused by errant conduction, ectopic foci or malfunctioning nodes, it can be curative to remove the automacity or conductive potential of those regions. This can be achieved through the use of Catheter Ablation, whereby an electrode tipped catheter is guided into the heart through a major vessel, and a burst of radio-frequency energy is directed at the aberrant region. Historically, other ablatives were used, such as direct current and cryogenics, but they cannot compare to the localised nature of radio-frequency ablation[19].

Catheter ablation can be used in situations where the condition is resistant to pharmacological intervention or the side-effects would be prohibitory [20]. Many types of atrial arrhythmia can be treated, including atrial fibrillation, atrial flutter, ectopic atrial tachycardia, and Wolff-Parkinson-White syndrome[19]. The procedure is also able to eliminate episodes of ventricular tachycardia in up to two-thirds of patients who have suffered myocardial infarction[20]. Ventricular tachycardia is significantly more difficult to treat than atrial due to the high variability in the location of the site requiring ablation. There are several established methods to localise arrhythmogenic foci.

The most prominent diagnostic electrophysiology technique is fluoroscopic cardiac angiography guided catheter-based mapping, such as activation mapping, pace mapping(stimulation of the heart with an electrical pulse delivered by an intra-cardio electrode), and anatomic mapping [19]. More recent developments in the localisation of arrhythmogenic focus involve non-invasive methods such as Magneto-cardiography (MCG). MCG has been specifically developed for studies of the electrical events in the heart[21].

However, an arrhythmogenic focus is not always easily localised, especially in cases of atrial tachycardia. In some invasive techniques, the point-by-point data acquisition for map creation is time consuming and, as it involves exposing the patient to ionising radiation, potentially dangerous. As well as this, activation mapping with a catheter is imprecise due to difficulties establishing landmarks on X-ray images that will enable the operator to return the electrode catheter to the exact arrhythmogenic focus which was localised in the mapping, and the lack of 3-dimensional spatial information. Furthermore, there are some cardiac tissues which are just difficult to reach with contact catheters.

More advanced methods have been developed that track the location of the catheter tip through echo-cardiography, RF signals and magnetic field measurements. These methods can be more spatially accurate and provide three dimensional location while also removing the time constraints applied by x-ray fluoroscopy. However, transient or hemodynamically unstable arrhythmias are not mappable at all with some techniques[22].

Prolonged mapping with a catheter can irritate the endocardium, and extended procedures increase the risk of complications due to perforations or damage to chordae[19]. Yet while extended mapping creates in own dangers, insufficient accuracy in the procedure can result in the quantity of tissue being ablated

increasing. With an ablation destroying an area some 5mm in diameter, the impact of a single treatment on an otherwise healthy heart is minimal. However, treatments near the primary pacing regions can damage the myocardium to an extent that external pacing becomes a requirement, and in an already damaged heart the results of any specific procedure become much less predictable[23].

Complex arrhythmia such as ventricular tachycardia and atrial fibrillation are difficult to treat without invasive methods due to the necessity of accurate localisation. If the arrhythmogenic focus or abnormal pathway of action potential could be localised non-invasively it would help guide catheter-based interventions, to the vicinity of the arrhythmic origin, allowing for fine mapping to finalise the location of the arrhythmogenic focus[21, 24].

Chapter 3

Digital Human Phantoms

Digital Human phantoms are a method of providing anthropomorphic, bio-physical models in a manner that can be utilised and operated on by computer software. Digital modelling allows for the computation of physical properties that would be inherently dangerous to discover using live subjects, provides a constant environment for repeated experiments that would be unobtainable with physical specimens, and reduces the reliance on donated cadavers for bio-medical research. Digital human phantoms are currently developing into valuable educational tools, being increasingly implemented in the teaching of anatomy [25].

3.1 Requirements for this Project

For the purposes of this project, we require a model that is high in both anatomical accuracy and data resolution. Solvers for the forward problem, the relationship between the electrical excitation in the heart and the output of the body surface electrocardiograph, reported in the literature often assume that the torso is a homogeneous conducting body[26]. Some studies take into account the physical structure of the torso with various levels of inhomogeneity, though the most detailed amongst these [27] set little more than conductivities for bones, lung, muscle and heart to different values.

Ignoring all torso inhomogeneities in these simulations, such as blood masses in the ventricles [28] and inaccuracies in electrode position, produces unrealistic electrocardiograms and introduces a systematic error into the calculation. The position of arrhythmogenic focus is often displaced by greater than 5 mm from its true physiological position whilst 2$\sim$3 mm accuracy is required for ablation[26].

This error could become problematic when attempting to match the location of the catheter tip to the location of arrhythmogenic focus, and so retain the requirement of significant invasive mapping to localise the ablation site.

The precision of the heart model is another important factor in the ideal simulator. Even a slight change in the heart model can result in significantly different simulation results. For example, the T-wave in the first limb lead for a homogeneous model is inverted in the anisotropic myocardial model[29]. Specific elements of the conductive system play a significant role in signal propagation, yet their effects are rarely modelled. The Purkinje fibres play an important role in the excitation process of the heart, yet only a few works such as Wie et al.[30] include the Purkinje fibres and set the different conduction velocity of atrial, ventricle and Purkinje fibres as 1.0 m/s, 0.5 m/s and 2.5 m/s.

In the literature, the conductivities of body tissues are ordinarily treated as frequency independent. The output signal at the sinoatrial node is known to include a frequency range of $0 \sim 2$ kHz, when the frequency components down to -60dB relative to the peak spectrum are taken into account. As an example, the conductivity of muscle has been measured to change from $4 \cdot 10^{-2}$ S/m to $2 \cdot 10^{-1}$ S/m as the signal frequency increases from 0 Hz to 2 kHz. Furthermore, many simulations such as that of Ramanathan & Rudy[27] set the relative permittivity of all included tissues to a constant value. The relative permittivity of tissue is known to be highly variable, that of muscle and lung being about 100 times higher than that of blood or bone. Therefore, the accuracy of [27] is limited by this relatively simplified electrophysiological modelling. Some papers such as Liu et al.[24] report that torso geometry does not affect the inverse results, however this statement can not be verified because their torso model is limited to a cubical or spherical homogeneous conductor. As such it is assumed that physiological accuracy is the preferable situation.

To accurately calculate the electromagnetic fields in the torso, it is necessary to solve Maxwell's full-wave equations. The Finite Difference Time Domain (FDTD) method is well suited to accurate evaluation of the electromagnetic field behaviour within complex biologic environments as it can take into account the effect of variations in conductivity and permittivity of various tissues with varying frequency. This level of accuracy will reveal the precise effect of the torso volume conductor[24] and contribute to the accurate solution of ECG inverse problem[31].

FDTD simulations are generally designed to work over a computational domain of cuboid cells, with each cell having well-defined electromagnetic properties. The cell sizes must be small enough to define the smallest geometrical features in the simulation and the geometrical features should match the size of the calls[32]. Because of the steepness of the myocardial action potential upstroke and the consequent steepness of the spatial distribution of transmembrane potential, the tissues inside the pericardium must have a high spatial resolution, optimally 0.1 $\sim$ 0.25 mm[33] to achieve high localisation accuracy.

The pericardium itself is a significant feature. As the first boundary between the heart and the rest of the body, it has a prominent position in the propagation of the electrical signals. The pericardium, being a fluid-filled double walled sack surrounding the heart, is difficult to model. The walls themselves are thin and prove difficult to image externally, while the serous fluid they contain is difficult to contain for measurement in a cadaver.

Ideally, all of these requirements could be met, and a phantom at 0.1 mm resolution containing all the biological and electromagnetic information definable at that scale could be created. In reality, phantoms are necessarily limited by the resolution of data we can collect from the human body, the time required for construction and the boundaries on simulation size imposed by the computer equipment available.

Further to these requirements, the Biological Physics group at Manchester have provided a pre-developed heart model. This model includes the various structures normally contained within the pericardium, though not the pericardium itself, and large section of the immediate vascular system. These are segmented into 18 different regions and tissues at a resolution of 0.33 mm^3. Integration of this model will add precise detail of the cardiac region to a phantom that is otherwise lacking in physiological accuracy.

Taking these requirements into account, there are a variety of options concerning the type of model developed.

3.2 Types of Model

Phantoms can be broadly classified as one of three varieties: mathematical, tomographic or a hybrid of the two. Mathematical (or equation-based) models are built from a series of geometrically defined regions, each used to describe the

placement, shape and properties of various organs. Tomographic phantoms are developed from MRI, CT or photographic data taken from human subjects. These consist of a large quantity of voxels of identical size but differing composition.

3.2.1 Mathematical Models

Mathematical models are commonly of the "MIRD-type", referring to the model first produced by the Medical Internal Radiation Dose committee of the US Society of Nuclear Medicine in 1967, and repeatedly updated and enhanced since then[34, 35]. Each generation of model adds to the structures and information in the phantom as the level of complexity that can be managed by computational systems increases. These are, however, not the only models available, with researchers adding and removing structures from the MIRD model, or designing entirely new phantoms that may, for example, be homogeneous in content, or simplify the torso shape to a sphere.

When a mathematical model is being designed or updated, it is commonly intended to match the characteristics of a "Reference Man" such as that specified by the International Commission on Radiological Protection (ICRP)[36, 37]. This is a collection of information that describes many of the anatomical features of the human body, with information available for both sexes and a variety of ages. The changing body proportions and organ volumes can thus be modelled for most scenarios.

The variation between individual models is therefore high, with large difference in heterogeneity, resolution and appearance. Models can be sex-specific or hermaphroditic, and a range of ages are available for each. These models, while physiologically relatively inaccurate, are easy to implement, can be easily scaled for simulating different body sizes and builds, and can be repositioned into different body poses with minimal editing[38].

3.2.2 Tomographic Models

Since the introduction of widely available MRI scanners, attempts have been made to enhance and expand upon earlier mathematical phantoms. These models are constructed from MRI and CT scans, with live volunteers or donated cadavers as their basis. More recently, the Visible Human Project provided photographic data that provides far greater resolution than MRI or CT, and models have been

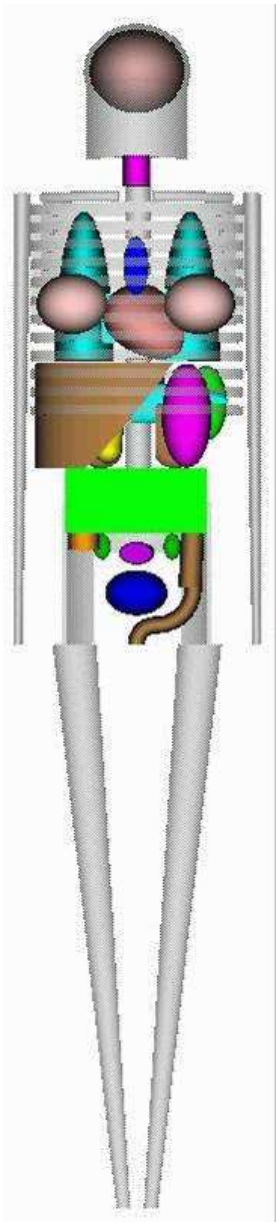

Figure 3.1: A rendering of an example MIRD-type mathematical phantom

constructed using this and other photographic data as their primary sources[39].

Tomographic models provide much greater physiological accuracy than their mathematical counterparts, lacking the simplified geometric structure. Their construction is limited by the inherent complexity of the human body, and the limitations of the information capture medium. MRI and CT data may cause difficulty in the separation of tissues with similar responses or regions where similar tissues, such as blood vessels, are intertwined. Photographic data relies on the ability to visually delineate the boundaries between structures. Many models are restricted to only containing the organs and tissues which are of interest to the primary research in order to reduce the complexity and construction time. This results in a model that produces highly accurate results in certain experiments, but could lack the necessary information for others.

Unlike mathematical models, scaling of the body is significantly more complicated. A simple enlargement must be carried out in a manner that does not disrupt other tissues, and this can prove difficult in highly heterogeneous regions. An operation such as changing the position of the arms becomes far more complicated than in a mathematical model, especially if retention of the high detail and full tissue connectivity is a priority. In either case, modifications must be made on a voxel basis, rather than the alteration of parameters[38].

While specialised models are created for specific purposes, there may still be a multitude available that are designed for the same experiment. Many countries are producing their own voxel phantoms developed from their own populace in order to correctly model racial variations in size, weight and organ structure[41]. The sources for these models are commonly chosen, and the results sometimes scaled[40], to approach the characteristics of a reference man that well defines the local population[42] rather than the ICRP specifications.

3.2.3 Hybrid Models

Hybrid models are an attempt to combine the physiological accuracy of tomographic phantoms, with the ease of use of mathematical. They may attempt this by making a mathematical model more realistic or, more usually, by making a tomographic phantom more flexible. A prime example of this technique comes in the use of Non-Uniform Rational B-Splines (NURBS) to define the structures in the phantom. NURBS are a mathematical method of defining smooth, continuous surfaces and are often used in computer graphics[43].

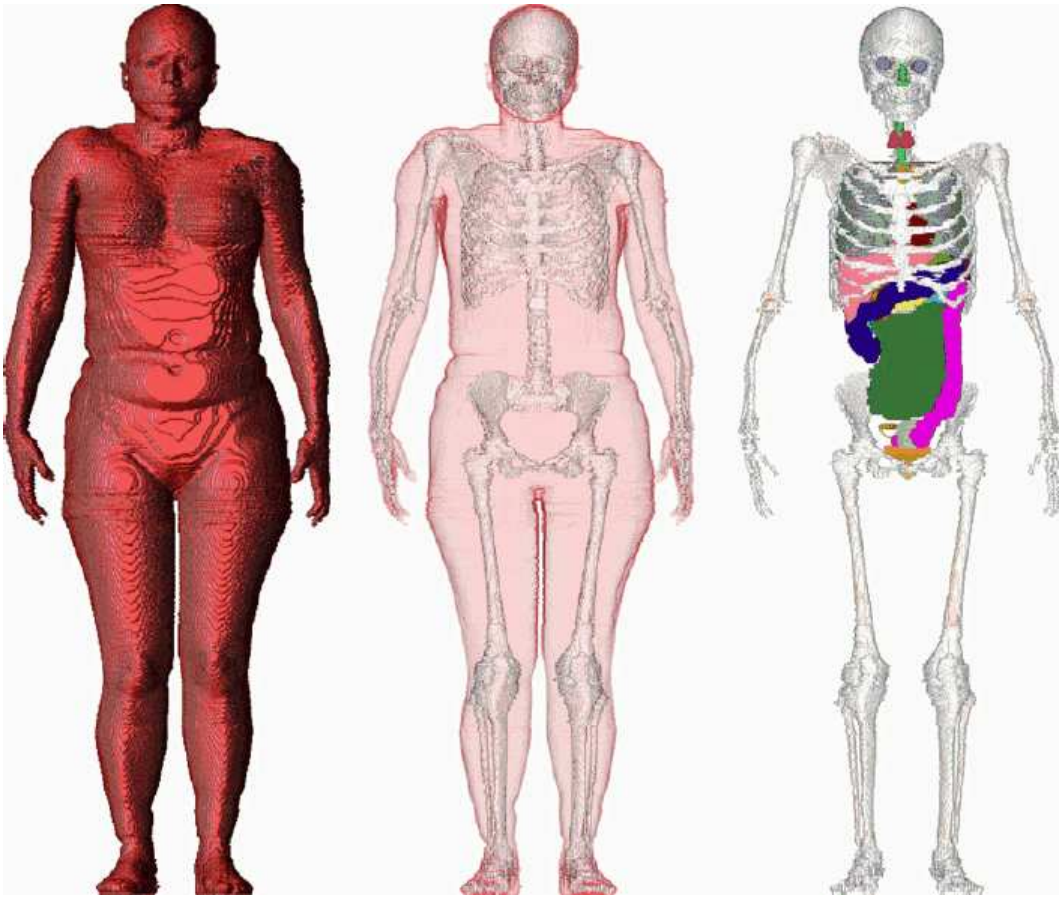

Figure 3.2: The female voxel phantom Naomi, produced by Peter Dimbylow[40]

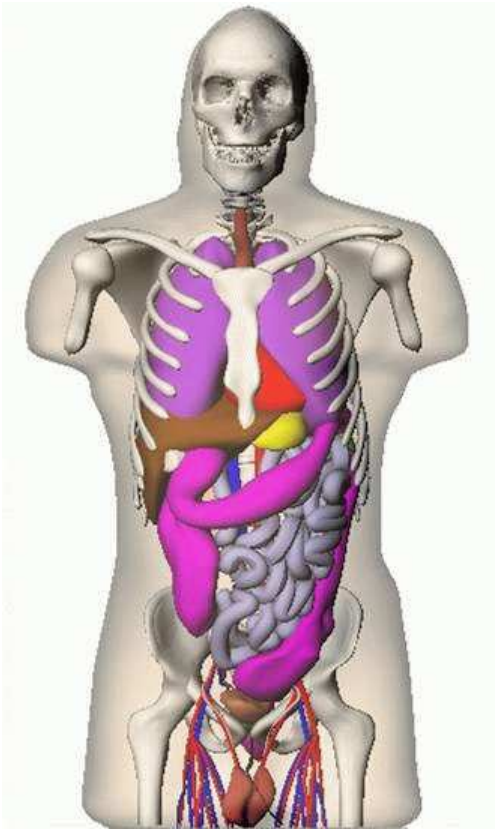

Figure 3.3: A 3-D rendering of the 4-D NCAT Phantom developed by Paul Segars[44]

A NURBS model, such as the NURBS-based CArdiac-Torso (NCAT), is constructed in stages. First the body and organ surfaces are extracted from a pre-existing model or medical data and converted into polygonal meshes. This may involve manual segmentation of medical images as in tomographic phantoms. The meshes are then converted into NURBS-based surfaces and combined into a single body framework. The NURBS system is inefficient at handling regions of high geometric complexity, so some regions may be left in their originally defined state. Once the NURBS surfaces are integrated, the result can be voxelised to produce a model compatible with most simulation software[38].

The strength of NURBS models comes in the middle phase of construction. At this point all of the organ shapes and alignments are comparable to their topographic counterparts, but described by a series of points and weightings allowing for the easy manipulation of structures. This makes repositioning and resizing

simple compared to tomographic models. while retaining the physiological accuracy. Once any desired alterations are carried out, the mathematical nature of the structures allows the voxelisation to be carried out at whatever resolution is desired without interpolation.

At the cost of some physical accuracy and fine detail, hybrid models can combine some of the best features of mathematical and topographic models. Adaptation at the NURBS stage can allow for the transformation of one model into a series containing a range of body shapes, or the modification of specific structures to facilitate the creation of 4-D models[45]. The computational and time costs associated with construction are not inconsiderable, and specialist software is required, but hybrid models provide a potentially powerful tool for the future.

3.3 Selecting a Phantom Type

Considering the requirements, each phantom variety has potential benefits. A mathematical model would be relatively simple to construct and work with, and the externally developed heart could be implanted without significant issue. The size of organs and their positioning is easily altered, and the mathematical way they are defined allows for the resolution of a voxel model to be whatever is desired. However, the physiological accuracy would be poor.

A tomographic model offers the best quality anatomical detail, at the cost of being the most difficult to alter. Modelling of fine structures is significantly more lifelike than in other model types. The complexity of the system makes altering organ sizes or other physical properties potentially prohibitively time consuming, and the insertion of an external model into a tomographic phantom is unlikely to be flawless in its result. The matching of size, shape and vascular structures will require significant alteration to the heart, body or both.

Hybrid models offer the potential for inserting the external heart in the NURBS stage, removing the existing heart structures, and replacing them with the external model, linking the vascular system and reshaping the other NURBS surfaces around the alterations. The model can then be sampled at whatever resolution is desired. However, this process would be damaging to the fine detail and complex structures that are explicitly requested. Attempts to retain such detail could result in the models construction being prohibitively time consuming.

Considering the options available, and aware of the time constraints, it was

decided that the final model would best be constructed as a tomographic phantom. Anatomical accuracy was the primary concern, and tomographic models are superior in this regard. Also, data sources for constructing such phantoms, and whole body phantoms previously constructed, were already accessible, reducing construction time.

Chapter 4

Available Data Sources and Phantoms

Three primary sources were available to aid in the construction of the Tomographic phantom. The first of these is data from the Visible human project, an information source that has been used in the construction of multiple previous phantoms. The second and third sources are phantoms that have been previously constructed by other research groups. The first of these is NORMAN, the NORmalised MAN, a phantom developed by Peter Dimbylow of the UK Health Protection Agency. The second is the phantom TARO, developed by Nagaoka et al.[41] for the National Institute of Information and Communications Technology (NIICT) in Japan.

4.1 The Visible Human Project

The Visual Human Project (VHP) is a creation of the US National Institutes of Health's National Library of Medicine (NLM). The goal of the NLM in the project is to create a dataset of images produced through medical scanning technologies and direct photography that allow for complete three dimensional modelling of standard male and female human bodies, both externally and internally. The NLM intends that these images and models can then be used for research in a variety of fields, including medical scanning, anatomical study and access of complex data sets through computer networking.

The Visual Human Project data was taken from cadavers of a man and woman who had chosen to donate their bodies to medical science after death. The Male

body is that of a 39-year old convicted murderer who had received the death penalty and been executed by lethal injection, while the female is that of a 59 year old woman believed to have died from a heart attack. Both bodies were classified as "normal", being under 60 years of age, under 6 feet tall, neither obese nor emaciated, free of infection and disease and having experienced no major traumas or surgeries[46].

The VHP Male data was released in November 1994, and the Female data in November 1995. Because of the time gap, there are some differences in the data provided and the specifics of the images. Both contain Magnetic Resonance Imaging (MRI) data collected by a General Electric Signa imager, stored in the Genesis format as $256 \times 256\times$ 16-bit grey-scale matrices. Also, both sets contain Computed Tomography (CT) scans of the fresh cadaver taken with a General Electric High Speed Advantage Scanner, stored as $512 \times 512\times$ 16-bit grey-scale matrices. The Male set also contains CT scans of the Frozen cadaver, stored in the same format as the unfrozen images. Both Male and Female data sets also contain photographic images taken of planes through the vertical axis of the cadavers.

Scripts for the extraction of all file types into basic image formats are provided in appendix A

4.1.1 Photographic Data

Male The photographic data for the male subject is included in three formats. The first is as .raw files containing non-interleaved 24-bit colour data. In this file format, each image is stored as three sequential arrays, the first containing the red intensity at each point, the second the green and the third the blue. Combining the three arrays provides trichromatic data for every pixel. Each of these files is 2048×1216 pixels, but contain a large amount of data surrounding the body section that serves to identify and characterise the section being imaged and has little value in modelling. These photographs are also included as preprocessed Portable Network Graphic (.png) files. As a lossless format, these should contain all the information that is present in the original .raw files.

The example image in figure 4.1 is a half-size example that displays the quality of the images and some features that explain how they were captured. The blue material that surrounds the cadaver is a frozen 3% gelatin solution that acted as a support for the body to ensure it did not move during the process[46]. The

cadaver was not cut into slices, but instead kept frozen at very low temperatures and milled away. This was a delicate process and completing work on the whole body took nearly 3 months. The black edges are a wooden structure designed to frame the image and remove the possibility of glare in the images from the dry ice used to keep the cadaver frozen. The blue areas in the centre of the image are latex that was injected into any exposed cavities as they were encountered to help maintain the body shape.

Along with these, there are included the original captured images taken on 70mm film, which are stored as 4096×2700 pixel images .rgb files, with 24-bit interleaved colour. This format stores the image as a single array with each point having the red, green and blue intensities in a single block. Each format has its own benefits and disadvantages depending on how it is to be used and the type of information that is being extracted.

Both photograph groups contain 1878 files, taken at 1mm separation through the cadaver. For the .raw files with 2048×1216 pixels, the pixel dimensions in the plane of the image are stated in the README file provided with the data as being 0.33×0.33 mm. Comparatively, the pixels in the plane of the .rgb images are stated as being 0.144×0.144 mm, with the scaling discrepancies caused by the removal of unnecessary data on the left and right hand side of each image.

The images contain a vast amount of information. Anatomists have detailed over 1400 separate structures that can be discerned within the VHM photography[47]. Figure 4.1 displays the heart and lungs, with the surrounding skeleton and elements of the vascular system clearly visible.

Female The female photographic data is only provided at one resolution, that of the smaller male set at 2048×1216 pixels, with each pixel having dimensions of 0.33×0.33 mm. Also the same is the images being packed as 24 bit colour, non-interleaved files with .png equivalents provided. However, unlike the male images, the separation between each image is only 0.33 mm rather than 1 mm. This higher vertical resolution allows for very fine details to be resolved that may be missed at 1mm separation. The images are denominated by their vertical position in mm, with a, b and c suffixes to provide the three images contained within each mm interval.

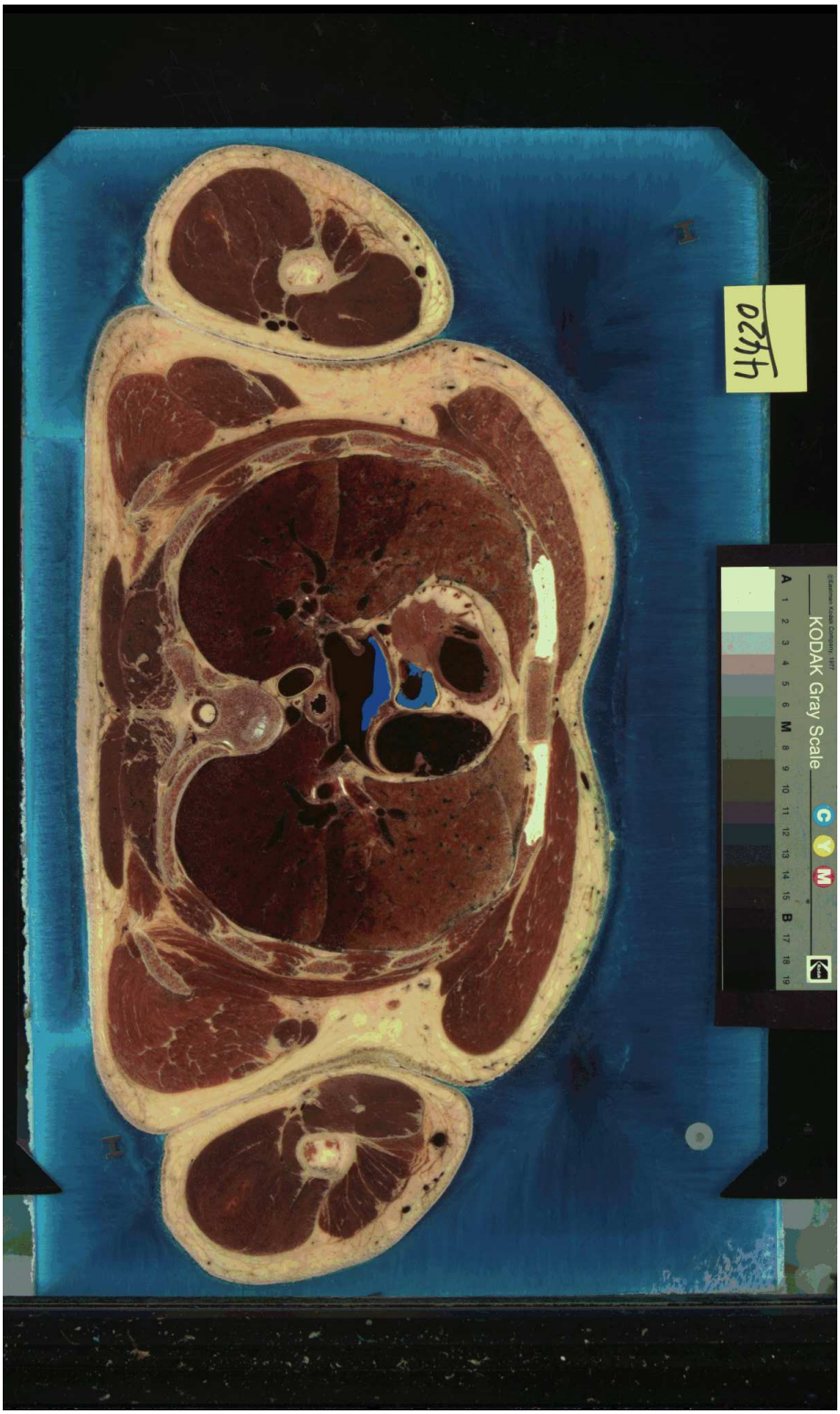

Figure 4.1: Image produced from a_vm1420.raw of the Visible Human Male, the image has been rotated 90° anti-clockwise. The body segment visible is arranged such that the rear of the torso is at the top and being viewed from the bottom, with the right arm on the right hand side of the image.

a) 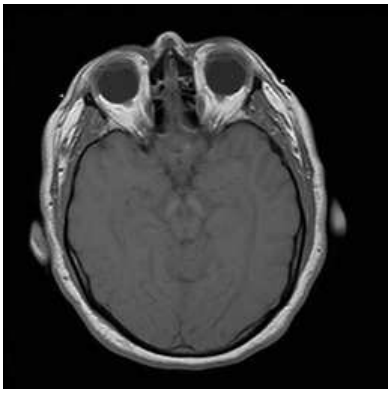 b) 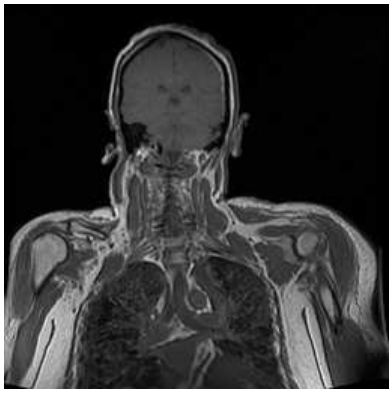

Figure 4.2: Axial and Coronal MRI scans from the VHP Female data set

4.1.2 Radiological Data

Magnetic Resonance Imaging

The male and female MRI datasets contain similar sets of MRI scans of the whole body, split into two parts. The first includes axial sections of the head, taking horizontal slices through the skull as in figure 4.2a, extending down to the bottom edge of the brain. The second part makes up the vast majority of the data and includes coronal images of the whole body. Coronal images are those taken with the image taken in a "human" orientation. The vertical axis of the image is the vertical axis of the body and the left side of the image is the left side of the body as in figure 4.2b. The body is not imaged as a whole piece, but is instead in five sections. The first is of the head and shoulders, the second of the torso, the third of the pelvis, the fourth of the thighs and knees, and the fifth of the lower extremities. There is significant overlap between the sections allowing for easier construction into a single image.

The MRI data is considerably more complicated to use than the photographic because of the manner in which it was collected. Rather than there being one MRI image of each section, there are three, with each displaying a specific type of measurement that the MRI machine is capable of collecting. MRI images are collected by measuring the response of protons (primarily those in hydrogen nuclei in water) in the body to various strong magnetic fields. The protons are first aligned with a powerful static field, and then an oscillating magnetic field pushes them out of alignment. As the protons return to alignment, they release a measurable radio-frequency signal. The protons return to their prior state through Longitudinal recovery and Transverse decay, responses that can be

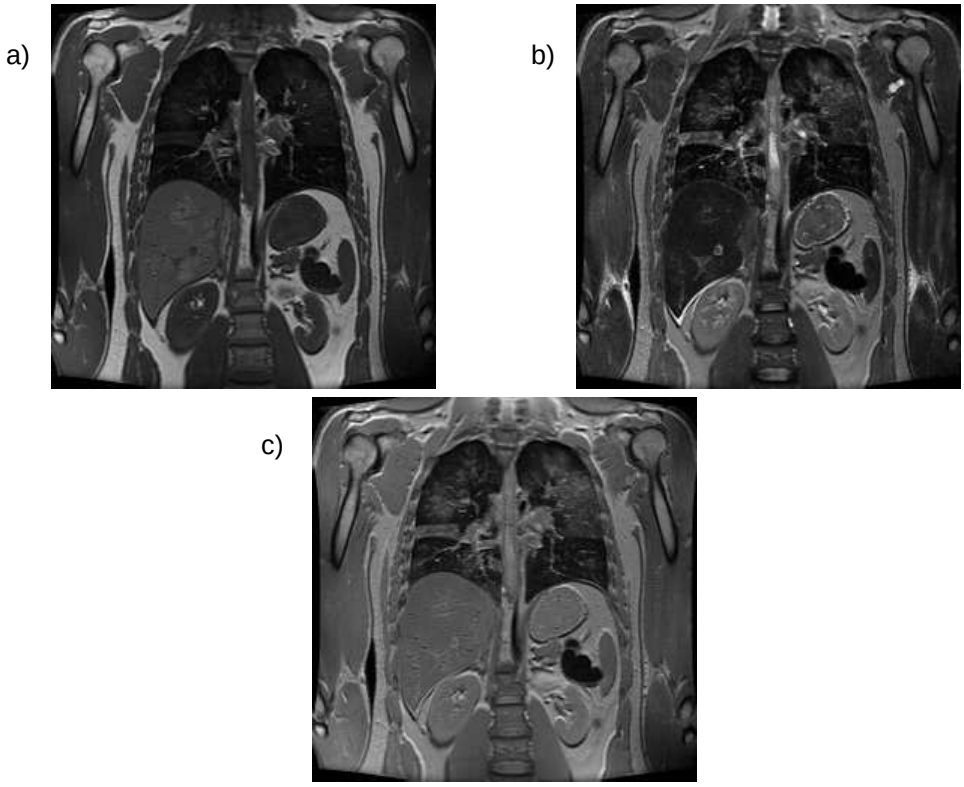

Figure 4.3: MRI scans of the same section of the VHM using a) T1, b) T2 and c) proton density imaging.

individually measured and recorded as T1 and T2 respectively. The third type of image, PD, is generated by adjusting the fields to produce minimal input from the T1 and T2 effects, providing an image that is dependant almost exclusively on the proton density. The same region scanned using all three methods is shown in figure 4.3.

The human body contains a large amount of water, with overall variation dependant on age, sex and levels of body fat. The variation between individual tissues in considerable, with the lungs being almost 90% water while dense bone may contain under 25%. This allows the MRI scan to take accurate images of soft, wet tissues that may be missed by other scans, with the three different imaging methods allowing differentiation of tissues that may appear identical in any one of them.

This range of data is the great strength of MRI, however, it is also the primary barrier to use by non-specialists. Understanding and interpretation of the specifics

of MRI output requires a not insignificant understanding of human anatomy, organ composition and their specific responses to MRI instrumentation. Identification of a specific tissue or assembly of a multiple tissue model from MRI data is not attainable without training.

The MRI data included with the VHM is made up of images 256×256 pixels in size. The axial brain images are at a resolution of 1.01562 mm^2 according to their accompanying header files, while the coronal images are at a resolution of 1.875 mm^2. The in-body separation between each image is 4mm in both sets.

Computed Tomography

CT images are created by a series of X-ray emitters and receivers that rotate around the body, measuring the absorption at each angle and then use this data to construct a two dimensional representation of the tissues in the plane. Modern scanners will commonly also move perpendicularly to the plane being scanned, tracing a helical path to obtain three dimensional information. CT scanning is much cheaper than MRI, and generally faster, also it does not require the removal of metallic implants and can easily provide images with sub-millimetre resolution. The use of ionising radiation for extended periods reduces the frequency at which CT scans can be used diagnostically, but the use of various contrast agents can provide a wealth of information about a variety of tissues that would otherwise be difficult to determine from density alone.

The CT data in the VHP is in sections taken axially through the cadaver, with the left hand side of the body on the left side of the image. Figure 4.4 is an example male image, the circularity is due to the rotating scanner and the surface on which the cadaver is resting is clearly visible. The male and female datasets are quite different in the case of CT images as the male cadaver began to decay rapidly during the imaging process, possibly due to the detrimental effects of the chemicals used in the lethal injection that caused his death[46]. The result of this is a section in the male set from just above the knees to above the ankles that is absent due to the increasing decay. It was decided that in order to minimise the effects of natural cell degradation, this area would be excluded to reduce the amount of time until the body could be frozen and preserved[46].

The decay of the cadaver also lead to the separation of the axial sections being altered as the work on the male cadaver continued. The separation begins at 1 mm in the head, increases to 3 mm in the torso and then to 5 mm in the legs.

Figure 4.4: A CT scan from the VHM.

In comparison, the female cadaver decayed much more slowly, and was imaged over the whole body at 1 mm intervals. This makes the male CT images slightly more difficult to work with than the photographical and MRI sets, as the vertical resolution changes have to be accounted for.

There is also added complexity due to a characteristic that is present in both the male and female set. Rather than a helical scan, the cadavers were scanned in independent planes for maximum accuracy, the need to minimise effects of patient movement and radiation exposure removed. During the CT scanning process, the Field of View (FOV) of the CT scanner was changed as the scanner was moved over the cadaver, while the dimension in pixels remained a constant 512×512. This resulted in the physical dimensions represented by each pixel changing between imaging groups. The specifics of the FOV and pixel sizes are given in the Header files provided for each image, and the variation is quite large. The range of FOV is between 250 and 480 mm, leading to pixel sizes ranging between 0.488281 and 0.9375 mm square. The variations and the points of change for the male data are detailed in table 4.1, and for the female data in

Image range	Slice thickness (mm)	FOV (mm)	Pixel size (mm)
1012-1019	1	250	0.488281
1020-1078	1	460	0.898438
1079-1161	1	345	0.673828
1162-1288	3	450	0.878906
1291-1957	3	460	0.898438
1958-2263	5	480	0.9375
2688-2893	5	480	0.9375

Table 4.1: Imaging specifications for the Male normalCT data

Image range	FOV (mm)	Pixel size (mm)
1001-1209	250	0.488281
1210-1227	370	0.722656
1228-1249	440	0.859375
1250-2106	480	0.9375
2107-2734	370	0.722656

Table 4.2: Imaging specifications for the Female CT data

table 4.2.

Computed Tomography - Frozen Male Cadaver

Because of the problems encountered while taking CT scans of the male cadaver, once the body had been cryogenically preserved a new series of scans were taken. As in the "fresh" CT images, the data is made up of axial slices through the body working from the head down, with the left side of the body on the left of the image. However, unlike the "fresh" images, the body was in a completely stable condition and could be worked upon without danger of degradation while the cryogenic preservation was maintained.

The lack of time limitations allowed the slice thickness to be kept at a constant 1mm. However, in a similar fashion to the unfrozen sets, the frozen CT images were recorded with a varying FOV, producing variable pixel sizes in the finished images, described in table 4.3. As the female cadaver had been fully imaged while unfrozen, this process was unnecessary in that case.

4.1.3 Applications of the VHP

Since its release, the VHP has been used in a variety of models and resources. The level of detail in the photographic data has led to the publication of the

Image range	FOV (mm)	Pixel size (mm)
1006-1236	270	0.527344
1237-1260	400	0.78125
1261-2882	480	0.9375

Table 4.3: Imaging specifications for the Male frozenCT data

Atlas of the Visible Human Male[47], a guide which labels some 1400 different structures within the human body. There has also been production of various models based on the information, though none which include all the structures previously mentioned.

The models produced range from the VHP range from small body sections[48] to including the whole body [49], with resolutions ranging from $5 \times 5 \times 5$ mm [50] to $0.33 \times 0.33 \times 1$ mm [49]. The specific tissues and organs delineated in the models are generally limited to some 20-40 types depending on the requirements in the model's construction.

4.1.4 Problems with the VHP

The VHP has not been an unblemished success. The use of an executed prisoner as the source for the male data produced a backlash from some groups who felt that the medical profession could not ethically use a cadaver obtained in such circumstances [51]. A common response to this is that the subject had declared his desire to donate his body to medical science, and that to refuse such a gesture would be unjustifiable[52].

The VHP photographs are not perfectly aligned, and so their use requires first identifying physical structures that can be used as markers to better fit the individual images together. Some sections of the body are also missing. Where the body was divided for the milling process, 1-2mm sections were lost in the cutting. Also, in some regions there are missing sections where milling has been disrupted or the surface has cut badly[46]. In the Male this may remove only a single image, but in the Female data with the considerable higher vertical resolution in can result in multiple losses that require more significant extrapolation to replace.

Further problems come from the characteristics of the two cadavers. Some critics argue that previous minor surgeries, including the previous surgical removal of the appendix and one testicle from the male cadaver render it inappropriate.

Along with this, there are areas of tissue damage around the point at which the lethal injection chemicals were inserted. Criticisms are also made concerning the the fact that though the male was not obese, he was overweight and had a higher than normal proportion of body fat[49].

The primary complaint about the female cadaver is that at age 59 the subject was too old to provide a valid representation of a 20-30 year old reference female. Anatomical study of the images has also shown that the subject displays several unusual characteristics, including an enlarged liver, kidney cysts and the absence of certain muscles[48]. As well as these, the photographs contain signs of cardiovascular and gastric disease.

4.1.5 Using the VHP

The Visible Human project is a huge resource full of valuable information that can be used in the production of high resolution, highly heterogeneous and accurate human models. However, the process of taking this data and translating it into such a model is neither simple nor expeditious. Production of a head model using only 120 images from the VHM required specialists with extensive reference to anatomic texts and the assistance of two practicing radiologists, for a final model containing 20 materials[53]. The pelvic region of the VHF was modelled at reduced resolution, producing an output model with 302 items identified as part of 220 structures, a task that was carried out by 11 supervised medical students who had completed anatomical training[48].

4.2 The Tomographic Models

The majority of digital human phantoms currently available can be utilised in a wide variety of research, but are designed for the numerical calculation of radiation dosimetry. Accurately calculating the absorbed dose from active sources, be they nuclear reactors or mobile phones, in a variety of tissues allows for the development of effective safety standards and have led to some models becoming a useful tool in commerce and industry.

NORMAN and TARO are both models of this type. Primarily designed for simulations of radiation interaction with the human body[41], the phantoms are designed to include a significant quantity of tissues but with specific care to include those that are particularly susceptible to radiation damage. This results

in phantoms that are not optimal for use in biological system modelling, but still offer a lot in terms of structure and come in scientifically recognised forms.

The two models are characteristically similar, both having been constructed from MRI scans taken of live volunteers, with voxel sizes of $2 \times 2 \times 2$ mm. NORMAN is some 5 voxels taller and would be slightly heavier[41], and there are differences between organ sizes, orientation and weight, but this is to be expected due to racial differences between the subjects the models were based on and the normal variation between healthy adults. This voxel size is not uncommon in tomographic phantoms. It represents a balance between the desire to obtain as high a resolution as possible when constructing a phantom, and the practical limitations of scanning a live volunteer. Higher resolution scans take significantly more time, but movement of the subject can create discontinuities and errors that must be avoided.

NORMAN is provided as a series of 871 text files. Each text file contains the information for a single z-normal plane of the phantom starting from the feet and travelling up to the head, stored as ASCII data with each line of the file containing a numerical value between 0 and 250 corresponding to the tissue type contained within a single voxel. An accompanying file contains a key that states the corresponding material for each value. The data is stored by rows, with 148 rows of 277 voxels, and can be converted to a .pgm image file such as that in figure 4.2 by adding the three line header:

```
P2
277 148
255
```

TARO is provided in a single file containing binary data. Rather than every line representing the contents of one voxel as with the NORMAN data, individual bytes are used, with each byte converting to an integer between 0 and 57. Again, an accompanying file provides the corresponding tissue or material for each number. The data is again stored by z-normal planes, starting from the top of the head and travelling down to the feet, working across each plane in rows. In TARO there are 866 z-normal planes, each of dimension 320×160. With the binary storage system, every plane requires the same storage in bytes, and so the individual z-normal planes can be extracted from the command line using the Unix *split* function:

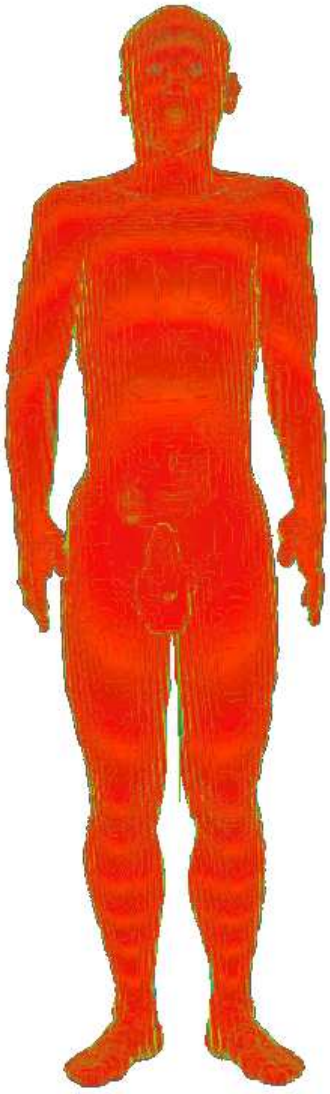

Figure 4.5: A Rendering of the TARO voxel phantom produced with the ParaView visualisation software

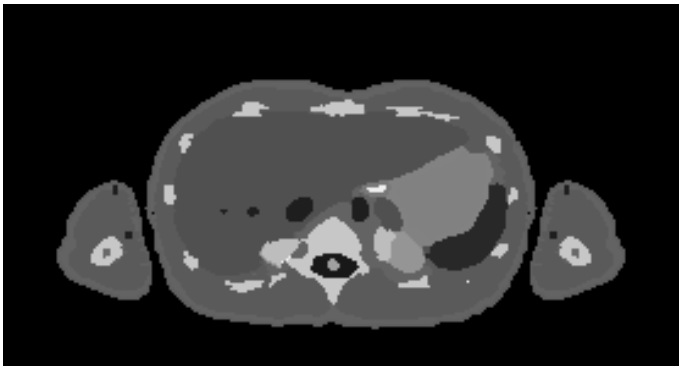

Figure 4.6: File 611.txt from the voxel phantom NORMAN converted to a .pgm image

Figure 4.7: Z-normal plane 220 from the voxel phantom TARO converted to a .pgm image

```
split -b 51200 -a 3 -d MALE-V1.RAW zplane
```

This will produce a series of 866 files titled zplane###, where ### is a number between 000 and 865. These can be converted into .pgm images by addition of the three line header:

```
P5
320 160
57
```

The defining difference between the two phantoms comes in the number of tissues and structures defined in each. Though the data values in NORMAN range from 0 to 250, there are only 38 distinct data types representing different tissues and materials. In contrast, the values in TARO range from 0 to 57 and contain 51. Our requirement of anatomical realism results in TARO being the more viable of the pair, though at 2 mm in all directions, the phantom resolution is significantly lower than desired.

4.3 The Basis for the Phantom

The VHM data is a strong candidate for providing the basis for a digital human phantom. The high resolution in the photographic imagery and the amount of available information concerning the structures that can be extracted from it[47] make it a very appealing option. However, after converting sections into easily manipulated formats and attempting to understand the information present in the various radiological file types, it was concluded that the amount of work required was simply too extensive, even when working with the various guides that have been produced. Previous phantoms based on the VHP have been very successful, but the time and expertise required to create such a model are simply not available.

Of the two pre-built phantoms, TARO was selected due to superior segmentation and inhomogeneity. As a 2 mm resolution model, fine detail has been lost and so the implanting of the external heart is a requirement to obtain the best possible results. Implementing this requires equal resolution between the two models, and so the TARO phantom must be adjusted to achieve a resolution of 0.33 mm, replacing every original voxel with 216 new ones.

Chapter 5

Increasing Resolution

To integrate the isolated heart into a tomographic phantom requires matching of the resolutions. Modern investment in digital image manipulation and enhancement has led to extensive development in fast, powerful and visually appealing algorithms that operate on two dimensional discrete data. A lot of scaling techniques are primarily targeted at decreasing image sizes while retaining as much information as possible in the reduced space. In contrast, increasing the size of an image provides no new information in the increased space and can reduce the aesthetic quality of the image. This is not to say that increasing the size of an image is necessarily destructive, but it is always preferable to obtain the desired size in the original capture. Image processing software will commonly provide a range of options when resizing an image as to how the scaling will be performed, with each offering a different balance of computational cost against visual appeal.

The simplest scaling is nearest neighbour interpolation. Each point in the new image is given a value according to the nearest defined point in the original. If, as in this case, the image is being scaled up by a whole number it is necessary only to replace each original element with the required number of new elements, the image will appear the same even though the resolution has improved. When the scaling is not by integer values the result may appear deformed when compared to the original, as shown in figure 5.1.

Up-scaling by a large amount produces a very jagged image such as that in figure 5.2. This is a small section extracted from a single z-plane of the TARO model scaled via nearest neighbour methods to increase the resolution 6 times. The region consists of a section of external air in the top left, extending down though the skin, fat, muscle and rib bone to lung in the lower right. What should

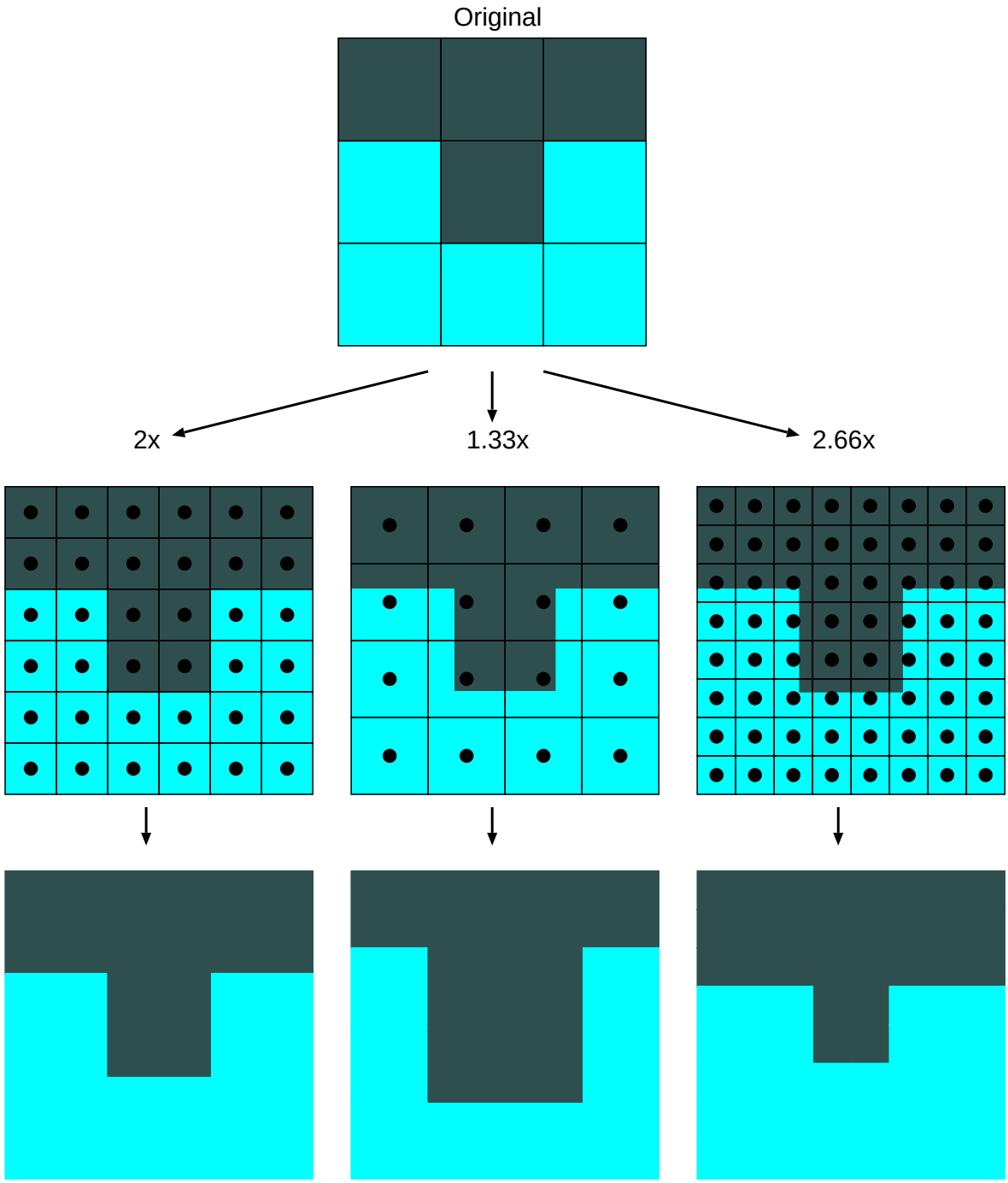

Figure 5.1: The results of increasing the resolution of a 3 pixel wide square image by 2×, 1.66× and 2.66× using a nearest neighbour algorithm

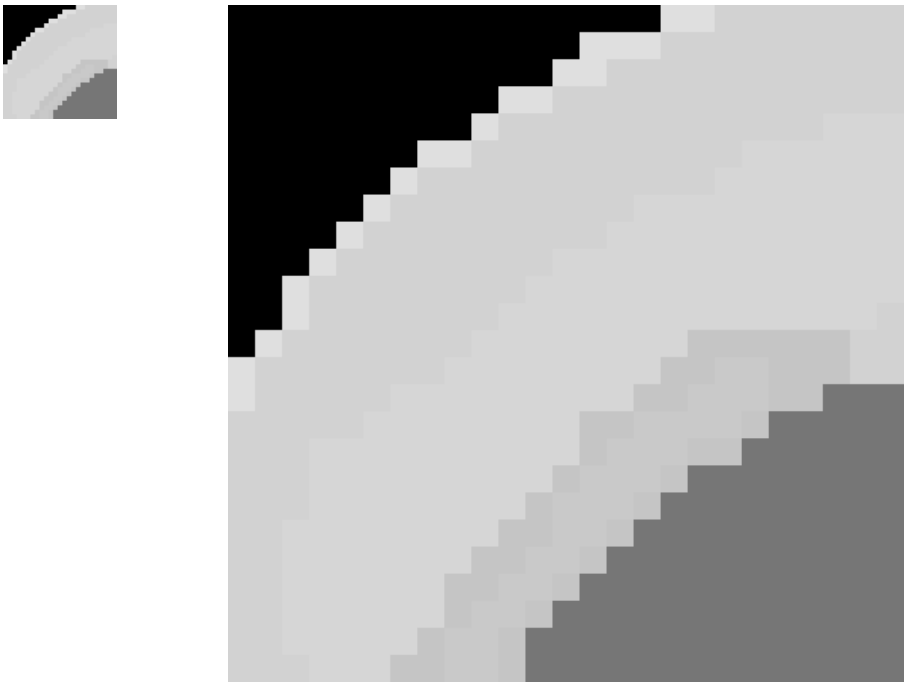

Figure 5.2: Nearest neighbour scaling to increase the resolution of a small section of a TARO z-plane from 2 mm to 0.33 mm. Pixel size has been kept constant.

be a series of smooth curves instead appears as a series of individual pixels in sharp steps.

With the intention of anatomical realism, the sharp corners and square elements detract heavily from the optimal scenario. More advanced scaling techniques reduce the blocky effects of the scaling through interpolation while scaling or applying anti-aliasing techniques on the scaled image. Two common interpolating methods used to smooth enlarged images are bilinear and bicubic interpolation. Figure 5 shows the effects of using these two methods on the same small section of a z-plane. The edges and corners are not as sharp as with the nearest neighbour scaling, but equally, the problem with using any method of this type becomes apparent. The original image contained seven different grey values, each of which directly correlates with a tissue type. The bilinearly and bicubically smoothed images contain 209 and 206 colours respectively. Most of the values in these images will be meaningless in the context of the known data, and some will almost certainly provide values for tissues that should not appear in that section of the body. Anti-aliasing works in a similar manner, blurring sharp edges to improve the visual appeal, and so is equally inappropriate.

It is important to remember that the information being dealt with is not

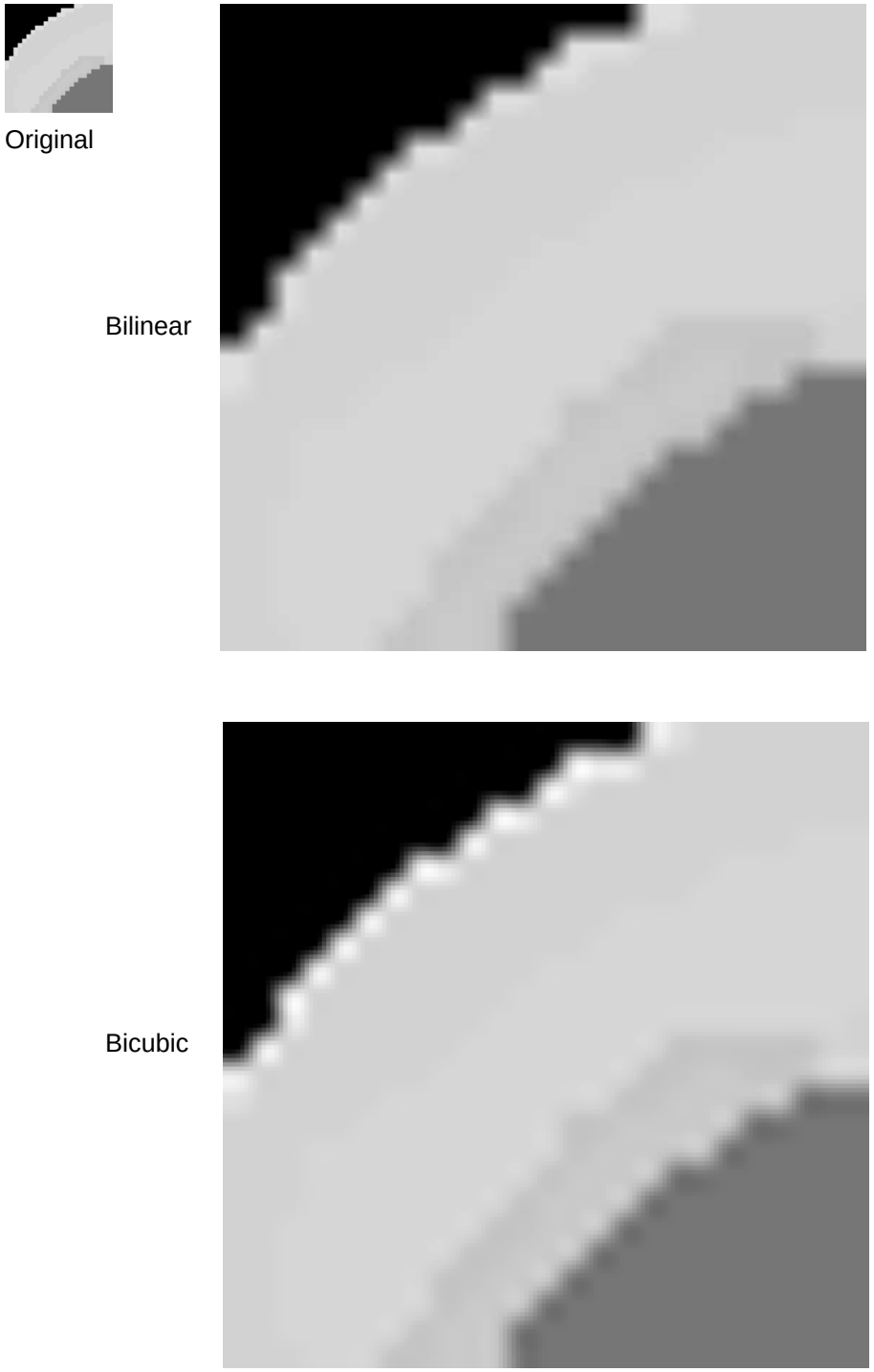

Figure 5.3: The same section of a TARO z-plane enlarged from 2 mm to 0.33 mm resolution using the standard bilinear and bicubic smoothing filters included in the GNU Image Manipulation Program version 2.2.13[54]

visual, but representative of the type of material present. While such jagged edges are inappropriate for the representation of surfaces that are known to be smooth, treating them as though they are visual images risks the introduction of information that is not present or the removal of information that is. Generalised smoothing may improve the state of sharp corners that should not be present, but also risks the possibility of removing sharp edges that should be.

As well as this, treating the data as two dimensional images makes interpretation and alteration relatively simple, but each pixel in the image is actually a three dimensional voxel. Altering a pixel in a single plane may improve the appearance of a curve or diagonal line, but in an orthogonal plane, the changed pixel may introduce irregularities that make structures disjointed or separate structures that should be connected.

Though awareness of the three dimensional requirements is important, the relative ease of working in two dimensions provides a practical base for the development of a method which provides acceptable three dimensional results.

5.1 Smoothing in Two Dimensions

As previously discussed, normal smoothing methods are inappropriate in this case. The use of interpolated values and averaging are liable to provide irrational results. There are, however, common method that can be adapted to provide more satisfactory results.

5.1.1 Convolution Filter Based

Convolution filter, or neighbourhood, operations determine an element's new value by operating on it and the surrounding elements. Neighbourhood based methods can be used to smooth, sharpen, detect edges, remove noise and perform a variety of other processes. In this scenario, we are interested in smoothing to remove the sharp corners present in the newly scaled data. In ordinary image manipulation, the simplest method to perform such an operation would be with a mean filter. The mean filter takes the mean average of the pixels in a certain region, and assigns this value to the position of the centre pixel in a new image. The new image is necessary as all the means must be taken from the original values.

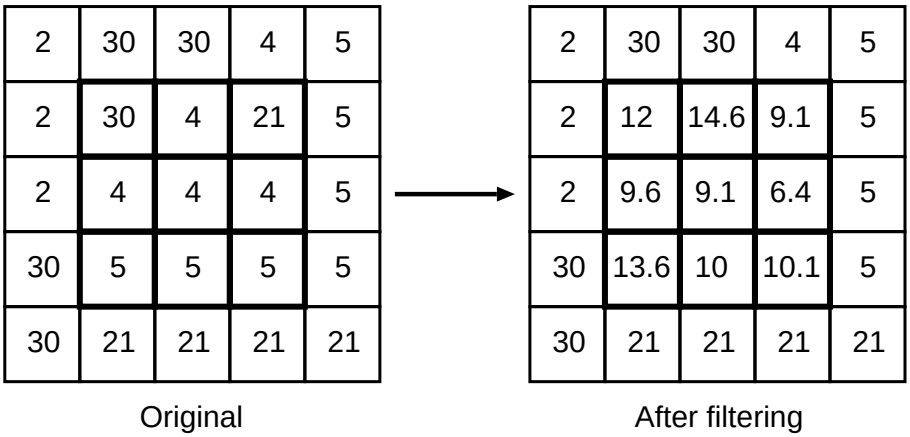

Figure 5.4: The result of applying a 3×3 mean filter to the central portion of a 5×5 grid of values

Figure 5.4 shows the result of applying a 3×3 mean filter to a 5×5 grid of values. Only the darker bordered region in the centre of the image has been operated on, with the edges simply copied over. As the edges possess a limited neighbourhood, their inclusion in the operation requires a slightly more complex algorithm, however the extensive amounts of empty space surrounding the TARO model renders this unnecessary.

Use of the mean filter brings the same problems as interpolation, the values created may represent nothing or a tissue that is inappropriate for the situation. However, while we cannot use the mean nor any other weighted averaging scheme, and the median average is likely to produce nonsensical output, the modal average provides a viable option. Use of the neighbourhood mode restricts the output to a value that is known to exist in the model and is appropriate for the region in question.

Defining pixels in the new image is a matter of extrapolating what is expected to be present from what is. If a pixel is isolated, it presents as a simple square. It is unlikely that anything within the human body can exactly represented by a square, so we instead assume that the structure is circular. While the chance of finding a perfectly circular internal structure is also minimal, the body contains many structures such as veins, arteries and ducts that do follow broadly cylindrical shapes.

The problem thus becomes one of attempting to create circles upon a grid of squares. While this in itself is not possible, attempts at circularisation can be made. The assumption is made that for a pixel to be assigned a certain value,

the tissue represented by said value comprised the majority of the region covered by said pixel. This region has now been expanded from being represented by one pixel to being represented by 36. As the intention is to remove sharp corners, the final outcome must remove these without altering any other regions. A lone pixel in the original should therefore both survive as an information point and retain more than 50% of its original area in the new image.

Considering the lone pixel, we know it converts into a square of 36 pixels in the scaled plane. The largest circle that would fit within this square would have an area of $\pi \cdot 3^2 = 28.27\ldots$ pixels. The result of the smoothing in this case is intended to be symmetrical, and so an equal amount of material must be removed from each corner. Removal of 1 pixel at each results in an area of 32, while removing three from each results in an area of 24. The next step would be the removal of 5 pixels from each corner, resulting in an area of only 16, below the self-imposed minimum.

In the case of a corner surrounded by a single media, single pixel reduction at each corner can be provided by a 3×3 modal filter, while 3 pixel reduction requires a 5×5 filter. Single pixel reduction results in an area closer to that of the ideal circle, but the overall smoothing effect is minimal, and so after considering various example situations, such as that in figure 5.5, originally the 5×5 filter was chosen for use.

However, while this appears a viable smoothing method when applied to examples, when applied to a whole image, the technique is not wholly successful. A code for applying the 5×5 filter to a TARO plane is provided in Appendix B. The outcome of this filter is shown in figure 5.6 where it is compared with the original plane scaled by 6 times without any smoothing. While there does appear to be some improvement, the effect is not large. What appears to work on a small scale does not produce high quality results on a global level. If we discard our lower limit on area retention and enlarge the filter to 9×9, which results in the reduction of an isolated point from 36 pixels down to 12, the smoothing appears better on a global scale as shown in figure 5.7

The filter based method produces reasonable results, but with drawbacks. Preservation of small structure size results in lesser reduction of sharp corners, while more effective smoothing results in the erosion of isolated features. While the concept of the filter is simple, computing the modal average requires counts of the materials present and the sorting of a list of values for each pixel being

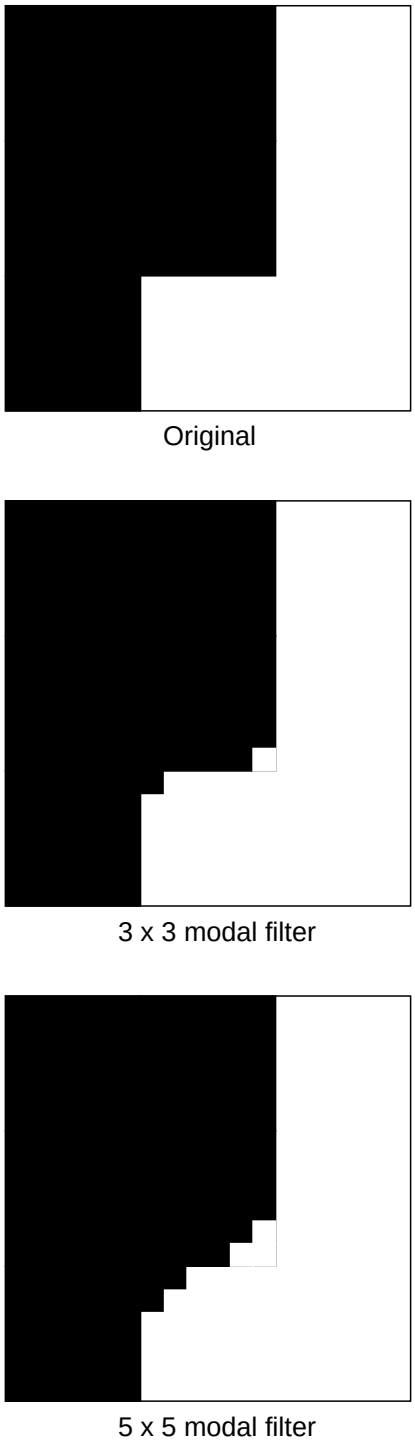

Figure 5.5: The result of applying a 3×3 and 5×5 modal filters in an example situation

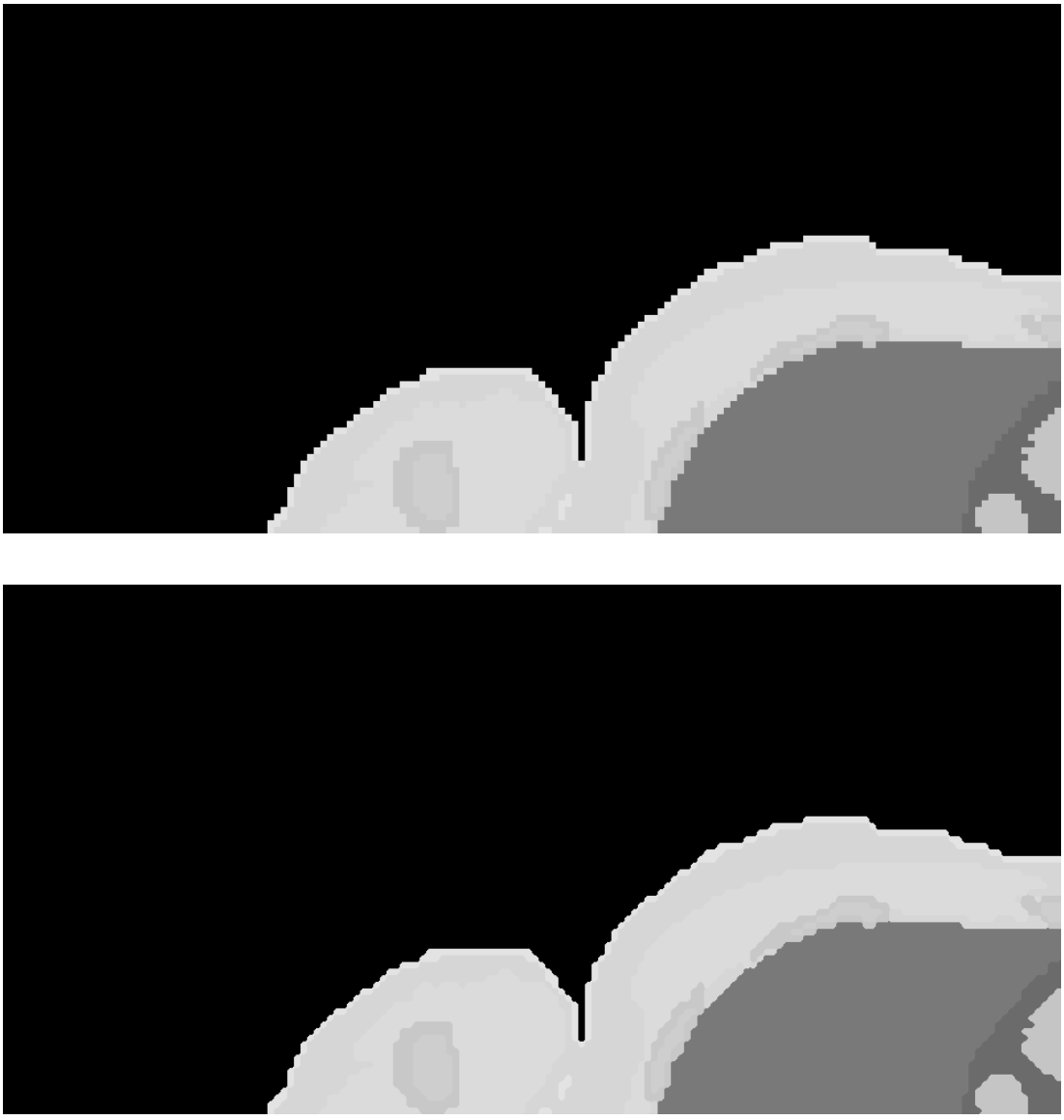

Figure 5.6: One quarter of TARO z-normal plane number 220, scaled by 6 times without smoothing (top) and with smoothing from a 5×5 modal filter(bottom)

Figure 5.7: One quarter of TARO z-normal plane number 220, scaled by 6 times and smoothed with a 9×9 modal filter

operated on in the final image.

5.1.2 Look-Up Table Based

Look-Up tables (LUTs) provide a method of overcoming the limitations of the neighbourhood based method. Rather than scaling the image and then considering the contents of the local region for a large amount of new pixels, the look-up table method uses the arrangement of similar pixels around an element in the original to determine the layout of the 36 pixels that will represent it in the new image. The layout of the final pixels is thus dependent not only on the original image, but the scheme chosen for the look up table to use.

Look-up table methods have previously been employed successfully in the field of computer gaming. Many old games run at resolutions much lower than modern hardware and require scaling and smoothing to be easily viewed. Common methods such as bilinear and bicubic scaling are seen as detrimental to the strong lines found in many computer games, and so a method was sought that would preserve the sharp edges of orthogonal lines while smoothing diagonals and curves to reduce the blocky effects.

An example of LUT based smoothing can be found in the hq$n$x family of scalers created by Maxim Stepin[55]. These filters compare a central pixel with the eight surrounding it, defining each as being either near or distant based on

how similar the colours are. Depending on the quantity and arrangement of the near pixels, an entry is chosen that describes how the colours of the new pixels should be chosen. The hq$n$x family includes hq2x, hq3x and hq4x, which scale by two, three and four times respectively.

The nearness of surrounding pixel values to that of the centre pixel is irrelevant in building the phantom. A value that is one away is as different as a value 20 away and so the only pixels that qualify as similar are those with exactly the same value. As there are 8 pixels surrounding the centre, there are 256 potential combinations of similar pixel arrangement. As the concern is with the removal of corners rather than the smoothing of edges, a not inconsiderable amount of these can be ignored, specifically those in which the two pixels either side of the centre in the x or y plane have values the same as it.

In this case, we do not require interpolation of colours, but the colours of the pixels have to be defined. As there is a limited colour set available, pixels that are not assigned to the original value can be instead assigned the value of the more common pixel value in the region. Hence a new pixel representing a corner of the original that is being assigned a new value will take it from the most common value in the three original pixel that intersect there. Should these three pixels be of different values, the layout of that region is uninterpretable and so it will remain as the original.

Figure 5.8 provides an example of the process. A full list of pixel combinations and the code that defines them is given in Appendix B. The pixel layout from the original is used to define the shape in the 36 pixel region. This shape is then combined with the value data from the original to produce the output region. In this case, it is assumed that two materials meeting along side a solid region will be infringed upon by that region.

Some combinations are more difficult to operate on than others. Figure 5.9 provides an example of two materials in a chess board pattern. The materials could be interpreted as being part of a diagonal line in either direction and produce appropriate output, but there is no reason to pick one material over the other. Any decision would be arbitrary due to the lack of information, and so the region is scaled without smoothing.

Output of the LUT method visually appears superior to that of the 9×9 filter in terms of smoothing, without risking the loss of data. Figure 5.10 shows the same section of a TARO plane as used in the filter examples after the LUT scaling

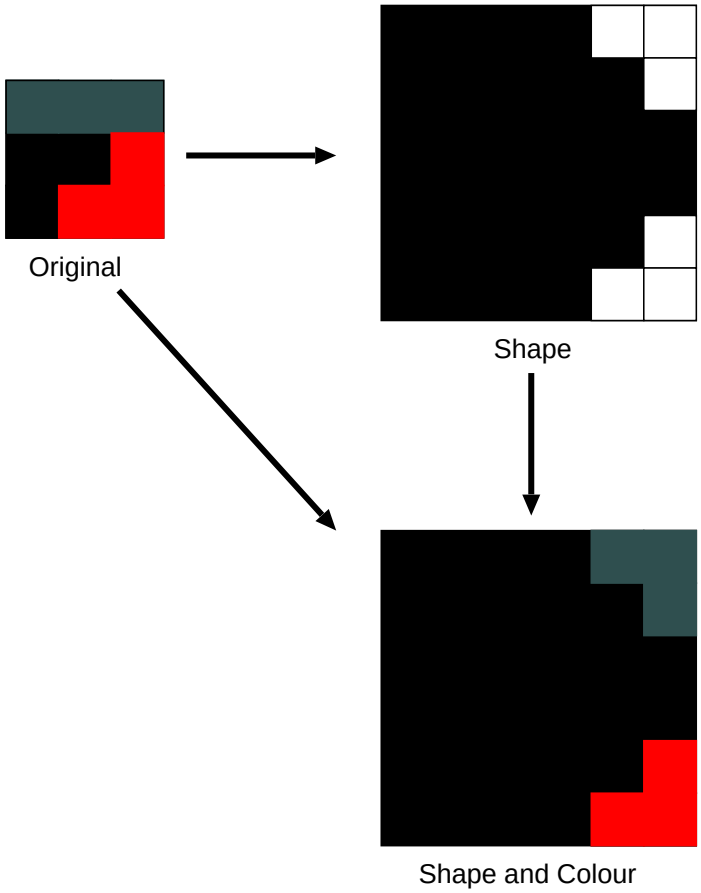

Figure 5.8: An example of the Look-Up Table process. The original data is used to select a output shape, and then this is used with the original data to apply values to the output pixels

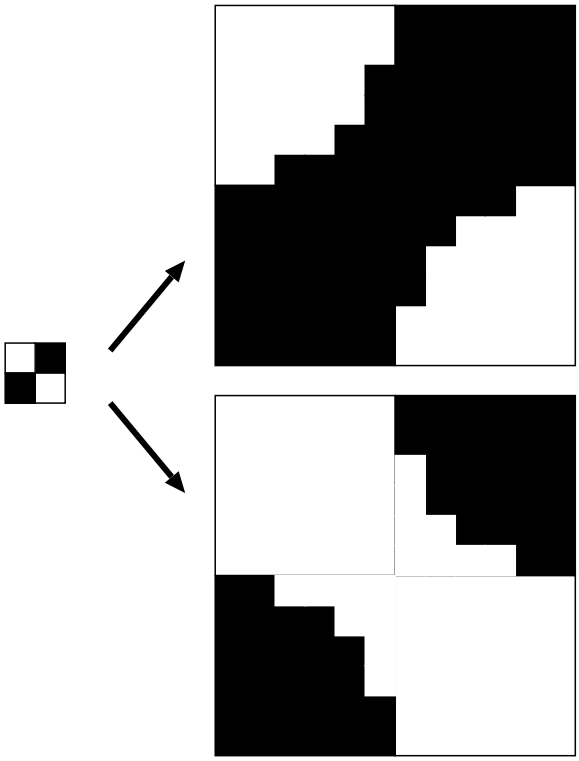

Figure 5.9: The four pixel arrangement on the left could be interpreted to produce either of the two 144 pixel outputs on the right. As there is no reason to pick one over the other, the region will simply be scaled without smoothing.

Figure 5.10: One quarter of TARO z-normal plane 220 scaled by 6 times and smoothed with the LUT method.

has been applied. Figure 5.11 displays smaller sections of the plane, scaled but unsmoothed, smoothed by the 5×5 and 9×9 filters and scaled with the LUT method for comparison.

While the output may appear visually superior, it cannot truly be said to be more accurate, reliable or anything other than possibly more probable and more aesthetically pleasing. While we know that the human body is more likely to consist of smooth curves than it is sharp edges, we cannot directly infer this from the information provided. No more information can be directly drawn from the phantom we have available, therefore to fully match the contents of any one plane in the final phantom to the expected tissues present in a plane from a human body would require the segmentation of the body at that level.

5.2 Smoothing in 3 Dimensions

Three dimensional smoothing is a complex procedure commonly achieved in human phantoms by converting the three dimensional voxel surface into a three dimensional mathematical surface such as is involved in a NURBS model[38, 45]. As well as requiring the conversion of the voxel data into a mathematical model, these methods smooth a single surface of a single material without regard to other structures. This would require the extraction of each individual material,

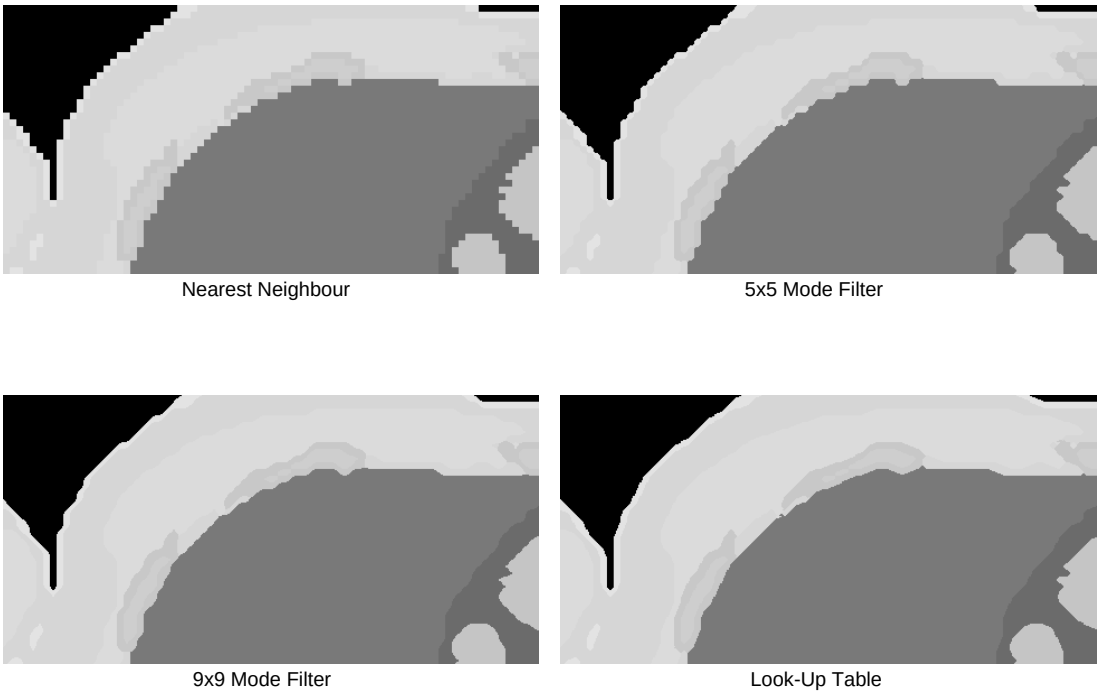

Figure 5.11: A section of TARO z-normal plane 220 after nearest neighbour scaling, scaling and smoothing with a 5×5 mode filter, scaling and smoothing with a 9×9 mode filter and scaling and smoothing via the LUT method.

its smoothing and its subsequent re-integration into the model, a process that may result in two tissues claiming to exist in the same location.

Extending the methods used in the two dimensional case into three dimensions is non-trivial. Use of a look-up table would provide a viable approach to producing smooth surfaces were it not for the computational complexity. While the two dimensional case produces 256 possible local configurations, the size of the problem grows as 2^n, where n is the number of pixels being considered. This results in the three dimensional case providing 2^{26}, over 67 million, potential pixel configurations. The total number of relevant configurations would be significantly reduced through ignoring all which place the central pixel as part of a line or inside a region, but the number would still be so large as to be insurmountable.

The filter method would provide a less complex scenario, but at not inconsiderable computational cost. The TARO phantom in its original state contains 44.3 million voxels of 2 mm in each direction. Increasing the resolution to 0.33 mm replaces every existing voxel with 216, producing a model of over 9.5 billion voxels. The 9×9 two dimensional filter produced reasonable results by taking into account 81 pixels to find the value for any pixel near a sharp corner. The three

dimensional equivalent would take the mode average of 729 voxels for each, and there could potentially be hundred of millions of voxels that require examination.

Due to time constraints, exploration of the three dimensional problem was never fully completed. Such large systems produce data management and access problems, and interpreting the quality of the results is in itself a difficult task. In order to progress, it was decided that the phantom would be built from the z-normal planes smoothed with the LUT method, with each plane simply copied 6 times rather than smoothing attempted between them.

Chapter 6

Implanting the Isolated Heart Model

6.1 The Heart Model

The isolated heart model includes 18 separated regions at a resolution of $0.33 \times 0.33 \times 0.33$ mm. These regions do not represent 18 different tissues, but define many of the larger structures in the heart and primary elements of the surrounding vascular system. Figure 6.1 is taken from Gray's Anatomy and shows the position of the heart within the chest and the large anatomy. The heart model includes the ascending aorta and the arch of the aorta, and large sections of the pulmonary arteries and vena cava, however it does not include a pericardium.

The heart model was provided as a single file containing point data. The file contains coordinates on the cardinal axes and the tissue type present at each voxel so defined. Large amounts of space within the model is therefore undefined in the original format, as to be expected when working with an isolated structure. The model is described as being $500 \times 325 \times 469$ pixels, but there is a certain amount of empty volume on the largest axis, reducing it to 486 pixels.

6.1.1 Reformatting and Viewing the Isolated Heart Model

Insertion of the isolated heart model into the body phantom requires that the file formats are similar. The isolated heart model thus required transference from being defined by coordinates to being defined by planes as the phantom is. At first it was assumed that the coordinates represented x, y and z in order, but it

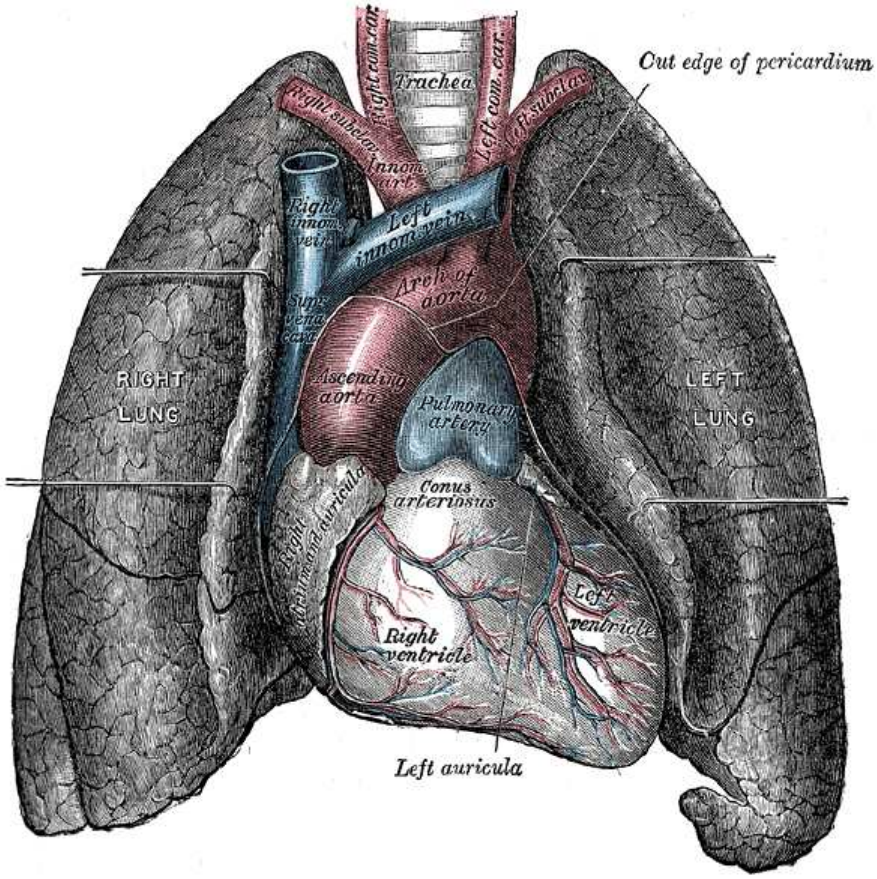

Figure 6.1: The position and large anatomy of the human heart, as shown in Gray's Anatomy[56] figure 490.

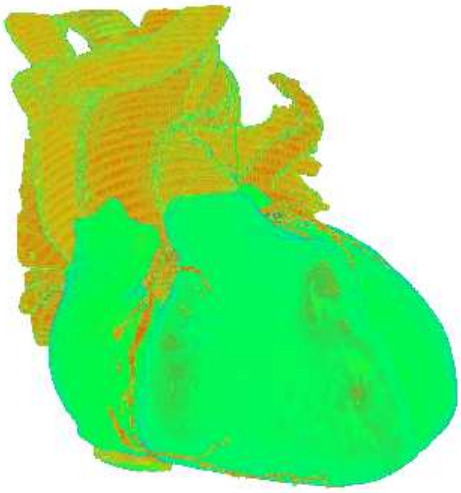

Figure 6.2: The isolated heart rendered in ParaView and viewed from the front.

became apparent that they were actually reversed, and the z coordinate was being given first. A program to carry out this procedure is included in Appendix C.

Once the file format had been changed, the result was viewed in the ParaView visualisation software[5]. This software provides a method of viewing three dimensional models and data stored in a wide variety of formats including raw binary files such as that created by the conversion procedure detailed above. Viewing the data in ParaView is a matter of informing the software of the data type, the storage format and the volume in which the data is contained. This can be done either through a header within the file, or manually in the software.

In this case the data is stored as single bytes representing values from 0-255, This is the scalar type represented by the "unsigned char" option. The byte order is LittleEndian, as defined by the system architecture, but as the data is stored in single bytes it is of little concern. The file is of dimensionality three, and the data spacing is constant in all directions. The data extent is 0-468 in the x-direction, 0-324 in the y-direction and 0-485 in the z-direction.

Viewing the model for the first time, it became apparent that the file was mirrored, and so a small program - given in appendix C - was used to resolve this problem. A ParaView rendering of the final output is shown in figure 6.2.

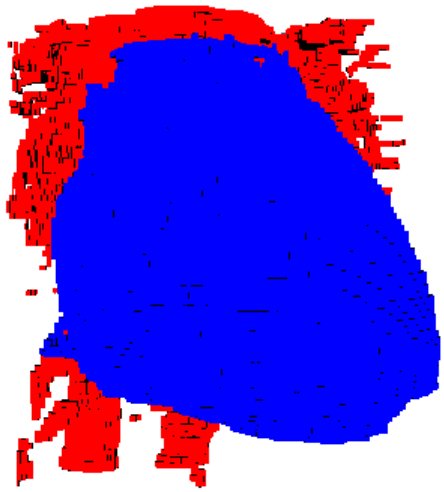

Figure 6.3: The heart (blue) - and local blood (red) - of the TARO model, extracted and rendered in ParaView and viewed from the front.

6.2 Insertion of the Isolated Heart

Insertion of the isolated heart into the body phantom requires two primary steps. The first of these is locating the position at which the insertion should be made, and the second is carrying out the procedure.

6.2.1 Orientation

Insertion of the heart model requires matching it with the best possible location in the body phantom. The TARO model includes a defined heart which can be viewed with the ParaView software by taking a threshold of the defined material. The TARO heart is shown from the front in figure 6.3, with the blue material representing “heart” and the red representing “blood”.

The two heart models available are from two different people and thus differ in both their size and their shape. The visual differences are considerable, but the dimensions and volume are relatively close. The separate heart model has a slightly larger transversal diameter than the TARO heart, while the TARO heart is larger in other dimensions. The difference in heart size can be considerable[57], so it is perhaps fortunate that these two examples are as similar as they are.

The reason for the large difference in appearance appears to be the role that

the pericardium has taken in the formation of the models. The NICT model appears to include everything within the pericardium except for blood as "heart" while the isolated model lacks any pericardial tissue or delimiters between veins and arteries inside and outside of the pericardial walls. As an example, the pulmonary trunk is completely contained by the pericardium[11], but the isolated model contains nothing that would suggest such information.

Using the ParaView software it is possible to align the isolated heart and the TARO phantom so that the two hearts occupy the same space. The smoothed and scaled phantom is over 9.5 GB in size, and so the whole model cannot be loaded in to memory on a normal computer. Appendix C includes a method of extracting a region of the phantom small enough to be visualised. This allows the determination of the volume in the body phantom which would best suit the positioning of the volume of the isolated heart. The ideal situation would be to insert the isolated heart inside the original heart space and use the boundary of it as a surrogate pericardium, however if we look at both hearts from below as in figure 6.4 it becomes clear that the isolated heart, while still smaller in volume, cannot fit inside the original heart boundaries in all directions.

Positioning of the heart is thus a matter of finding the position at which the phantom and the heart intersect the most. Rotation and scaling of the isolated heart would produce a better fit, but could damage the model, while alignment of the associated venous systems requires misaligning the heart chambers.

6.2.2 Insertion

Once the location of the insertion is determined, the implantation is a relatively simple process. The full size phantom is split into sections to avoid having to work with the whole phantom, only the vertical region containing the planes which will be altered is operated on. This can be performed using the standard Unix `head` and `tail` commands, as storing it as a single binary file allows exact knowledge of the size of each z-plane.

Using the extracted region, insertion is then only a matter of overwriting the isolated heart in the correct region of the phantom. Any non-zero voxel in the heart model overwrites the information present in the body phantom. Tissue identifiers are written as their original value+100 to avoid conflicts in enumeration. Code to achieve this is given in appendix C.

When the heart has been inserted, the phantom is reconstructed by simply

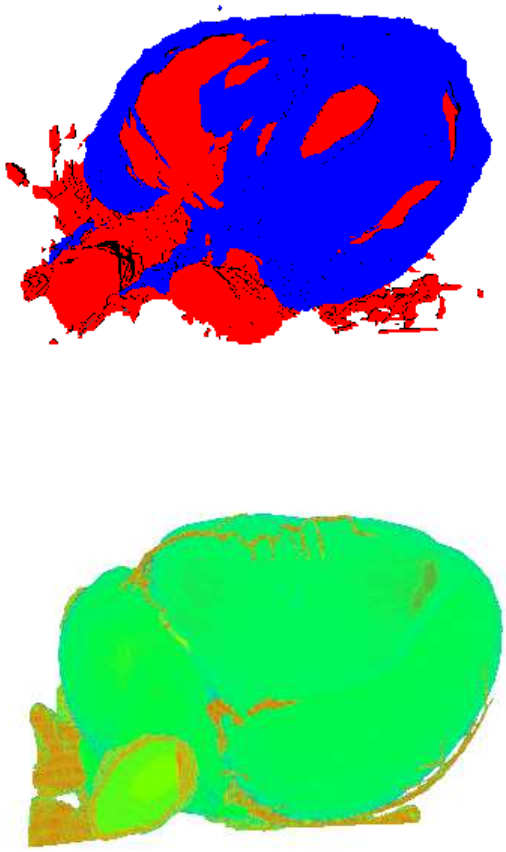

Figure 6.4: The TARO model heart (top) and the isolated heart (bottom) rendered in ParaView and viewed from below.

concatenating the previously removed sections together with the new inserted section.

6.3 Preparing the phantom for use

When used, the phantom will be accessed as a series of files, each containing one z-plane of the model stored as ASCII data, with the tissue content of one voxel per line. Converting the whole phantom into this format from the single, raw binary file requires three steps.

Firstly, the phantom must be split into 5196 separate planes. As every plane is represented by 1843200 bytes, this can be performed with the UNIX `split` command:

```
split -d -a 4 -b 1843200 final.raw z
```

This produces a series of files named z#### where #### is a 4 digit suffix.

Each of these files can then be converted from binary data into ASCII by use of the `od` command:

```
od -t u1 -v -A n --width=1 z#### > k####
```

This will convert the file z#### into a file k#### which stores each voxel value on a new line.

The final step is to reduce the data value ranges to a minimum. Due to avoiding number conflicts in the insertion and some numbers lacking a defined tissue, the phantom will have values ranging from 0 to 170, while containing only 70 tissues. This can be reduced through extensive use of the `awk` command, and an example script that converts all files in the phantom is given in appendix C

The final model is contained in a series of 5196 files each in the region of 4 MB in size, combined they require approximately 19.5 GB of storage space. Resolution in the $x - y$ plane is 0.33 mm throughout, while vertical resolution is 0.33 mm with the structure of 2 mm resolution for all materials except those implanted with the isolated heart. A full list of the materials and structures present is given in appendix D.

Chapter 7

Conclusions

This thesis has described the motivation for, and construction of, a Digital Human Phantom. The produced model and it's surrounding space are constructed of over 9.5 billion $0.33 \times 0.33 \times 0.33$ mm voxels and contain 70 different defined tissues, materials and structures. An externally produced isolated heart model has been integrated into the phantom for superior accuracy in the cardiac tissues. The produced phantom is intended for use in an exploratory study into the use of FDTD to simulate the body surface potential response to cardiac arrhythmia.

The fundamental requirements for this project were achieving high spatial resolution combined with physiological realism. Production of the phantom from raw medical data was determined to be overly complex and beyond the capabilities of the author. A previous tomographic phantom was chosen as the basis for the project over a mathematical model to maximise the anatomical realism, though the available models were at a resolution below that desired.

Scaling of the model was necessary to increase the resolution towards the required value. Direct scaling produced a model with sharp corners and formations that would not be expected to appear in the human body. Smoothing was attempted to reduce the impact of the corners and the common methods were discarded due to their introducing and removing information as part of the process. Modal and look-up table based methods were developed to smooth individual planes of the phantom but their extension into three dimensions provided an obstacle insurmountable in the time available. The result is that the model is smoothed in only one plane and would visually appear to be at 2 mm resolution in the vertical axis. Achievement of three dimensional smoothing would greatly enhance the physical realism through reduction of tissues appearing as stratified

layers.

The inclusion of the the isolated heart provides a source of accurate anatomy, but introduces the considerable complexity of interfacing between the two models. Tomographic models are the most difficult to adapt to new parameters, and so the interactions between two are overly complex. Accurately linking the cardiovascular systems together would require alterations at the voxel level over a region containing tens of millions of voxels. The implanted heart provides a very accurate cardiac system to simulate over, but introduces irregularities in the rest of the torso that could potentially effect the results of simulations.

7.1 Future Work

There is potential for further development of this model and many reasons to consider the creation of next generation models to replace it.

In this phantom, three dimensional smoothing before the isolated heart insertion would be the primary route to enhancement, but the specific integration of the isolated heart also offers scope for refinement. There is also potential for a pericardium to be manually added or adapted from an existing source. In chapter 2 the importance of the cardiac conduction system to arrhythmia development was discussed, and currently the phantom lacks any system of modelling even the larger structures in this. The SA and AV nodes are large enough to be defined at this resolution, and while the Purkinje fibres are too small to be modelled, the bundle of His and the left and right bundle branches could potentially be included.

The option of replacing the model offers many benefits, especially if a phantom could be constructed for the specific purpose of electro-cardiology simulation. This phantom could be planned at the desired resolution, removing the need for scaling and smoothing, ensuring anatomical accuracy and reducing the chance of data loss or addition. Unlike the majority of phantoms which are produced for dosimetry, the structures and tissues required for accurate modelling would be present and well defined.

A new phantom could also offer a significantly more adaptable simulation space. A hybrid model constructed with the previously described characteristics would allow for the simple alteration of structures to simulate varying scenarios. With the variable nature of heart size, the ability to increase and decrease the

heart dimensions without overly affecting the surrounding structures and the ability to resize the entire phantom, would allow for simulation of cardiac arrhythmia in patients of many ages. A hybrid phantom constructed to lesser specifications would still be considerably easier to integrate with externally developed organs. Finally, the use of a hybrid model would potentially allow the inclusion of dynamic elements[45].

Appendix A

Methods for the Visualisation of Data

A.1 Viewing VHP data

The complete Visual Human Project data is currently stored at 130.88.154.30/local/visualhumanproject/. The scripts below extract from this location to the folder they are run in. Currently they are located at 130.88.154.30/local/michael/Male/ and stored in their respective folders.

A.1.1 Photographic

.RAW Files

This script extracts 10 files from the VHP photographic data stored as 2048×1216 pixel .RAW files and converts them into .ppm colour image files that can be viewed on the majority of systems. This example is extracting data from the Male set, but the female set is stored and extracted in similar manner.

```
#!/bin/csh

set datadir = "/local/visiblehumanproject/Male/Fullcolor/fullbody"

set k = 1001

while (k < 1011)
echo $k

if(! -e $datadir/a_vm$k.raw.Z) then
```

```
@ k ++
continue
else

echo "P3" > full$k.ppm
echo "2048 1216" >> full$k.ppm
echo "255" >> full$k.ppm

cp  $datadir/a_vm$k.raw.Z .
gunzip a_vm$k.raw.Z

od -t u1 -v -A n --width=1 a_vm$k.raw > temp
split -l 2490368 temp
paste xaa xab xac > output

cat output >> full$k.ppm

rm a_vm$k.raw

endif

@ k ++
end

exit 0
```

.rgb Files

This script extracts the 4096×2700 pixel colour images found only in the male dataset, converting them into .ppm files.

```
#!/bin/csh

set datadir = "/local/visiblehumanproject/Male/70mm/fullbody"

set k = 1001
while($k < 1011)

echo $k

if(! -e $datadir/$k.rgb.gz) then
@ k ++
```

```
continue
else

echo "P3" > large$k.ppm
echo "4096 2700" >> large$k.ppm
echo "255" >> large$k.ppm

cp  $datadir/$k.rgb.gz .
gunzip $k.rgb.gz

od -t u1 -v -A n --width=3 $k.rgb > temp

cat temp >> large$k.ppm

rm $k.rgb

endif

@ k ++
end

exit 0
```

A.1.2 Radiological

MRI

This script extracts images from a group of MRI files converting them into greyscale .pgm files. While this script extracts only T1 images from the male dataset, the T2 and proton density scans, and their female counterparts, are stored in the same fashion and so the only difference in their extraction scripts comes in file names.

```
#!/bin/csh

set datadir = "/local/visiblehumanproject/Male/radiological/mri"


set k = 1005
while($k < 1100 )

echo $k
```

```
if(! -e $datadir/m_vm$k.t1.Z) then
@ k ++
continue
else

echo "P2" > mri$k.pgm
echo "256 256" >> mri$k.pgm

cp  $datadir/m_vm$k.t1.Z  .

gunzip m_vm$k.t1.Z

dd conv=swab if=m_vm$k.t1 of=swap >& /dev/null
od -j 7900 -t u2 -v -A n --width=2 swap > temp
set max = `sort -gr temp | head -1 `
echo $max >> mri$k.pgm

cat temp >> mri$k.pgm

rm m_vm$k.t1

endif

@ k ++
end

exit 0
```

CT scans

This script extracts a small group of unfrozen CT images found in the male set and converts them into greyscale .pgm files. The unfrozen CT images in the female set and the frozen CT images in the male set can be extracted in the same way.

```
#!/bin/csh

set datadir = "/local/visiblehumanproject/Male/radiological/normalCT"

set k = 1012
```

```
while($k < 1030 )

echo $k

if(! -e $datadir/c_vm$k.fre.Z) then
@ k ++
continue
else

echo "P2" > ct$k.pgm
echo "512 512" >> ct$k.pgm

cp  $datadir/c_vm$k.fre.Z  .

gunzip c_vm$k.fre.Z

dd conv=swab if=c_vm$k.fre of=swap >& /dev/null
od -j 3416 -t u2 -v -A n --width=2 swap > temp
set max = `sort -gr temp | head -1 `
echo $max >> ct$k.pgm

cat temp >> ct$k.pgm

rm c_vm$k.fre

endif

@ k ++
end

exit 0
```

Appendix B

Methods for Scaling and Smoothing

B.1 Modal Filter

This Program smooths a single file from the local directory for testing purposes

```
PROGRAM filter
!
! This program scales an input TARO z-normal plane to 6 times larger and
! smooths with a 5x5 modal filter
!
IMPLICIT NONE

 INTEGER :: input(320,160), tissue(0:57), temp(57), mode(1)
 INTEGER :: work(1920,960)
 CHARACTER (LEN=1) :: a
 INTEGER :: i, j, k, l, zonei, zonej, temp2, temp3
 INTEGER, ALLOCATABLE :: counts(:,:)

! Input and output files are both binary, with each tissue represented
! by a single byte

OPEN(101,FILE='zplane220', ACCESS='STREAM', STATUS='OLD')

!
! Read information into array and record which tissues are present
! in the tissue array for faster modal sorting
!
```

```
tissue = 0
input = 0

DO j=1,160
  DO i=1,320
    READ(101) a
    input(i,j) = ICHAR(a)
    tissue(input(i,j)) = tissue(input(i,j))+1
  END DO
END DO
CLOSE(101)

!
! Find the total number of tissues in the plane
!
l=0
DO i=0,57
  IF (tissue(i) /= 0) then
     l=l+1
     temp(l)=i
  END IF
END DO

!
! Create a counting array, with two columns and as many rows as there
! are tissues in the plane
!
ALLOCATE (counts(l,2))
counts(1:l,1) = temp(1:l)

!
! Scale the image by 6 times in each direction
!
DO j=1,960
  DO i=1,1920
     work(i,j) = readin(ceiling(i/6.0),ceiling(j/6.0))
  END DO
END DO

OPEN(201,file='zlarge220', ACCESS='STREAM', STATUS='NEW')

!
```

```
! Begin the smoothing
!
DO j = 1,960
  DO i = 1,1920
!
! Operate only on regions which are away from the plane boundaries
! and near corners in materials.
!
   IF (j-2 >= 1 .AND. j+2 <= 960 .AND. i-2 >= 1 &
          .AND. i+2 <=  1920) THEN
     IF ((work(i,j-2) == work(i,j) .AND. &
         work(i,j+2) == work(i,j)) .OR. &
        (work(i-2,j) == work(i,j) .AND. &
         work(i+2,j) == work(i,j))) THEN
!
! If not near a corner, copy output from the scaled.
!
       WRITE(201) ACHAR(work(i,j))
     ELSE
!
! Count the tissues in the 5x5 region surrounding the pixel of interest
!
       counts(:,2)=0
       DO zonej=-2,2
         DO  zonei=-2,2
           DO k = 1,l
             IF (counts(k,1) == work(i+zonei,j+zonej)) then
               counts(k,2) = counts(k,2) + 1
             END IF
           END DO
         END DO
       END DO
!
! Find the most common.
!
         mode=maxloc(counts(:,2))
         temp2=mode(1)
         temp3=counts(temp2,1)
!
! Write out the result
!
         WRITE(201) ACHAR(temp3)
```

```
     END IF
    ELSE
!
! If near the image boundary, copy output from the scaled
!
     WRITE(201) ACHAR(work(i,j))
    END IF
 END DO
END DO

CLOSE(201)
END PROGRAM
```

B.2 Look-Up Table

B.2.1 The Main Program

This program operates on the TARO phantom in it's original form. It is currently located on 130.88.154.36 in /local/michael/NICT/codes/.

```
PROGRAM lookup
!
! This program scales by 6 times and smooths at the same time using a
! look-up table of potential results. It operates on the z-normal planes
! of the TARO phantom.
!

IMPLICIT NONE

INTEGER :: i,j,k,ni,nj,pix,m,l ! counting and holding variables
INTEGER :: d2, d1, d0 ! naming numbers
INTEGER :: inp(320,160), outp(1920,960)
INTEGER :: mask(320,160)
CHARACTER (len=30) :: num
CHARACTER (LEN=1) :: a
!
! The TARO phantom is opened and a single voxel layer is read
!
OPEN(101, FILE='/local/michael/NICT/MALE-V1.RAW',&
          ACCESS='STREAM', STATUS='OLD')

DO k=1,866
```

```
  DO j=1,160
    DO i=1,320
     READ(101) a
     inp(i,j) = ICHAR(a)
    END DO
  END DO

 write(*,*) k
!
! An output file for this level is created
!
   d2=k/100; d1=(k-d2*100)/10; d0=(k-d2*100)-d1*10;
   num='/local/michael/NICT/big/big' // CHAR(48+d2) &
           // CHAR(48+d1) // CHAR(48+d0)

 OPEN(201, FILE=num, ACCESS='STREAM', STATUS='NEW')
!
! Corners in the image are located and stored
!
 DO j=2,159
   DO i=2,319
     IF ((inp(i,j-1) == inp(i,j) .and. &
             inp(i,j+1) == inp(i,j)) .OR. &
             (inp(i-1,j) == inp(i,j) .and. &
             inp(i+1,j) == inp(i,j))) THEN
        mask(i,j) = 0
     ELSE
        mask(i,j) = 1
     END IF
   END DO
 END DO
!
! The output base is scaled from the input
!
 DO j=1,960
   DO i=1,1920
     outp(i,j) = inp(ceiling(i/6.0),ceiling(j/6.0))
   END DO
 END DO
!
! Operate on the corners found in the mask
!
```

```
 DO i=2,319
   DO j=2,159
     IF (mask(i,j) == 1) THEN
        l=0 ! counter
        pix=0 ! pixel code combination
!
! Check the pattern for the original 8 surrounding pixels
! to see which match
!
        DO nj=-1,1
          DO ni=-1,1
            IF (ni == 0 .AND. nj == 0) THEN
              ELSE
              IF (inp(i+ni,j+nj) == inp(i,j)) THEN
                pix=pix+2**l
                l=l+1
              ELSE
                l=l+1
              END IF
            END IF
          END DO
        END DO
!
! Give a value to isolated pixels
!
        IF (pix == 0) THEN
           pix = 254
        END IF
!
! Revalue the position in the mask with the code for the pixel pattern
!
        mask(i,j) = pix
      END IF
   END DO
 END DO
!
! Send the code and the information to the mask subroutine to
! determine the pattern of the resulting 36 pixels. These overwrite the
! previously generated scaled image.
!
DO i=2,319
  DO j=2,159
```

```
     IF (mask(i,j) /= 0) THEN
       CALL table(mask(i,j), inp(i-1:i+1,j-1:j+1), outp(6*i-5:6*i,6*j-5:6*j))
     END IF
  END DO
END DO
!
! Write out the result
!
DO j=1,960
  DO i=1,1920
    m = outp(i,j)
    WRITE(201) achar(m)
  END DO
END DO
!
! Close the current output file and start on the next layer
!
CLOSE(201)

END DO

CLOSE(101)

END PROGRAM
```

B.2.2 The Look-Up Table

```
SUBROUTINE table(num, local, out)

IMPLICIT NONE

INTEGER, INTENT(IN) :: local(3,3)
INTEGER :: num, act,i,j
INTEGER, INTENT(OUT) :: out(6,6)
!
! Match the input with the relevent output. Unlisted values use the
! DEFAULT case.
!
Tab:  SELECT CASE(NUM)
      CASE(254)
        act=0
      CASE(1)
```

```
      act=1
    CASE(2)
      act=2
    CASE(3)
      act=2
    CASE(4)
      act=3
    CASE(5)
      act=2
    CASE(6)
      act=2
    CASE(7)
      act=2
    CASE(8)
      act=4
    CASE(9)
      act=4
    CASE(10)
      act=5
    CASE(11)
      act=5
    CASE(12)
      act=6
    CASE(13)
      act=6
    CASE(14)
      act=6
    CASE(15)
      act=6
    CASE(16)
      act=7
    CASE(17)
      act=8
    CASE(18)
      act=9
    CASE(19)
      act=8
    CASE(20)
      act=7
    CASE(21)
      act=8
    CASE(22)
```

```
  act=9
CASE(23)
  act=8
CASE(32)
  act=10
CASE(33)
  act=4
CASE(34)
  act=11
CASE(35)
  act=11
CASE(36)
  act=12
CASE(37)
  act=13
CASE(38)
  act=13
CASE(39)
  act=13
CASE(40)
  act=4
CASE(41)
  act=4
CASE(42)
  act=11
CASE(43)
  act=11
CASE(44)
  act=13
CASE(45)
  act=13
CASE(46)
  act=13
CASE(47)
  act=13
CASE(48)
  act=14
CASE(52)
  act=15
CASE(64)
  act=16
CASE(65)
```

```
  act=17
CASE(68)
  act=18
CASE(72)
  act=19
CASE(73)
  act=17
CASE(80)
  act=20
CASE(84)
  act=18
CASE(96)
  act=16
CASE(97)
  act=17
CASE(100)
  act=15
CASE(104)
  act=19
CASE(105)
  act=17
CASE(112)
  act=14
CASE(116)
  act=15
CASE(128)
  act=21
CASE(129)
  act=22
CASE(130)
  act=23
CASE(131)
  act=24
CASE(132)
  act=7
CASE(133)
  act=24
CASE(134)
  act=23
CASE(135)
  act=24
CASE(136)
```

```
  act=25
CASE(137)
  act=26
CASE(144)
  act=7
CASE(145)
  act=24
CASE(146)
  act=23
CASE(147)
  act=24
CASE(148)
  act=7
CASE(149)
  act=24
CASE(150)
  act=23
CASE(151)
  act=24
CASE(160)
  act=16
CASE(161)
  act=26
CASE(164)
  act=15
CASE(168)
  act=25
CASE(169)
  act=26
CASE(176)
  act=14
CASE(180)
  act=15
CASE(192)
  act=16
CASE(193)
  act=26
CASE(196)
  act=18
CASE(200)
  act=25
CASE(201)
```

```
        act=26
      CASE(208)
        act=20
      CASE(212)
        act=18
      CASE(224)
        act=16
      CASE(225)
        act=26
      CASE(228)
        act=15
      CASE(232)
        act=25
      CASE(233)
        act=26
      CASE(240)
        act=14
      CASE(244)
        act=15
      CASE DEFAULT
        act=255

END SELECT Tab
!
! Apply the appropriate case to alter the output region
!
result: SELECT CASE(act)
      CASE(0)
        IF (local(2,1) == local(1,2)) THEN
          out(1,1) = local(1,2); out(1,2) = local(1,2); out(2,1) = local(1,2)
        ELSE IF (local(1,1) == local(1,2)) THEN
          out(1,1) = local(1,1); out(1,2) = local(1,1); out(2,1) = local(1,1)
        ELSE IF (local(1,1) == local(2,1)) THEN
          out(1,1) = local(1,1); out(2,1) = local(2,1); out(1,2) = local(1,1)
        ELSE

        END IF

        IF (local(2,1) == local(3,2)) THEN
          out(6,1) = local(3,2); out(6,2) = local(3,2); out(5,1) = local(3,2)
        ELSE IF (local(3,1) == local(3,2)) THEN
          out(6,1) = local(3,1); out(6,2) = local(3,1); out(5,1) = local(3,1)
```

```
  ELSE IF (local(3,1) == local(2,1)) THEN
    out(6,1) = local(3,1); out(5,1) = local(3,1); out(6,2) = local(3,1)
  ELSE

  END IF

  IF(local(2,3) == local(1,2)) THEN
    out(1,6) = local(1,2); out(1,5) = local(1,2); out(2,6) = local(1,2)
  ELSE IF (local(1,3) == local(1,2)) THEN
    out(1,6) = local(1,3); out(1,5) = local(1,3); out(2,6) = local(1,3)
  ELSE IF (local(1,3) == local(2,3)) THEN
    out(1,6) = local(1,3); out(2,6) = local(1,3); out(1,5) = local(1,3)
  ELSE

  END IF

  IF (local(2,3) == local(3,2)) THEN
    out(6,6) = local(3,2); out(6,5) = local(3,2); out(5,6) = local(3,2)
  ELSE IF (local(3,3) == local(3,2)) THEN
    out(6,6) = local(3,3); out(6,5) = local(3,3); out(5,6) = local(3,3)
  ELSE IF (local(3,3) == local(2,3)) THEN
    out(6,6) = local(3,3); out(6,5) = local(3,3); out(5,6) = local(3,3)
  ELSE

  END IF

CASE(1)
  IF (local(1,2) == local(2,3)) THEN
    out(1,4:6) = local(2,3); out(2,5:6) = local(2,3)
    out(3,6) = local(2,3)
  ELSE IF (local(1,3) == local(2,3)) THEN
    out(1:3,6) = local(2,3); out(2,5) = local(2,3)
    out(1,4:5) = local(1,2)
  ELSE IF (local(1,3) == local(1,2)) THEN
    out(1,4:6) = local(1,2); out(2,5) = local(1,2)
    out(2:3,6) = local(2,3)
  ELSE

  END IF

  IF (local(2,1) == local(3,2)) THEN
    out(6,1) = local(3,2); out(5,1) = local(3,2); out(6,2) = local(3,2)
```

```
  ELSE IF (local(3,1) == local(2,1) .OR. local(3,1) == local(3,2)) THEN
    out(5,1) = local(3,1); out(6,1) = local(3,1); out(6,2) = local(3,1)
  ELSE

  END IF

  IF (local(2,3) == local(3,2)) THEN
    out(6,6) = local(3,2); out(6,5) = local(3,2); out(5,6) = local(3,2)
  ELSE IF (local(3,3) == local(3,2) .OR. local(3,3) == local(2,3)) THEN
    out(6,6) = local(3,3); out(6,5) = local(3,3); out(5,6) = local(3,3)
  ELSE

  END IF

CASE(2)
  IF (local(1,2) == local(2,3)) THEN
    out(1,6) = local(2,3); out(2,6) = local(2,3); out(1,5) = local(2,3)
  ELSE IF (local(1,3) == local(2,3) .OR. local(1,3) == local(1,2)) THEN
    out(1,6) = local(1,3); out(1,5) = local(1,3); out(2,6) = local(1,3)
  ELSE

  END IF

  IF (local(2,3) == local(3,2)) THEN
    out(6,6) = local(3,2); out(6,5) = local(3,2); out(5,6) = local(3,2)
  ELSE IF (local(3,3) == local(3,2) .OR. local(3,3) == local(2,3)) THEN
    out(6,6) = local(3,3); out(6,5) = local(3,3); out(5,6) = local(3,3)
  ELSE

  END IF

CASE(3)
  IF (local(2,1) == local(1,2)) THEN
    out(1:3,1) = local(1,2); out(1:2,2) = local(1,2)
    out(1,3) = local(1,2)
  ELSE IF (local(1,1) == local(1,2)) THEN
    out(1,1:3) = local(1,1); out(2,2) = local(1,1)
    out(2:3,1) = local(2,1)
  ELSE IF (local(1,1) == local(2,1)) THEN
    out(1:3,1) = local(1,1); out(2,2) = local(1,1)
    out(1,2:3) = local(1,2)
  ELSE
```

```
  END IF

  IF (local(1,2) == local(2,3)) THEN
    out(1,6) = local(2,3); out(2,6) = local(2,3); out(1,5) = local(2,3)
  ELSE IF (local(1,3) == local(2,3) .OR. local(1,3) == local(1,2)) THEN
    out(1,6) = local(1,3); out(1,5) = local(1,3); out(2,6) = local(1,3)
  ELSE

  END IF

  IF (local(2,3) == local(3,2)) THEN
    out(6,6) = local(3,2); out(6,5) = local(3,2); out(5,6) = local(3,2)
  ELSE IF (local(3,3) == local(3,2) .OR. local(3,3) == local(2,3)) THEN
    out(6,6) = local(3,3); out(6,5) = local(3,3); out(5,6) = local(3,3)
  ELSE

  END IF

CASE(4)

  IF (local(2,1) == local(3,2)) THEN
    out(6,1) = local(3,2); out(5,1) = local(3,2); out(6,2) = local(3,2)
  ELSE IF (local(3,1) == local(2,1) .OR. local(3,1) == local(3,2)) THEN
    out(5,1) = local(3,1); out(6,1) = local(3,1); out(6,2) = local(3,1)
  ELSE

  END IF

  IF (local(2,3) == local(3,2)) THEN
    out(6,6) = local(3,2); out(6,5) = local(3,2); out(5,6) = local(3,2)
  ELSE IF (local(3,3) == local(3,2) .OR. local(3,3) == local(2,3)) THEN
    out(6,6) = local(3,3); out(6,5) = local(3,3); out(5,6) = local(3,3)
  ELSE

  END IF

CASE(5)
  IF (local(2,3) == local(3,2)) THEN
    out(4:6,6) = local(3,2); out(5:6,5) = local(3,2)
    out(6,4) = local(3,2)
  ELSE IF (local(3,3) == local(3,2)) THEN
```

```
      out(6,4:6) = local(3,3); out(5,5) = local(3,3)
      out(4:5,6) = local(3,3)
    ELSE IF (local(3,3) == local(2,3)) THEN
      out(6,4:5) = local(3,3); out(5,5) = local(3,3)
      out(4:6,6) = local(3,3)
    ELSE

    END IF

  CASE(6)
    IF (local(3,2) == local(1,3)) THEN
      IF (local(3,2) == local(2,3)) THEN
        out(1:6,6) = local(2,3); out(3:6,5) = local(2,3)
        out(6,4) = local(2,3)
      ELSE IF (local(2,3) == local(3,3)) THEN
        out(1:6,6) = local(2,3); out(3:5,5) = local(2,3)
        out(6,4:5) = local(3,2)

      END IF
    ELSE
      IF (local(2,3) == local(3,2)) THEN
        out(6,6) = local(3,2); out(6,5) = local(3,2); out(5,6) = local(3,2)
      ELSE IF (local(3,3) == local(3,2) .OR. local(3,3) == local(2,3)) THEN
        out(6,6) = local(3,3); out(6,5) = local(3,3); out(5,6) = local(3,3)
      ELSE

      END IF
    END IF

  CASE(7)

    IF (local(1,2) == local(2,3)) THEN
      out(1,6) = local(2,3); out(2,6) = local(2,3); out(1,5) = local(2,3)
    ELSE IF (local(1,3) == local(2,3) .OR. local(1,3) == local(1,2)) THEN
      out(1,6) = local(1,3); out(1,5) = local(1,3); out(2,6) = local(1,3)
    ELSE

    END IF

    IF (local(2,1) == local(1,2)) THEN
      out(1,1) = local(1,2); out(1,2) = local(1,2); out(2,1) = local(1,2)
    ELSE IF (local(1,1) == local(1,2) .OR. local(1,1) == local(2,1)) THEN
```

```
      out(1,1) = local(1,1); out(2,1) = local(1,1); out(1,2) = local(1,1)
    ELSE

    END IF

  CASE(8)
    IF (local(1,2) == local(3,3)) THEN
      IF (local(2,3) == local(1,2)) THEN
        out(1:6,6) = local(2,3); out(1:4,5) = local(2,3)
        out(1,4) = local(2,3)
      ELSE IF (local(1,2) == local(1,3)) THEN
        out(2:6,6) = local(2,3); out(3:4,5) = local(2,3)
        out(2,5) = local(1,2); out(1,4:6) = local(1,2)
      ELSE

      END IF
    ELSE
      IF (local(1,2) == local(2,3)) THEN
        out(1,6) = local(2,3); out(2,6) = local(2,3); out(1,5) = local(2,3)
      ELSE IF (local(1,3) == local(2,3) .OR. local(1,3) == local(1,2)) THEN
        out(1,6) = local(1,3); out(1,5) = local(1,3); out(2,6) = local(1,3)
      ELSE

      END IF
    END IF

  CASE(9)
    IF (local(1,2) == local(2,3)) THEN
      out(1:3,6) = local(2,3); out(1:2,5) = local(2,3)
      out(1,3) = local(2,3)
    ELSE IF (local(1,3) == local(2,3)) THEN
      out(1:3,6) = local(1,3); out(2,5) = local(1,3)
      out(1,4:5) = local(1,3)
    ELSE IF (local(1,3) == local(1,2)) THEN
      out(2:3,6) = local(1,3); out(2,5) = local(1,3)
      out(1,4:6) = local(1,3)
    ELSE

    END IF

  CASE(10)
    IF (local(2,1) == local(1,2)) THEN
```

```
      out(1:3,1) = local(1,2); out(1:2,2) = local(1,2)
      out(1,3) = local(1,2)
    ELSE IF (local(1,1) == local(1,2)) THEN
      out(1,1:3) = local(1,1); out(2,2) = local(1,1)
      out(2:3,1) = local(2,1)
    ELSE IF (local(1,1) == local(2,1)) THEN
      out(1:3,1) = local(1,1); out(2,2) = local(1,1)
      out(1,2:3) = local(1,2)
    ELSE

    END IF

    IF (local(2,1) == local(3,2)) THEN
      out(6,1) = local(3,2); out(5,1) = local(3,2); out(6,2) = local(3,2)
    ELSE IF (local(3,1) == local(2,1) .OR. local(3,1) == local(3,2)) THEN
      out(5,1) = local(3,1); out(6,1) = local(3,1); out(6,2) = local(3,1)
    ELSE

    END IF

    IF (local(2,3) == local(3,2)) THEN
      out(6,6) = local(3,2); out(6,5) = local(3,2); out(5,6) = local(3,2)
    ELSE IF (local(3,3) == local(3,2) .OR. local(3,3) == local(2,3)) THEN
      out(6,6) = local(3,3); out(6,5) = local(3,3); out(5,6) = local(3,3)
    ELSE

    END IF

  CASE(11)
    IF (local(2,3) == local(3,1)) THEN
      IF (local(3,2) == local(2,3)) THEN
        out(6,1:6) = local(2,3); out(5,3:6) = local(2,3)
        out(4,6) = local(2,3)
      ELSE IF (local(2,3) == local(3,3)) THEN
        out(6,1:5) = local(3,2); out(5,3:4) = local(3,2)
        out(5,5) = local(2,3); out(4:6,6) = local(2,3)
      ELSE

      END IF
    ELSE
      IF (local(2,3) == local(3,2)) THEN
        out(6,6) = local(3,2); out(6,5) = local(3,2); out(5,6) = local(3,2)
```

```
      ELSE IF (local(3,3) == local(3,2) .OR. local(3,3) == local(2,3)) THEN
        out(6,6) = local(3,3); out(6,5) = local(3,3); out(5,6) = local(3,3)
      ELSE

      END IF
    END IF

  CASE(12)
    IF (local(2,1) == local(1,2)) THEN
      out(1:3,1) = local(1,2); out(1:2,2) = local(1,2)
      out(1,3) = local(1,2)
    ELSE IF (local(1,1) == local(1,2)) THEN
      out(1,1:3) = local(1,1); out(2,2) = local(1,1)
      out(2:3,1) = local(2,1)
    ELSE IF (local(1,1) == local(2,1)) THEN
      out(1:3,1) = local(1,1); out(2,2) = local(1,1)
      out(1,2:3) = local(1,2)
    ELSE

    END IF

    IF (local(2,3) == local(3,2)) THEN
      out(6,6) = local(3,2); out(6,5) = local(3,2); out(5,6) = local(3,2)
    ELSE IF (local(3,3) == local(3,2) .OR. local(3,3) == local(2,3)) THEN
      out(6,6) = local(3,3); out(6,5) = local(3,3); out(5,6) = local(3,3)
    ELSE

    END IF

  CASE(13)
    IF (local(2,3) == local(3,2)) THEN
      out(6,6) = local(3,2); out(6,5) = local(3,2); out(5,6) = local(3,2)
    ELSE IF (local(3,3) == local(3,2) .OR. local(3,3) == local(2,3)) THEN
      out(6,6) = local(3,3); out(6,5) = local(3,3); out(5,6) = local(3,3)
    ELSE

    END IF

  CASE(14)
    IF (local(1,2) == local(3,1)) THEN
      IF (local(1,2) == local(2,1)) THEN
        out(1:6,1) = local(2,1); out(1:4,2) = local(2,1)
```

```
      out(1,3) = local(2,1)
    ELSE IF (local(1,2) == local(1,1)) THEN
      out(2:6,1) = local(2,1); out(3:4,2) = local(2,1)
      out(2,2) = local(1,2); out(1,1:3) = local(1,2)
    ELSE

    END IF
  ELSE
    IF (local(2,1) == local(1,2)) THEN
      out(1,1) = local(1,2); out(1,2) = local(1,2); out(2,1) = local(1,2)
    ELSE IF (local(1,1) == local(1,2) .OR. local(1,1) == local(2,1)) THEN
      out(1,1) = local(1,1); out(2,1) = local(1,1); out(1,2) = local(1,1)
    ELSE

    END IF
  END IF

CASE(15)

  IF (local(2,1) == local(1,2)) THEN
    out(1:3,1) = local(1,2); out(1:2,2) = local(1,2)
    out(1,3) = local(1,2)
  ELSE IF (local(1,1) == local(1,2)) THEN
    out(1,1:3) = local(1,1); out(2,2) = local(1,1)
    out(2:3,1) = local(2,1)
  ELSE IF (local(1,1) == local(2,1)) THEN
    out(1:3,1) = local(1,1); out(2,2) = local(1,1)
    out(1,2:3) = local(1,2)
  ELSE

  END IF

CASE(16)
  IF (local(2,1) == local(3,2)) THEN
    out(6,1) = local(3,2); out(5,1) = local(3,2); out(6,2) = local(3,2)
  ELSE IF (local(3,1) == local(2,1) .OR.local(3,1) == local(3,2)) THEN
    out(5,1) = local(3,1); out(6,1) = local(3,1); out(6,2) = local(3,1)
  ELSE

  END IF

  IF (local(2,1) == local(1,2)) THEN
```

```
      out(1,1) = local(1,2); out(2,1) = local(1,2); out(1,2) = local(1,2)
    ELSE IF (local(1,1) == local(2,1) .OR. local(1,1) == local(1,2)) THEN
      out(1,1) = local(1,1); out(2,1) = local(1,1); out(1,2) = local(1,1)
    ELSE

    END IF

  CASE(17)
    IF (local(2,1) == local(3,3)) THEN
      IF (local(3,2) == local(2,1)) THEN
        out(6,1:6) = local(3,2); out(5,1:4) = local(3,2)
        out(4,1) = local(3,2)
      ELSE IF (local(2,1) == local(3,1)) THEN
        out(6,2:6) = local(3,2); out(5,3:4) = local(3,2)
        out(5,2) = local(2,1); out(4:6,1) = local(2,1)
      ELSE

      END IF
    ELSE
      IF (local(2,1) == local(3,2)) THEN
        out(6,1) = local(3,2); out(5,1) = local(3,2); out(6,2) = local(3,2)
      ELSE IF (local(3,1) == local(2,1) .OR.local(3,1) == local(3,2)) THEN
        out(5,1) = local(3,1); out(6,1) = local(3,1); out(6,2) = local(3,1)
      ELSE

      END IF
    END IF

  CASE(18)
    IF (local(2,1) == local(1,3)) THEN
      IF (local(1,2) == local(2,1)) THEN
        out(1,1:6) = local(1,2); out(2,1:4) = local(1,2)
        out(3,1) = local(1,2)
      ELSE IF (local(2,1) == local(1,1)) THEN
        out(1,2:6) = local(1,2); out(2,3:4) = local(1,2)
        out(2,2) = local(2,1); out(1:3,1) = local(2,1)
      ELSE

      END IF
    ELSE
      IF (local(2,1) == local(1,2)) THEN
        out(1,1) = local(1,2); out(1,2) = local(1,2); out(2,1) = local(1,2)
```

```
    ELSE IF (local(1,1) == local(1,2) .OR. local(1,1) == local(2,1)) THEN
      out(1,1) = local(1,1); out(2,1) = local(1,1); out(1,2) = local(1,1)
    ELSE

    END IF
  END IF

CASE(19)
  IF (local(2,1) == local(3,2)) THEN
    out(4:6,1) = local(3,2); out(5:6,2) = local(3,2)
    out(6,3) = local(3,2)
  ELSE IF (local(3,1) == local(3,2)) THEN
    out(6,1:3) = local(3,1); out(5,2) = local(3,1)
    out(4:5,1) = local(3,1)
  ELSE IF (local(3,1) == local(2,1)) THEN
    out(6,2:3) = local(3,1); out(5,2) = local(3,1)
    out(4:6,1) = local(3,1)
  ELSE

  END IF

CASE(20)
  IF (local(2,1) == local(1,2)) THEN
    out(1:3,1) = local(1,2); out(1:2,2) = local(1,2)
    out(1,3) = local(1,2)
  ELSE IF (local(1,1) == local(1,2)) THEN
    out(1,1:3) = local(1,1); out(2,2) = local(1,1)
    out(2:3,1) = local(1,1)
  ELSE IF (local(1,1) == local(2,1)) THEN
    out(1,2:3) = local(1,1); out(2,2) = local(1,1)
    out(1:3,1) = local(1,1)
  ELSE

  END IF

CASE(21)
  IF (local(2,1) == local(1,2)) THEN
    out(1:3,1) = local(1,2); out(1:2,2) = local(1,2)
    out(1,3) = local(1,2)
  ELSE IF (local(1,1) == local(1,2)) THEN
    out(1,1:3) = local(1,1); out(2,2) = local(1,1)
    out(2:3,1) = local(2,1)
```

```
    ELSE IF (local(1,1) == local(2,1)) THEN
      out(1:3,1) = local(1,1); out(2,2) = local(1,1)
      out(1,2:3) = local(1,2)
    ELSE

    END IF

    IF (local(2,1) == local(3,2)) THEN
      out(6,1) = local(3,2); out(5,1) = local(3,2); out(6,2) = local(3,2)
    ELSE IF (local(3,1) == local(2,1) .OR. local(3,1) == local(3,2)) THEN
      out(5,1) = local(3,1); out(6,1) = local(3,1); out(6,2) = local(3,1)
    ELSE

    END IF

    IF (local(1,2) == local(2,3)) THEN
      out(1,6) = local(2,3); out(2,6) = local(2,3); out(1,5) = local(2,3)
    ELSE IF (local(1,3) == local(2,3) .OR. local(1,3) == local(1,2)) THEN
      out(1,6) = local(1,3); out(1,5) = local(1,3); out(2,6) = local(1,3)
    ELSE

    END IF

  CASE(22)
    IF (local(1,2) == local(2,3)) THEN
      out(1,4:6) = local(2,3); out(2,5:6) = local(2,3)
      out(3,6) = local(2,3)
    ELSE IF (local(1,3) == local(2,3)) THEN
      out(1:3,6) = local(2,3); out(2,5) = local(2,3)
      out(1,4:5) = local(1,2)
    ELSE IF (local(1,3) == local(1,2)) THEN
      out(1,4:6) = local(1,2); out(2,5) = local(1,2)
      out(2:3,6) = local(2,3)
    ELSE

    END IF

    IF (local(2,1) == local(3,2)) THEN
      out(6,1) = local(3,2); out(5,1) = local(3,2); out(6,2) = local(3,2)
    ELSE IF (local(3,1) == local(2,1) .OR. local(3,1) == local(3,2)) THEN
      out(5,1) = local(3,1); out(6,1) = local(3,1); out(6,2) = local(3,1)
    ELSE
```

```
  END IF

CASE(23)
  IF (local(2,3) == local(1,1)) THEN
    IF (local(1,2) == local(2,3)) THEN
      out(1,1:6) = local(1,2); out(2,3:6) = local(1,2)
      out(3,6) = local(1,2)
    ELSE IF (local(2,1) == local(1,3)) THEN
      out(1,1:5) = local(1,2); out(2,3:4) = local(1,2)
      out(2,5) = local(2,3); out(1:3,6) = local(2,3)
    ELSE

    END IF
  ELSE
    IF (local(1,2) == local(2,3)) THEN
      out(1,6) = local(2,3); out(2,6) = local(2,3); out(1,5) = local(2,3)
    ELSE IF (local(1,3) == local(2,3) .OR. local(1,3) == local(1,2)) THEN
      out(1,6) = local(1,3); out(1,5) = local(1,3); out(2,6) = local(1,3)
    ELSE

    END IF
  END IF

CASE(24)
  IF (local(1,2) == local(2,3)) THEN
    out(1,4:6) = local(2,3); out(2,5:6) = local(1,2)
    out(3,6) = local(1,2)
  ELSE IF (local(1,3) == local(2,3)) THEN
    out(1:3,6) = local(2,3); out(2,5) = local(2,3)
    out(1,4:5) = local(1,2)
  ELSE IF (local(1,3) == local(1,2)) THEN
    out(1,4:6) = local(1,2); out(2,5) = local(1,2)
    out(2:3,6) = local(2,3)
  ELSE

  END IF

CASE(25)
  IF (local(3,2) == local(1,1)) THEN
    IF (local(3,2) == local(2,1)) THEN
      out(1:6,1) = local(2,1); out(3:6,2) = local(2,1)
```

```
            out(6,3) = local(2,1)
          ELSE IF (local(3,2) == local(3,1)) THEN
            out(1:5,1) = local(2,1); out(3:4,2) = local(2,1)
            out(5,2) = local(3,2); out(6,1:3) = local(3,2)
          ELSE

          END IF
        ELSE
          IF (local(2,1) == local(3,2)) THEN
            out(6,1) = local(3,2); out(5,1) = local(3,2); out(6,2) = local(3,2)
          ELSE IF (local(3,1) == local(2,1) .OR. local(3,1) == local(3,2)) THEN
            out(5,1) = local(3,1); out(6,1) = local(3,1); out(6,2) = local(3,1)
          ELSE

          END IF
        END IF

      CASE(26)
        IF (local(2,1) == local(3,2)) THEN
          out(6,1) = local(2,1); out(5,1) = local(2,1); out(6,2) = local(2,1)
        ELSE IF (local(3,1) == local(2,1) .OR. local(3,1) == local(3,2)) THEN
          out(5,1) = local(3,1); out(6,1) = local(3,1); out(6,2) = local(3,1)
        ELSE

        END IF

      CASE(255)
!
! In the default case, the output either requires no change or is
! unpredictable enough to leave alone
!
END SELECT result
END SUBROUTINE table
```

B.2.3 Pictoral Representation of the LUT Shape Choices

Each output shape can be the result of one or more input pixel combinations. The combinations are binary in their nature with only pixels having values that match the centre exactly being considered as similar, and everything else as different. In the graphics on the following pages every 36 pixel square is the shape assigned to the region represented by the pixel that forms the centre of the 9

pixel combinations to its left. Any pixel combinations that are not represented in these diagrams leave all 36 output pixels at their original value.

B.2.4 Recombining the Files

This script combines the produced files into a single large binary file of the type the TARO phantom is originally provided in. It is currently located at /local/michael/NICT/huge/build.sh

```
#!/bin/csh

set k = 1
while ( $k < 10 )
set j=1
while ($j < 7)
cat /local/michael/NICT/big/big00$k >> /local/michael/NICT/huge/mass
@ j ++
end
@ k ++
end

set k = 10
while ( $k < 100 )
set j=1
while ($j < 7)
cat /local/michael/NICT/big/big0$k >> /local/michael/NICT/huge/mass
@ j ++
end
@ k ++
end

set k = 100
while ( $k < 867 )
set j=1
while ($j < 7)
cat /local/michael/NICT/big/big$k >> /local/michael/NICT/huge/mass
@ j ++
end
@ k ++
end

exit 0
```

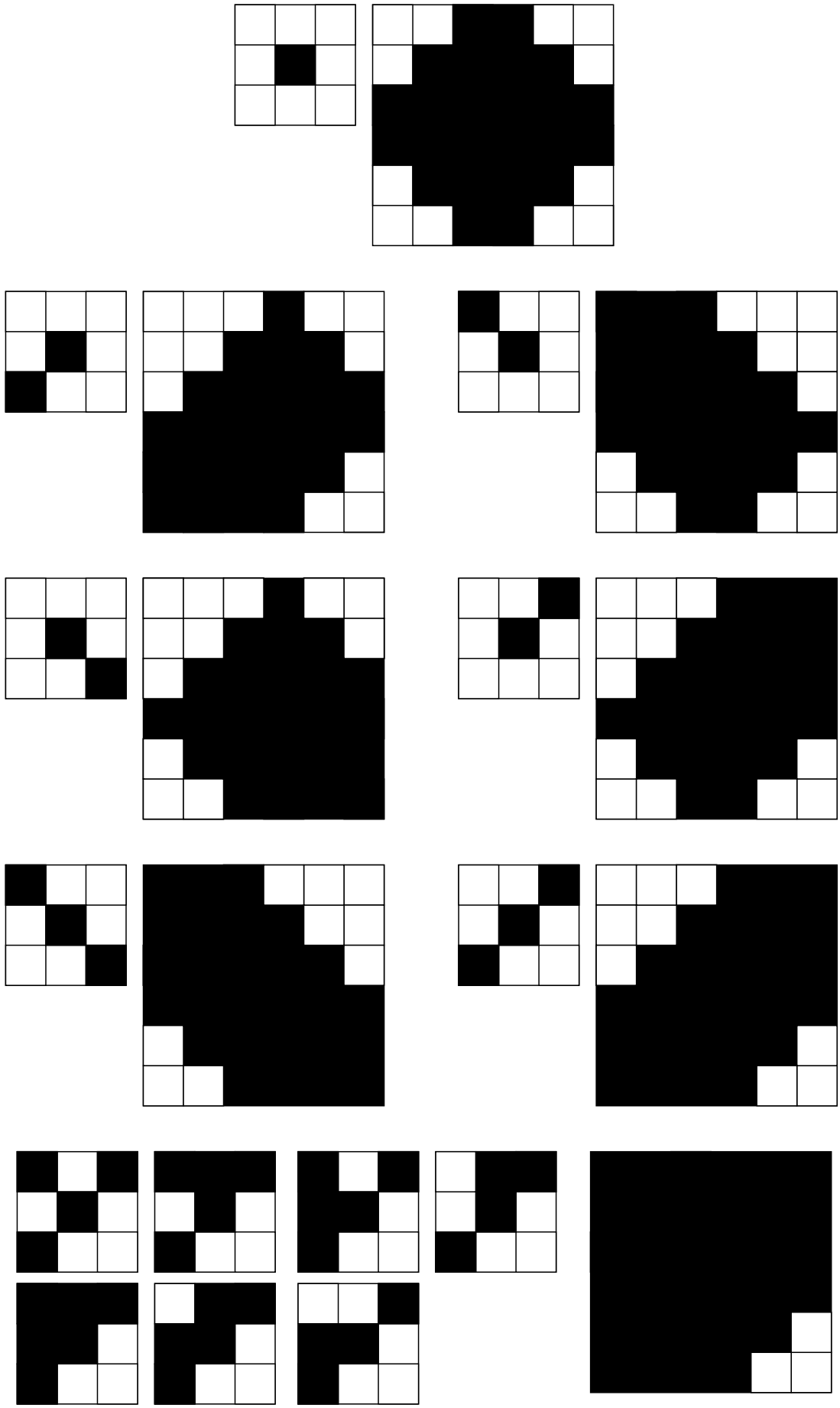

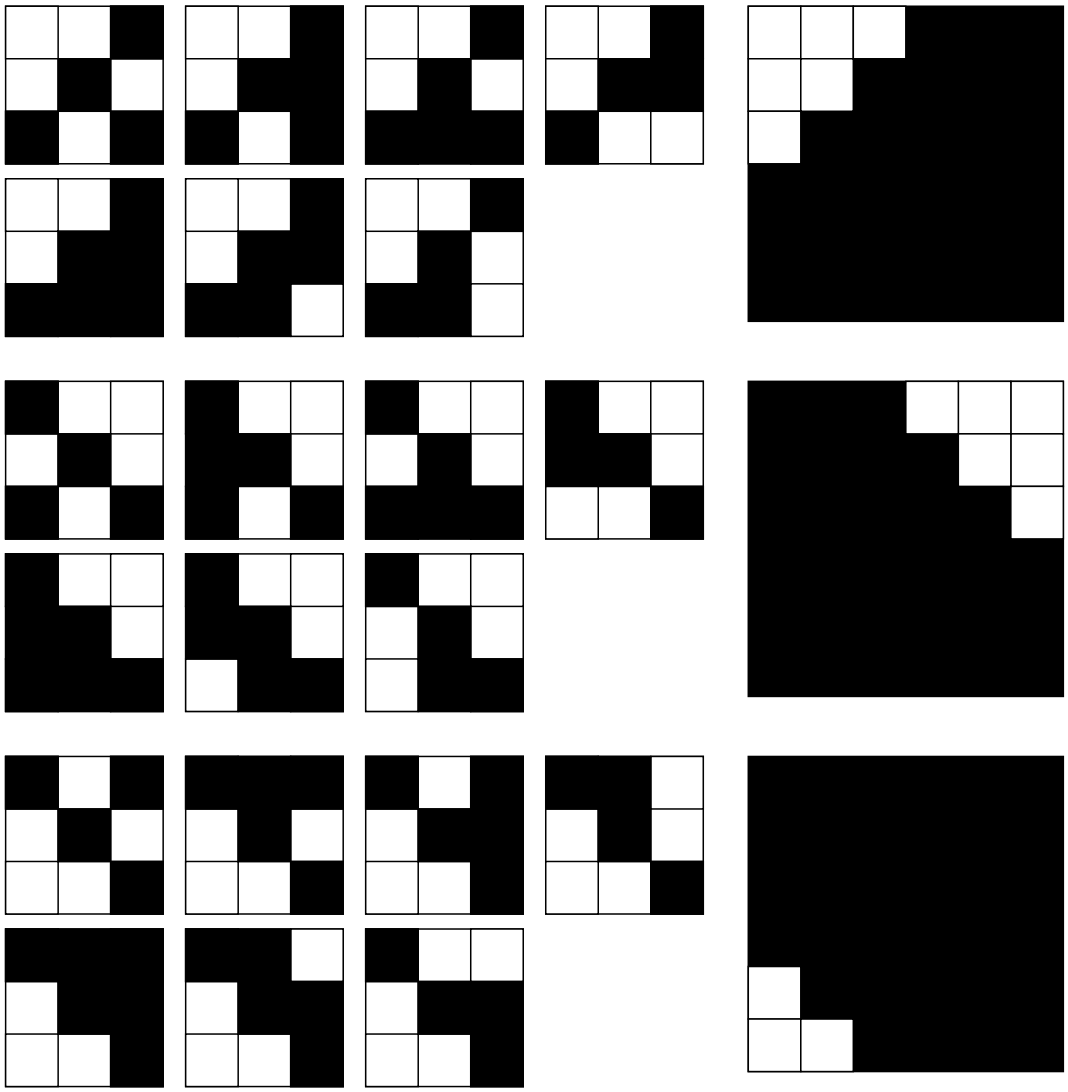

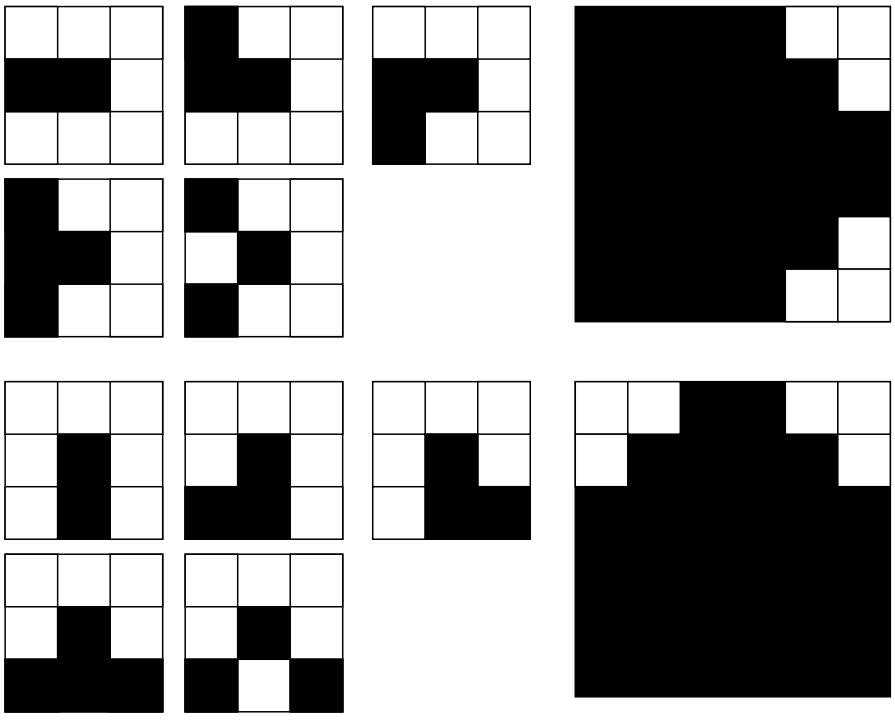

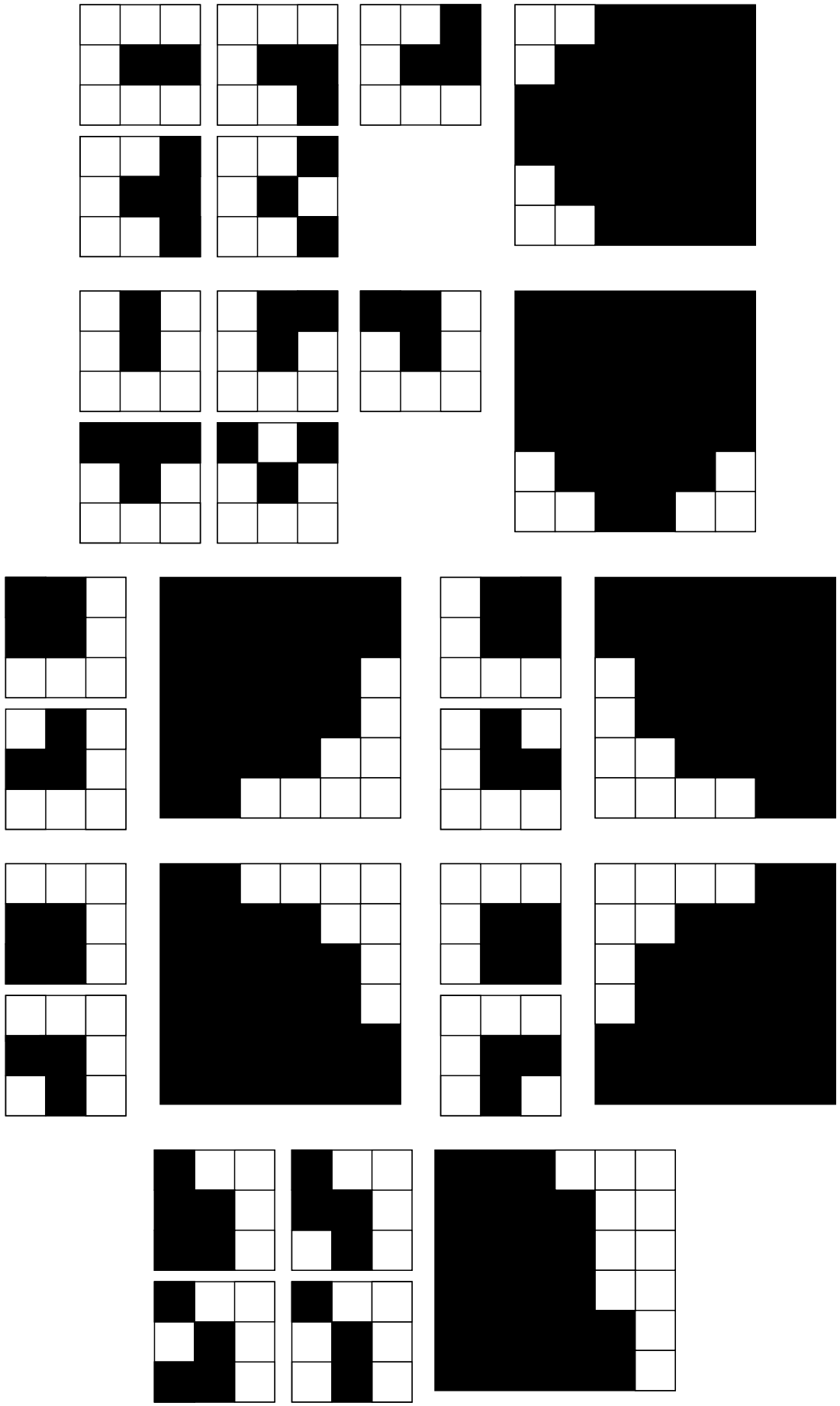

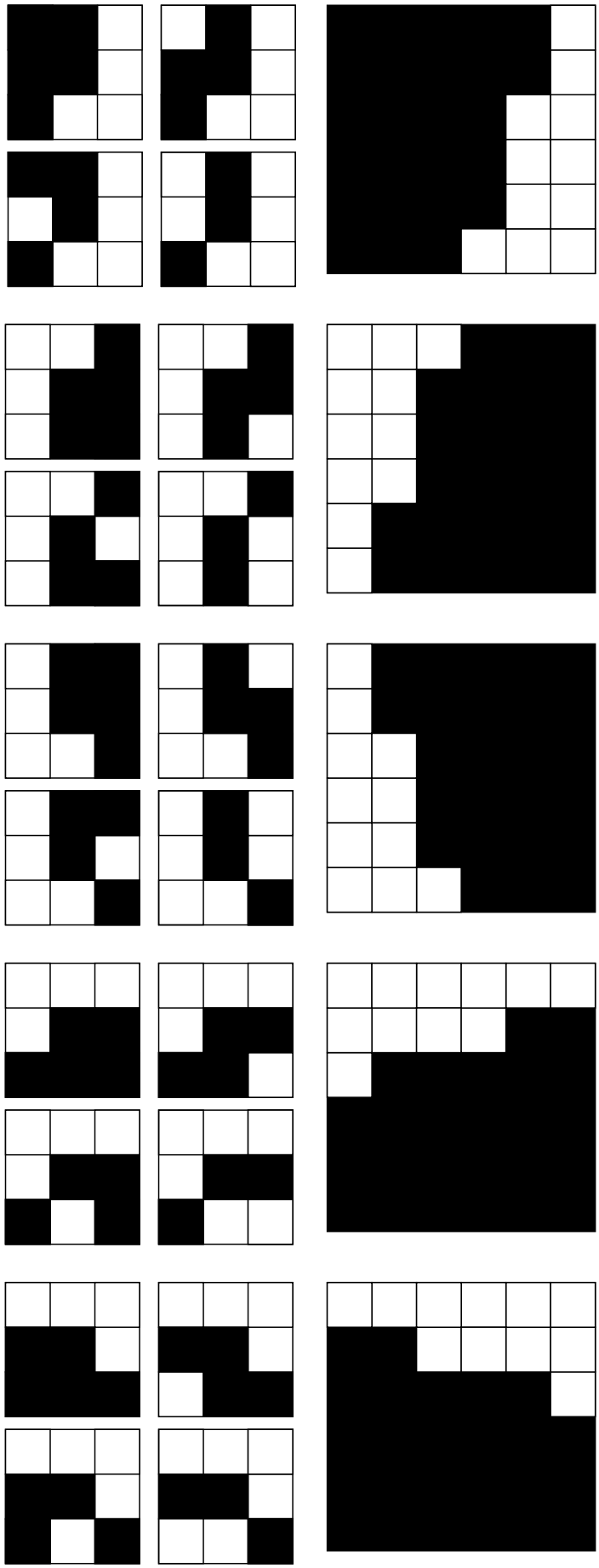

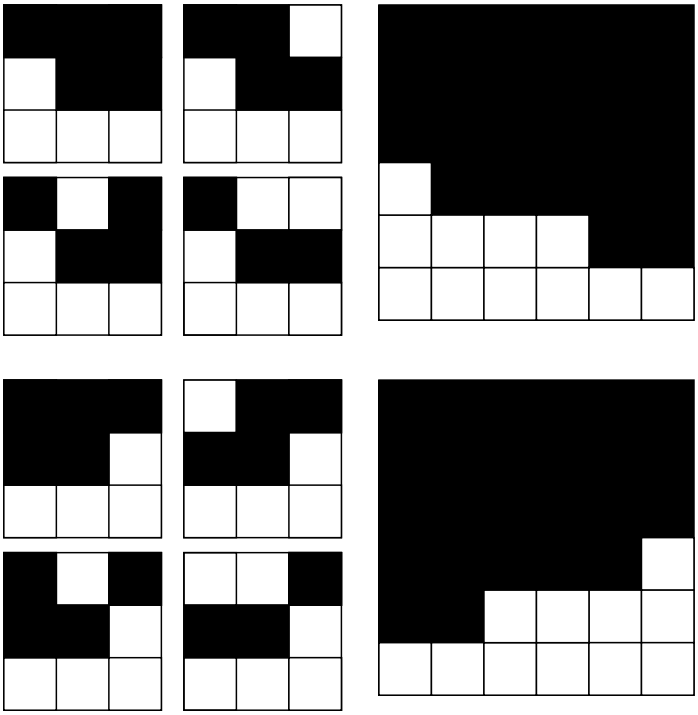

Appendix C

Isolated Heart Codes

C.1 Reformatting

This code takes input from the file out.dat, the original file containing the isolated heart model, and converts it from defining individual points to storing every voxel in the model space.

```
PROGRAM transfer
IMPLICIT NONE

INTEGER :: zold, x, y, z, t, err, i, j
! The file stores in 0-based coordinates
INTEGER :: plane(0:324,0:468)

!
! Set the array and plane variables to zero
!
plane = 0 ! The empty space is given a value of zero
zold = 0 ! The first z value is 0
!
! Read the first line of volume information
!
OPEN(101,file='../out.dat')
READ(101,*) z, y, x
!
! Set the error variable state to 0
!
 err = 0
OPEN(201, file='heart.out', ACCESS='STREAM', STATUS='NEW')
!
! Continue until there is no information left in the file
```

```
!
DO WHILE (err .eq. 0)
  READ(1,*,IOSTAT=err) z,y,x,t
!
! If the plane being worked on hasn't changed, keep
! storing information
!
  IF (z .EQ. zold) THEN
    plane(y,x) = t
!
! If the plane has changed, write out the contents of the last one
! then set z to the new plane, wipe it clean and continue
!
  ELSE
    DO i=0,324
      DO j=0,468
        WRITE(201) CHAR(plane(i,j))
      END DO
    END DO
    zold = z
    plane = 0
    plane(y,x) = t
  END IF
END DO

CLOSE(101)
CLOSE(201)

END PROGRAM
```

C.2 Mirroring

This program was used to reflet the heart model into the required orientation.

```
PROGRAM mirror

IMPLICIT NONE

INTEGER :: i,j,k
CHARACTER (len=1) :: heart(469,324)

OPEN(101,FILE='heart.raw', ACCESS='STREAM')
```

```
OPEN(201,FILE='heart2.raw', ACCESS='STREAM')
!
! reading in
!
DO k=1,486
  DO j=1,325
    DO i=1,469
      READ(101) heart(i,j)
    END DO
  END DO
!
! Mirroring
!
  DO j=325,1,-1
    DO i=1,469
      WRITE(201) heart(i,j)
    END DO
  END DO
END DO

CLOSE(101)
CLOSE(201)

END PROGRAM
```

C.3 Extracting a Phantom Section for Visualising

The system on which the PavaView simulation is being used has only 4 GB of system RAM, and the smoothed phantom is 9.5 GB in size in its binary form. Visualising the heart in this dataset is not possible, but it is possible to extract a section around the heart that is small enough to work with. The original TARO phantom is small enough to view as a whole entity, so the heart can be located and its position in the scaled phantom calculated.

The section in which the heart is located can then be extracted in two steps. The first is to trim the vertical excess through simple file management commands. Every layer is known to be 1843200 bytes in size, and the bottom edge of the heart can be found in the original model. The 500 layers between 1151-1650 can be obtained with two commands:

```
head -c 3041280000 mass > upper
tail -c 921600000 upper > section
```

The first command takes the top 1650 layers from the `mass` file that contains the whole smoothed phantom. The second takes the bottom 500 layers from these. This section is under 900 MB but still too large to use.

The second stage is the removal of the unnecessary tissue. The following program extracts a section of 500×400 pixels from every plane, producing a final `heartsec.raw` file that is just over 95 MB in size.

```
PROGRAM piece
IMPLICIT NONE

INTEGER :: i,j,k
CHARACTER (LEN=1) :: stack(1920,960), a

OPEN(101,file='section',ACCESS='STREAM', STATUS='OLD')
OPEN(201,file='heartsec.raw',ACCESS='STREAM', STATUS='NEW')

DO k = 1,500
  DO j = 1,960
    DO i = 1,1920
      READ(101) stack(i,j)
    END DO
  END DO
  DO j = 251,650
    DO i = 776,1275
      WRITE(201) stack(i,j)
    END DO
  END DO
 END DO

CLOSE(101)
CLOSE(201)

END PROGRAM
```

From visualisation of this section and the isolated heart, the insertion region was defined as $786 - 1254$ in the x axis, $268 - 592$ in the y axis and $1147 - 1632$ in the z-axis/

C.4 Insertion

This code inserts the isolated heart model into a section extracted from the body phantom. `sec2` is the phantom section that contains only the required region of the z-axis, `heart2.raw` is the formatted and mirrored isolated heart.

```
PROGRAM insert
IMPLICIT NONE

INTEGER :: i,j,k,l
CHARACTER (LEN=1):: slice(1920,960), a

OPEN(101, FILE='sec2', ACCESS='STREAM', STATUS='OLD')
OPEN(102, FILE='../heart2.raw', ACCESS='STREAM', STATUS='OLD')
OPEN(201, FILE='inserted.raw', ACCESS='STREAM', STATUS='NEW')

!
! Read in the body section one plane at a time
!
DO k = 1,486
  DO j = 1,960
    DO i = 1,1920
      READ(101) slice(i,j)
    END DO
  END DO
!
! Overwrite the heart in the correct region
!
  DO j = 268,592
    DO i = 786,1254
      READ(102) a
!
! Ignore all 0 cells, add 100 to avoid number conflicts
!
        IF(ICHAR(a) /= 0) THEN
          l=ICHAR(a)
          l=l+100
          a=CHAR(l)
          slice(i,j) = a
        END IF
    END DO
  END DO
!
```

```
! Write out the plane with the inserted information
!
  DO j = 1,960
    DO i = 1,1920
      WRITE(201) slice(i,j)
    END DO
  END DO
END DO

CLOSE(101)
CLOSE(102)
CLOSE(201)

END PROGRAM
```

C.5 Reducing the Range of Tissue Values

This script reduces the range of tissue values in the final phantom files from 0-170 to 0-69.

```
#!/bin/csh

set k = 0
while($k <  10)
echo $k

cat k000$k  | awk '($1 == 0){print 0}($1 == 1){ print 1}
($1 == 2){ print 2}($1 == 3){ print 3}($1 == 5){ print 4}
($1 == 6){ print 5}($1 == 7){ print 6}($1 == 8){ print 7}
($1 == 9){ print 8}($1 == 10){ print 9}($1 == 11){ print 10}
($1 == 12){ print 11}($1 == 13){ print 12}($1 == 14){ print 13}
($1 == 15){ print 14}($1 == 16){ print 15}($1 == 18){ print 16}
($1 == 19){ print 17}($1 == 20){ print 18}($1 == 21){ print 19}
($1 == 22){ print 20}($1 == 23){ print 21}($1 == 24){ print 22}
($1 == 25){ print 23}($1 == 26){ print 24}($1 == 27){ print 25}
($1 == 29){ print 26}($1 == 30){ print 27}($1 == 31){ print 28}
($1 == 32){ print 29}($1 == 33){ print 30}($1 == 34){ print 31}
($1 == 35){ print 32}($1 == 36){ print 33}($1 == 38){ print 34}
($1 == 39){ print 35}($1 == 20){ print 36}($1 == 43){ print 37}
($1 == 44){ print 38}($1 == 45){ print 39}($1 == 46){ print 40}
($1 == 47){ print 41}($1 == 48){ print 42}($1 == 49){ print 43}
($1 == 50){ print 44}($1 == 51){ print 45}($1 == 52){ print 46}
```

```
($1 == 53){ print 47}($1 == 54){ print 48}($1 == 55){ print 49}
($1 == 56){ print 50}($1 == 57){ print 51}($1 == 130){ print 52}
($1 == 131){ print 53}($1 == 132){ print 54}($1 == 133){ print 55}
($1 == 143){ print 56}($1 == 144){ print 57}($1 == 146){ print 58}
($1 == 147){ print 59}($1 == 148){ print 60}($1 == 149){ print 61}
($1 == 160){ print 62}($1 == 161){ print 63}($1 == 162){ print 64}
($1 == 163){ print 65}($1 == 164){ print 66}($1 == 165){ print 67}
($1 == 169){ print 68}($1 == 170){ print 69}' > a000$k

@ k ++
end

set k = 10
while($k <  100)
echo $k

cat k00$k  | '($1 == 0){print 0}($1 == 1){ print 1}
($1 == 2){ print 2}($1 == 3){ print 3}($1 == 5){ print 4}
($1 == 6){ print 5}($1 == 7){ print 6}($1 == 8){ print 7}
($1 == 9){ print 8}($1 == 10){ print 9}($1 == 11){ print 10}
($1 == 12){ print 11}($1 == 13){ print 12}($1 == 14){ print 13}
($1 == 15){ print 14}($1 == 16){ print 15}($1 == 18){ print 16}
($1 == 19){ print 17}($1 == 20){ print 18}($1 == 21){ print 19}
($1 == 22){ print 20}($1 == 23){ print 21}($1 == 24){ print 22}
($1 == 25){ print 23}($1 == 26){ print 24}($1 == 27){ print 25}
($1 == 29){ print 26}($1 == 30){ print 27}($1 == 31){ print 28}
($1 == 32){ print 29}($1 == 33){ print 30}($1 == 34){ print 31}
($1 == 35){ print 32}($1 == 36){ print 33}($1 == 38){ print 34}
($1 == 39){ print 35}($1 == 20){ print 36}($1 == 43){ print 37}
($1 == 44){ print 38}($1 == 45){ print 39}($1 == 46){ print 40}
($1 == 47){ print 41}($1 == 48){ print 42}($1 == 49){ print 43}
($1 == 50){ print 44}($1 == 51){ print 45}($1 == 52){ print 46}
($1 == 53){ print 47}($1 == 54){ print 48}($1 == 55){ print 49}
($1 == 56){ print 50}($1 == 57){ print 51}($1 == 130){ print 52}
($1 == 131){ print 53}($1 == 132){ print 54}($1 == 133){ print 55}
($1 == 143){ print 56}($1 == 144){ print 57}($1 == 146){ print 58}
($1 == 147){ print 59}($1 == 148){ print 60}($1 == 149){ print 61}
($1 == 160){ print 62}($1 == 161){ print 63}($1 == 162){ print 64}
($1 == 163){ print 65}($1 == 164){ print 66}($1 == 165){ print 67}
($1 == 169){ print 68}($1 == 170){ print 69}' > a00$k

@ k ++
```

```
end

set k = 100
while($k <  1000)
echo $k

cat k0$k  | awk '($1 == 0){print 0}($1 == 1){ print 1}
($1 == 2){ print 2}($1 == 3){ print 3}($1 == 5){ print 4}
($1 == 6){ print 5}($1 == 7){ print 6}($1 == 8){ print 7}
($1 == 9){ print 8}($1 == 10){ print 9}($1 == 11){ print 10}
($1 == 12){ print 11}($1 == 13){ print 12}($1 == 14){ print 13}
($1 == 15){ print 14}($1 == 16){ print 15}($1 == 18){ print 16}
($1 == 19){ print 17}($1 == 20){ print 18}($1 == 21){ print 19}
($1 == 22){ print 20}($1 == 23){ print 21}($1 == 24){ print 22}
($1 == 25){ print 23}($1 == 26){ print 24}($1 == 27){ print 25}
($1 == 29){ print 26}($1 == 30){ print 27}($1 == 31){ print 28}
($1 == 32){ print 29}($1 == 33){ print 30}($1 == 34){ print 31}
($1 == 35){ print 32}($1 == 36){ print 33}($1 == 38){ print 34}
($1 == 39){ print 35}($1 == 20){ print 36}($1 == 43){ print 37}
($1 == 44){ print 38}($1 == 45){ print 39}($1 == 46){ print 40}
($1 == 47){ print 41}($1 == 48){ print 42}($1 == 49){ print 43}
($1 == 50){ print 44}($1 == 51){ print 45}($1 == 52){ print 46}
($1 == 53){ print 47}($1 == 54){ print 48}($1 == 55){ print 49}
($1 == 56){ print 50}($1 == 57){ print 51}($1 == 130){ print 52}
($1 == 131){ print 53}($1 == 132){ print 54}($1 == 133){ print 55}
($1 == 143){ print 56}($1 == 144){ print 57}($1 == 146){ print 58}
($1 == 147){ print 59}($1 == 148){ print 60}($1 == 149){ print 61}
($1 == 160){ print 62}($1 == 161){ print 63}($1 == 162){ print 64}
($1 == 163){ print 65}($1 == 164){ print 66}($1 == 165){ print 67}
($1 == 169){ print 68}($1 == 170){ print 69}' > a0$k

@ k ++
end

set k = 1000
while($k <  5196)
echo $k

cat k$k  | awk '($1 == 0){print 0}($1 == 1){ print 1}
($1 == 2){ print 2}($1 == 3){ print 3}($1 == 5){ print 4}
($1 == 6){ print 5}($1 == 7){ print 6}($1 == 8){ print 7}
($1 == 9){ print 8}($1 == 10){ print 9}($1 == 11){ print 10}
```

```
($1 == 12){ print 11}($1 == 13){ print 12}($1 == 14){ print 13}
($1 == 15){ print 14}($1 == 16){ print 15}($1 == 18){ print 16}
($1 == 19){ print 17}($1 == 20){ print 18}($1 == 21){ print 19}
($1 == 22){ print 20}($1 == 23){ print 21}($1 == 24){ print 22}
($1 == 25){ print 23}($1 == 26){ print 24}($1 == 27){ print 25}
($1 == 29){ print 26}($1 == 30){ print 27}($1 == 31){ print 28}
($1 == 32){ print 29}($1 == 33){ print 30}($1 == 34){ print 31}
($1 == 35){ print 32}($1 == 36){ print 33}($1 == 38){ print 34}
($1 == 39){ print 35}($1 == 20){ print 36}($1 == 43){ print 37}
($1 == 44){ print 38}($1 == 45){ print 39}($1 == 46){ print 40}
($1 == 47){ print 41}($1 == 48){ print 42}($1 == 49){ print 43}
($1 == 50){ print 44}($1 == 51){ print 45}($1 == 52){ print 46}
($1 == 53){ print 47}($1 == 54){ print 48}($1 == 55){ print 49}
($1 == 56){ print 50}($1 == 57){ print 51}($1 == 130){ print 52}
($1 == 131){ print 53}($1 == 132){ print 54}($1 == 133){ print 55}
($1 == 143){ print 56}($1 == 144){ print 57}($1 == 146){ print 58}
($1 == 147){ print 59}($1 == 148){ print 60}($1 == 149){ print 61}
($1 == 160){ print 62}($1 == 161){ print 63}($1 == 162){ print 64}
($1 == 163){ print 65}($1 == 164){ print 66}($1 == 165){ print 67}
($1 == 169){ print 68}($1 == 170){ print 69}' > a$k

@ k ++
end

exit 0
```

Appendix D

Contents of the Final Phantom

The following list provides the 70 different tissues, structures and materials present in the final phantom. Number 0 to 51 are all those present in the original TARO model, while 52 to 69 are those from the isolated heart.

0 External Air
1 Cerebellum
2 CSF
3 Cornea
4 Eye tissue (Sclera)
5 Gray Matter
6 Hypothalamus
7 Lens
8 Pineal Glands
9 Pituitary
10 salivary gland
11 Thalamus
12 Tongue
13 White Matter
14 Adrenals
15 Bladder
16 Large Intestine
17 Large Intestine Contents
18 Duodenum
19 Esophagus
20 Bile

21 Gall Bladder
22 Heart
23 Kidney
24 Liver
25 Lung
26 Pancreas
27 Prostate
28 Small Intestine
29 Spleen
30 Stomach
31 Stomach Contents
32 Tendon
33 Testis
34 Thyroid
35 Trachea
36 Urine
37 Air (Internal)
38 Blood
39 Cortical Bone
40 Bone Marrow and Cancellous Bone
41 Cartilage
42 Fat
43 Muscle
44 Nerve (Spinal cord)
45 Skin
46 Tooth
47 Ligament
48 Small Intestine Contents
49 Diaphragm
50 Seminal Vesicle
51 Cavernous Body
52 Right Ventricle
53 Left Ventricle
54 Right Atrium
55 Left Atrium

56 Blood, venous
57 Blood, arterial
58 AV valve, left
59 AV valve, right
60 Aortic valve
61 Pulmonal Valve
62 Vena-Cava
63 Pulmonary Trunk
64 Aorta
65 Pulmonary vein
66 Blood, coronary veins
67 Blood, cononary arteries
68 Muscle Papillaries, left
69 Muscle Papillaries, right

Bibliography

[1] Judith Mackay, George A. Mensah, Shanthi Mendis, and Kurt Greenlund. *The Atlas of Heart Disease and Stroke*. World Health Organisation, 2004.

[2] UK National Office of Statistics. Mid-year population estimates. `http://www.statistics.gov.uk/cci/nugget.asp?ID=949`, August 2008.

[3] Yee Guan Yap, Trinh Duong, Martin Bland, Marel Malik, Christian Torp-Pederson, Lars Køber, Stuart J. Connolly, Bradley Marchant, and John Camm. Temporal trends on the risk of arrhythmic vs. non-arrhythmic deaths in high-risk patients after myocardial infarction: a combined analysis from multicentre trials. *European Heart Journal*, 26(14):1385–1393, 2005.

[4] A. A. Armoundas, A. B. Feldman, R. Mukkamala, and R. J. Cohen. A single equivalent moving dipole model: An efficient approach for localizing sites of origin of ventricular electrical activation. *Annals Biomedical Engineering*, 31:564–576, 2003.

[5] Amy Squillacote. *The ParaView Guide*. Kitware, Inc., 2004.

[6] Hamish Watson. *Disorders of Cardiac Rate Rhythm and Conduction*. Beaconsfield Publishers Ltd., 1984.

[7] GE Healthcare. MAC 5500 ECG diagnosis system brochure.

[8] Dewar D. Finlay, Chris D. Nugent, Paul J McCullagh, and Norman D Black. Mining for diagnostic information in body surface potential maps: a comparison of feature selection techniques. *BioMedical Engineering OnLine*, 4(51), 2005.

[9] R. Hoekema, G. J. H Uijen, and A. van Oosterom. On selecting a body surface mapping procedure. *Journal of Electrocardiology*, 32(2):93–101, 1999.

[10] L. Ambroggi and A. D. Corlan. Clinical use of body surface potential mapping in cardiac arrhythmias. *Anatol. J. Cardiol.*, pages 8–10, 2007.

[11] R. D. Lockhart, G.F. Hamilton, and F. W. Fyfe. *Anatomy of the Human Body*. Faber and Faber Ltd, 1965.

[12] Susan L. Woods, Erika Sivarajan Froelicher, Sandra Adams Motzer, and Elizabeth J. Bridges, editors. *Cardiac Nursing*, chapter Cardiac Anatomy and Physiology. Lippincott Williams & Wilkins, 5th edition, 2005.

[13] Michel Hassaguerre, Pierre Jas, Dipen C. Shah, Atsushi Takahashi, Mélèze Hocini, Gilles Quiniou, Stéphane Garrigue, Alain Le Mouroux, Philippe Le Mtayer, and Jacques Clémenty. Sponataneous initiation of atrial fibrillation by ectopic beats originating in the pulmonary veins. *The New England Journal of Medicine*, 339:659–666, 1998.

[14] Ian H. Law, Nicholas H. Von Bergen, Gingerich Jean C, Elizabeth V. Saarel, Peter S. Fischbach, and Macdonald Dick II. Transcatheter cryothermal ablation of junctional ectopic tachycardia in the normal heart. *Heart Rhythm*, 3:903–907, 2006.

[15] D. P. Redfearn, J. D. Hill, R. Keal, W. D. Toff, and P. J. Stafford. Left ventricular dysfunction resulting from frequent unifocal ventricular ectopics with resolution following radiofrequency ablation. *Europace*, 5(3):247–250, 2003.

[16] C. Beane, M. Bodruzzaman, M. Essawy, M. Malkani, and R. Smith. Localization of ventricular arrhythmogenic foci. In *IEEE Symp. System Theory*, pages 75–79, 1998.

[17] Christopher S. Simpson. Implantable cardioverter defibrillators work - so why aren't we using them? *Canadian Medical Association Journal*, 177:49–51, 2007.

[18] Fred M. Kusumoto and Nora F. Goldschlager, editors. *Cardiac Pacing for the Clinician*. Springer, 2008.

[19] Denise L. Janosik, Antonella Quattromani, and Lisa Schiller. *Cardiac Catheterization Handbook*, chapter Electro-Physiologic Studies and Ablation Techniques. Mosby Inc, 1999.

[20] Fei Lü, Scott Sakaguchi, and David G. Benditt. *Handbook of Cardiac Anatomy, Physiology and Devices*, chapter Cardiac Arrhythmias and Transcatheter Ablation. Humana Press Inc, 2005.

[21] P. L. Agren, H. Goranson, H. Jonsson, and L. Bergfeldt. Magnetocardiographic and magnetic resonance imaging for noninvasive localization of ventricular arrhythmia origin in a model of nonischemic cardiomyopathy. *Pacing and Clinical Electrophysiology*, 25:161–166, 2002.

[22] D. Darbar, J. E. Olgin, J. M. Miller, and P. A. Friedman. Localization of the origin of arrhythmias for ablation:from electrocardiography to advanced endocardial mapping systems. *J. Cardiovascular Electrophysiology*, 12:1309–1325, 2001.

[23] Shih-Ann Chen, Chern-En Chiang, Ching-Tai Tai, Chen-Chuen Cheng, Cheun-Wang Chiou, Shih-Huang Lee, Kwo-Chang Ueng, Zu-Chi Wen, and Mau-Song Chang. Complications of diagnostic electrophysiologic studies and radiofrequency catheter ablation in patients with tachyarrhythmias: an eight-year survey if 3,966 consecutive procedures in a tertiary referral center. *The American Journal of Cardiology*, 77(1):41–46, 1996.

[24] C. Liu, G. Li, and B. He. Localization of the site of origin of reentrant arrhythmia from body surface potential maps: a model study. *Phys. Med. Biol.*, 50:1421–1432, 2005.

[25] The National Library of Medicine. The national library of medicine's visual human project. `http://www.nlm.nih.gov/research/visible/visible_human.html`. Accessed on 04/Feb/2008.

[26] M. E. Barley and R. J. Cohen. High-precision guidance of ablation catheters to arrhythmic sites using electrocardiographic signals. In *IEEE Int. Conf. EMBS*, pages 6297–6300, 2006.

[27] C. Ramanathan and Y. Rudy. Electrocardiographic imaging: I. effect of torso inhomogeneities on body surface electrocardiographic potentials. *J. Cardiovascular Electrophysiol.*, 12:229–240, 2001.

[28] M. S. Lynn, A. C. L. Barnard, J. H. Holt, and L. T. A. Sheffield. A proposed method for the inverse problem in electrocardiology. *Biophys. J.*, 7:925–945, 1967.

[29] M. Boulakia, M. A. Fernandez, J.-F. Gerbeau, and N. Zemzemi. Towards the numerical simulation of electrocardiograms. In *IEEE Int. Conf. Functional Imaginand Modeling of the Heart*, pages 420–429, 2007.

[30] D. Wei, O. Okazaki, K. Hatumi, E. Harasawa, and H. Hosaka. Comparative simulation of excitation and body surface electrocardiogram with isotropic and anisotropic computer heart models. *IEEE Trans. Biomed. Eng.*, 42:343–357, 1995.

[31] M. Seger, B. Tilg, R. Modre-Osprian, G. Fischer, F. Hanser, and B. Messnarz. Ecg mapping and imaging of cardiac electrical function. *Stud. Health Technol. Inform.*, 95:56–61, 2003.

[32] Rudolf Kopecký and Mikael Persson. Subgridding method for fdtd modeling in the inner ear. In *Proceedings of SPIE*, volume 5445, pages 398–401, 2003.

[33] M. Potse, A.-R. LeBlanc, and A. Vinet. Why do we need supercomputers to understand the electrocardiographic t-wave? *Anatol. J. Cardiol.*, Suppl. 1:123–4, 2007.

[34] Nina Petoussi-Henss, Maria Zankl, Ute Fill, and Dieter Regulla. The GSF family of voxel phantoms. *Physics in Medicine and Biology*, 47:89–106, 2002.

[35] Walter S. Snyder, Mary R. Ford, and Gordon G. Warner. *MIRD Pamphlet no. 5, revised: Estimates of Specific Absorbed Fractions for Photon Sources Uniformly Distributed in Various Organs of a Heterogeneous Phantom.* Society of Nuclear Medicine, 1978.

[36] W. S. Snyder, M. J. Cook, E. S. Nasset, L. R. Karhausen, G. Parry Howells, and I. H. Tipton. Report on the task group on reference man. *Annals of the ICRP*, 23, 1975.

[37] J. Valentin. Basic anatomical and physiological data for use in radiological protection: Reference values ICRP publication 89. *Annals of the ICRP*, 32:1–277, 2002.

[38] Choonsik Lee, Choonik Lee, Daniel Lodwick, and Wesley E. Bolch. NURBS-based 3-d anthropomorphic computational phantoms for radiation dosimetry applications. *Radiation Protection Dosimetry*, 127:227–232, 2007.

[39] Binquan Zhang, Jizeng Ma, Liye Liu, and Jianping Cheng. CNMAN: A chinese adult male voxel phantom constructed from color photographs of a visible anatomical data set. *Radiation Protection Dosimetry*, 124:130–136, 2007.

[40] Peter Dimbylow. Development of the female voxel phantom, NAOMI, and its application to calculations of induced current densities and electric fields from applied low frequency magnetic and electric fields. *Physics in Medicine and Biology*, 50:1047–1070, 2005.

[41] Tomoaki Nagaoka, Soichi Watanabe, Kiyoko Sakurai, Etsuo Kunieda, Satoshi Watanabe, Masao Taki, and Yukio Yamanaka. Development of realistic high-resolution whole-body voxel models of japanese adult males and females of average height and weight, and application of models to radio-frequency electromagnetic-field dosimetry. *Physics in Medicine and Biology*, 49:1–15, 2004.

[42] G. Tanaka, H. Kawamura, R. V. Griffith, M. Cristy, and K. F. Eckerman. Reference man models for males and females of six age groups of asian populations. *Radiation Protection Dosimetry*, 79:383–386, 1998.

[43] Les Piegl. On NURBS: A survey. *IEEE Computer Graphics and Applications*, 11:55–71, 1991.

[44] William Paul Segars. *Development and Application of the new Dynamic NURBS-based cardiac-torso (NCAT) phantom.* PhD thesis, University of North Carolina at Chapel Hill, 2001.

[45] W. Paul Segars, David S. Lalush, and Benjamin M. W. Tsui. A realistic spline-based dynamic heart phantom. *IEEE Transactions on Nuclear Science*, 46:503–506, 1999.

[46] Victor Spitzer, Michael J. Ackerman, Ann L. Scherzinger, and David Whitlock. The visible human male: A technical report. *The Journal of the American Medical Informatic Association*, 3:118–130, 1996.

[47] V.M. Spitzer and D.G. Whitlock. *Atlas of the visible human male.* Jones and Bartlett Publishers, 1998.

[48] M. Bajka, M. Manestar, J. Hug, G. Székely, and U. Hallerand P. Groscurth. Detailed anatomy of the abdomen and pelvis of the visible human female. *Clinical Anatomy*, 17:252–260, 2004.

[49] X. G. Xu, T. C. Chao, and A Bozkurt. VIP-man: An image-based whole-body adult male model constructed from colour photographs of the visible human project for multi-particle monte carlo calculations. *Health Physics*, 78(5):476–486, 2000.

[50] REMCOM Inc. Xfdtd. `http://www.remcom.com`, 2005.

[51] G. Roeggla, U. Landesmann, and M. Roeggla. Ethics of executed person on the internet. *The Lancet, letters*, 345:260, 1995.

[52] R. Glynn Owens. Ethics of executed person on the internet. *The Lancet, letters*, 345:653, 1995.

[53] Christopher M. Collins and Michael B. Smith. Signal-to-noise ratio and absorbed power as functions of main magnetic field strength, and definition of "90°" rf pulse for the head in the birdcage coil. *Magnetic Resonance in Medicine*, 45, 2001.

[54] Spencer Kimball ad Peter Mattis. The gnu image manipulation project. `http://www.gimp.org/`.

[55] Maxim Stepin. hq3x magnification filter. `http://www.hiend3d.com/hq3x.html`.

[56] Henry Gray. *Henry Gray's Anatomy of the Human Body.* Lea & Febiger, 20th edition, 1918.

[57] Albert Oberman, Allen R. Myers, Thomas M. Karunas, and Frederick H. Epstein. Heart size of adults in a natural population - tecumseh, michigan: Variation by sex, age, height and weight. *Circulation: Journal of the American Heart Association*, 50:724–733, 1967.